FOREWORD

This report was prepared by Arthur D. Little, Inc., under USAF Contract No. AF 33(616)-6154. This contract was initiated under Project No. 7350, "Refractory, Inorganic and Non-Metallic Materials," Task 735001 "Non-Graphitic." This work was administered under the direction of the Directorate of Materials and Processes, Deputy for Technology, Aeronautical Systems Division, with Mr. Fred Vahldiek acting as project engineer.

This report covers the period of work from September 1959 to July 1962.

Personnel participating in the work included J. Berkowitz-Mattuck, J. T. Larson, R. F. Quigley, and W. Christiansen.

ABSTRACT

SECTION I: OXIDATION OF COPPER

An apparatus is described for continuous measurement of the rate of oxidation of metallic materials at temperatures between 900° and 2100°C. The samples, enclosed in an all-glass constant pressure flow system, are heated inductively and a thermal conductivity cell of the type employed in vapor phase chromatography is used to compare the oxygen concentration in a helium stream before and after removal of a portion of the oxygen by reaction with the heated specimens. Quantitative results obtained by this technique for the oxidation of copper between 975° and 1044°C at oxygen partial pressures of 2-10 mm are in good agreement with previously reported values, obtained by conventional methods.

SECTION II: OXIDATION OF CARBIDES

For the highest carbides of the metals of Groups IV-A (Ti, Zr, Hf), V-A (V, Nb, Ta), and VI-A (Cr, Mo, W) of the periodic table, the results of calculations of the pressures of carbon monoxide and carbon dioxide over an equilibrium mixture of metal carbide and the corresponding metal oxide are given. On the basis of thermodynamics, a coherent oxide film on the carbide surfaces would be ruptured by evolution of $CO(g)$ and $CO_2(g)$ from the carbide/oxide interface at temperatures above: 1230°C for TiO_2 (rut.) on TiC, 1730°C for ZrO_2 on ZrC, 1730°C for HfO_2 on HfC, 1230°C for V_2O_3 on VC, 830°C for NbO_2 on NbC, 1030°C for Ta_2O_5 on TaC, 1130°C for Cr_2O_3 on Cr_3C_2, and 730°C for WO_2 on WC. These are maximum temperatures for oxidation resistance of the carbides. Experimental data obtained under this contract and in other laboratories indicates that many of the carbides oxidize rapidly at even lower temperatures due to the poor adherence between oxide and substrate. The most promising refractory carbide is HfC.

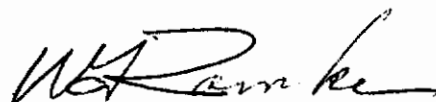SECTION III: OXIDATION OF MOLYBDENUM SILICIDES

The oxidation of Mo_3Si, Mo_5Si_3, and $MoSi_2$ between 1300° and 2100°K at oxygen pressures of 2-20 Torr was studied by oxygen consumption and metallographic techniques.

SECTION IV: OXIDATION OF MISCELLANEOUS MATERIALS

The oxidation of W_5Si_3 and WSi_2 was studied by the thermal conductivity method at temperatures between 1600° and 2030°K.

A measurement of the rate of oxygen consumption of Ta_2Be_{17} was made at 1664°K and an oxygen partial pressure of 8.4 Torr.

This report has been reviewed and is approved.

W. G. Ramke
Chief, Ceramics and Graphite Branch
Metals and Ceramics Laboratory
Materials Central

TABLE OF CONTENTS

vi

LIST OF FIGURES

viii

LIST OF TABLES

KINETICS OF OXIDATION OF REFRACTORY METALS AND ALLOYS
AT 1000°-2000°C

SECTION I - OXIDATION OF COPPER

1. INTRODUCTION

In the past 30 years, extensive studies have been made of the oxidation
of metals and alloys in the 300°-1000°C range, where the Wagner mechanism[1]
is frequently applicable after the first few minutes of reaction. A major
experimental tool for this work has been the vacuum microbalance,[2] which
permits continuous measurement of weight changes during oxidation, with a sen-
sitivity of 3×10^{-7} g. Supplementary measurements of the electrical properties
of oxide films and diffusion through the oxide layers have given firm support
to Wagner's ideas. More recently, with the development of electron microscopy
and electron probe analysis, attention has been directed toward the
earliest stages of oxidation, where Mott's[3] theory for the growth of thin
films can be tested, but interest has again centered on pure metals at
temperatures below 1000°C.

The growing need for structural materials for space and technological
applications in the 1000° and 3000°C range has emphasized the importance of
fundamental studies of the oxidation process at higher temperatures. Theoreti-
cal extrapolations from oxidation behavior at low temperatures is, for the most
part, not possible, due largely to the enhanced volatility of alloy constitu-
ents and product oxides as the temperature is raised. Experimentally, many of
the low temperature techniques are either difficult to adapt or inapplicable,
and new methods must be developed.

As temperature increases, rates of chemical reactions are greatly
accelerated, and the possible container materials in which a reaction can be
studied become more and more limited. If the sample is a metallic conductor,
induction heating provides an excellent means for maintaining it at a high
temperature, while keeping non-conducting walls and supports relatively cool.
The choice of induction heating, however, almost precludes the use of
continuous weighing techniques for following an oxidation reaction, since the
r.f. field generates an upward force on the heated sample. In this paper, the

---

1

use of a thermal conductivity bridge, of the type employed in vapor phase
chromatography, to compare the oxygen concentration in a helium stream before
and after reaction with an inductively heated sample pellet is described. The
method gives rates of oxidation directly and continuously with a sensitivity
of about 10^{-4} g/min-millivolt, where voltage differences of the order of 0.01
millivolt are readily detectable. Although the general technique was first
suggested by E. R. Weaver of the National Bureau of Standards[4] in 1951, it
has received little attention for physical chemical studies[5] and has
apparently never been applied to oxidation kinetics.

2. EXPERIMENTAL

(a) Apparatus

A schematic diagram of the apparatus in operation in this laboratory
is shown in Figure 1. Samples under study are machined in the form of cylin-
ders, 0.8 cm in diameter and 0.3 cm in height, and are mounted by point
contact with three alumina or thoria rods, 3 cm in length (L). The ceramic
support rods are in turn fastened with gold wire to an aluminum sample holder.
A screw at the bottom of the sample holder permits positioning of the pellet
optimally with respect to the concentrator and r.f. coils of a Sylvania 5 kw
induction unit. The samples are completely enclosed in a constant pressure
flow system, constructed entirely of pyrex, except for a short length of quartz
tubing in the immediate neighborhood of the pellet.

The flow system is of conventional design. Helium from tank A flows
through a purification train of magnesium perchlorate, Ascarite, drierite, and
glass wool, B, that removes water vapor, carbon dioxide, and dust. Flow rate
is measured with a dibutylphthalate capillary flow meter, D, flanked by liquid
nitrogen traps C and C'. Oxygen can be introduced into the helium stream at
partial pressures between 0 and 20 mm by allowing the helium to flow through
heated CuO (E). The helium-oxygen mixture passes through a cold trap, G, at
dry-ice acetone temperature (-80°C), and enters the reference side of the
thermal conductivity cell at H. The stream flows through a second -80°C cold
trap at J, and over the hot refractory button L, where a portion of the
oxygen is removed by chemical reaction. The gas stream, depleted in oxygen,

2
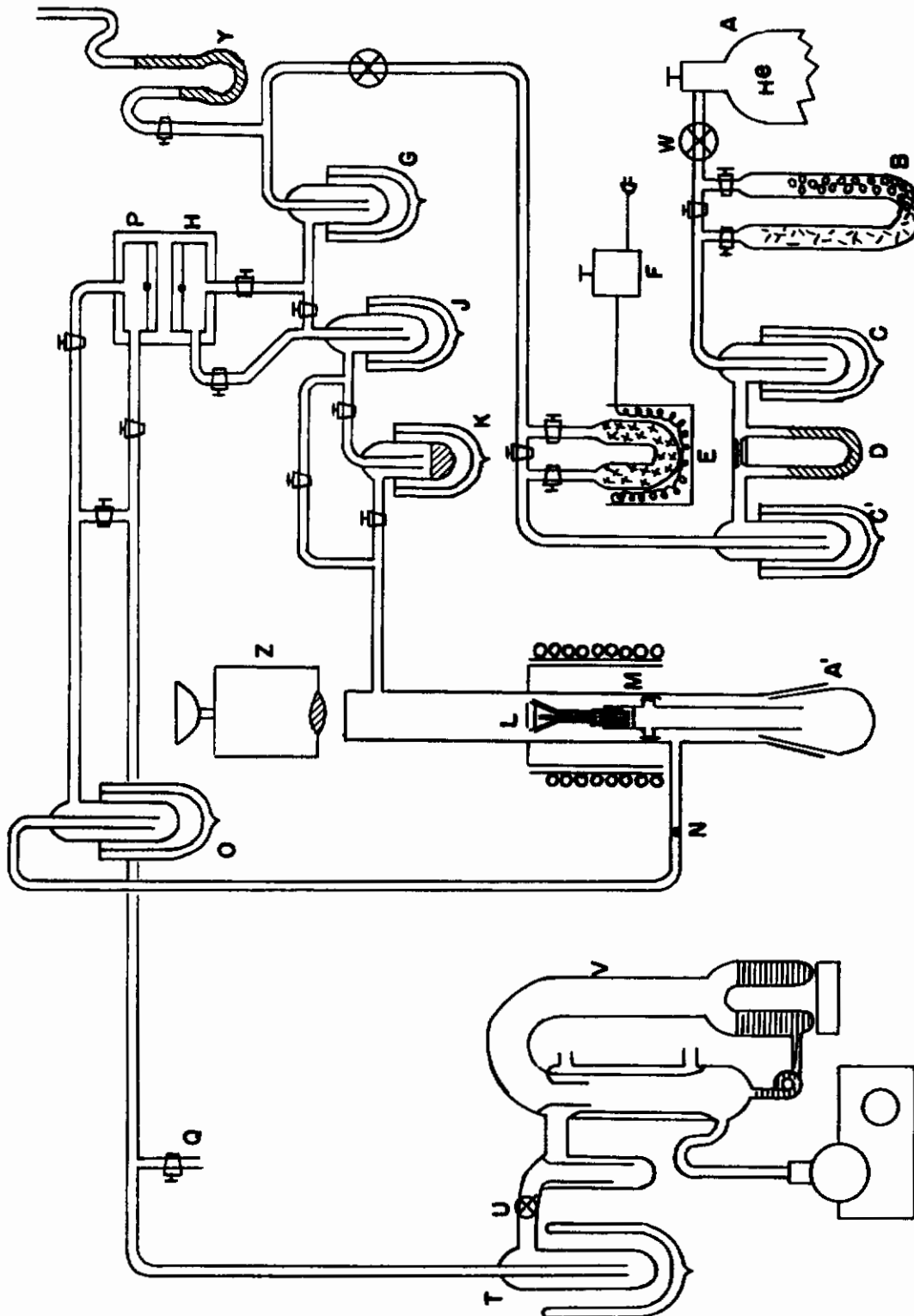
FIGURE I-1   DIAGRAM OF APPARATUS

3

flows across a coarse glass frit N, that removes particulate matter, through a dry-ice acetone trap, O, and enters the sampling side of the thermal conductivity cell, P. The stream is ultimately vented to the atmosphere at Q.

The two sides of the thermal conductivity cell, P and H, form two arms of a Wheatstone bridge whose output is fed into a recorder.[6] The recorder signal is, of course, proportional to the difference in oxygen concentration in the two sides of the cell, or to the rate of oxygen consumption by the heated sample.

(b) Calibration

(1) Optical Pyrometer and Flow Meter

An optical flat is blown onto the system at R, and temperatures are measured by sighting an optical pyrometer on an image of the sample pellet in a plane mirror. The pyrometer is calibrated against a General Electric standardized tungsten filament lamp, viewed through the same optical flat as the heated samples. Observed temperatures are corrected for sample emissivities, on the basis of literature data, if possible. In cases where emissivities are unknown, they can be measured by comparing observed temperatures of the surface of oxidized and unoxidized sample pellets with those of a blackbody cavity drilled ultrasonically in the specimen. It is important to recognize that the emissivity correction is large; it amounts to 85°C, for example, for an observed temperature of 1600°C on a sample with an emissivity of 0.6.[7] Surface temperatures on the inductively heated specimens are uniform to $\pm$ 5°C.

The flow meter can be calibrated in situ over the range 0 to 100 cc/min by water displacement from a Mariotte flask.[8]

(2) Thermal Conductivity Apparatus

To establish the relationship between recorder deflection and oxygen concentration differences in the two sides of the thermal conductivity cell, measured slugs of oxygen can be introduced into the helium stream by means of a manometric device[9] blown onto the main flow system at Z (Figure 1). A typical recorder tracing for a single calibration point is shown in Figure 2. The first peak occurs as the oxygen slug passes through

4
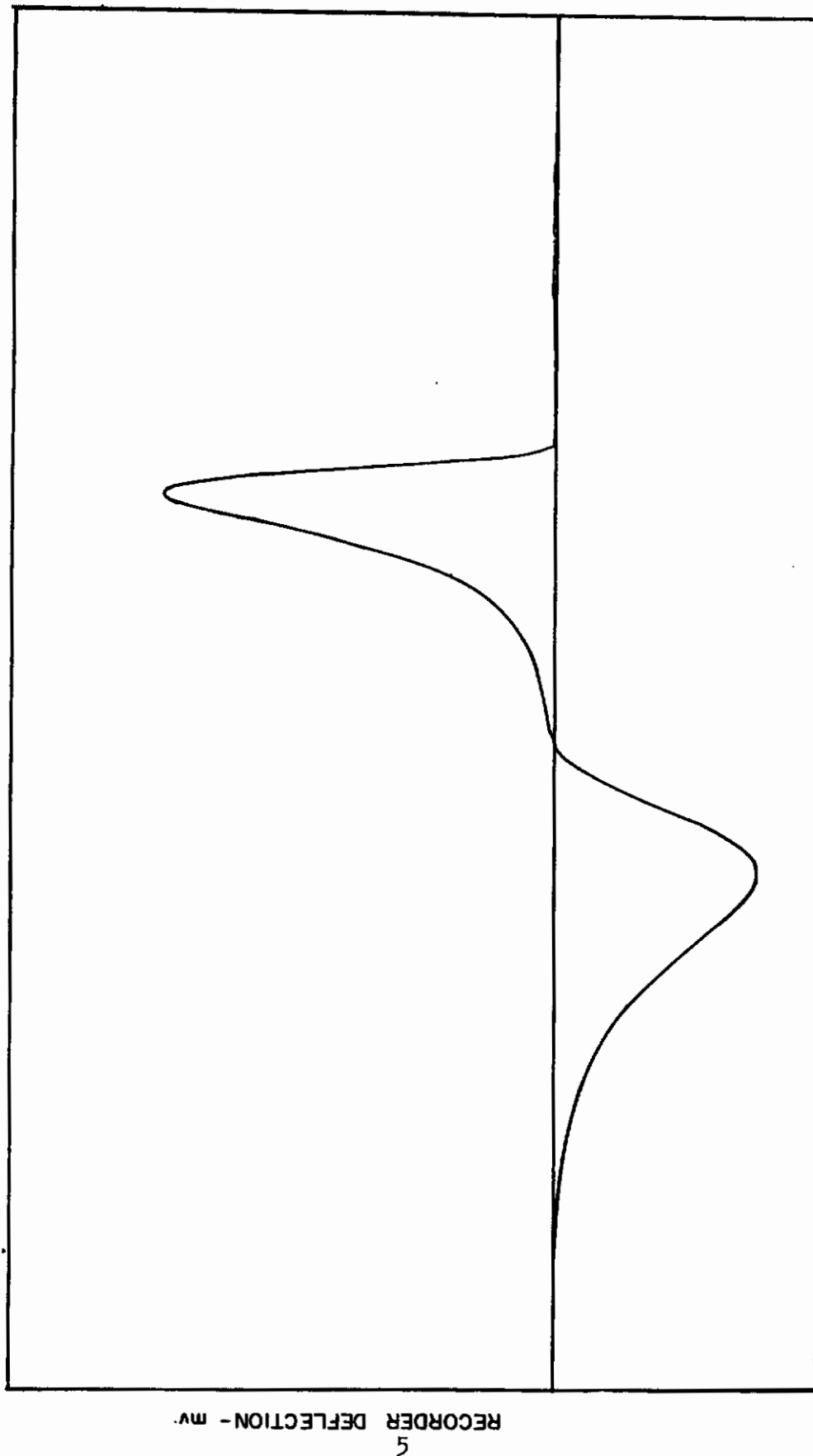
FIGURE I-2   RECORDER TRACING FOR A SINGLE CALIBRATION POINT

5

the reference side of the thermal conductivity cell, while the sampling side
is filled with pure helium. The first peak declines and a reverse peak is
observed when the reference side is once more filled with pure helium, and
the oxygen slug passes through the sampling side. The area under either peak
is proportional to the total weight of oxygen that was introduced. From the
area calibration factor in g/mm^2 and the measured recorder speed in mm/min,
peak heights can be related to rates of change of oxygen concentration in the
sampling cell in g/min for constant oxygen concentration in the reference
cell.

A calibration curve for a Burrell 340-148[10] thermal conduc-
tivity cell operated from a 6 volt storage battery with a current of 300 ma
and a helium flow rate of 95 ml/min is given in Figure 3. The curve is seen
to be linear, and to pass through the origin as expected. Separate calibrations
are required for each flow rate and current setting. For the conditions
described here, a signal of one millivolt (full scale, 256 mm) corresponds to
an oxidation rate of about 1.3×10^{-4} g/min. A calibration is reproducible to
$\pm 3.5\%$. The sensitivity is approximately proportional to the square of the
current, and to the reciprocal of the flow rate. Gow-Mac[11] hot wire and
thermistor cells have also been used successfully in work in this laboratory.

The calibration given in Figure 3 was checked by using heated
$CuO(s)$ in equilibrium with $Cu_2O(s)$ as a source of oxygen. The free energy of
decomposition of CuO to Cu_2O and oxygen is known to ± 0.5 kcal in the range
$298°-1300°K,$[12] so that the equilibrium pressure of oxygen at a given tempera-
ture is readily calculated. Up to 1300°K, the further decomposition of Cu_2O
to Cu is comparatively insignificant. In order to determine whether equilibrium
conditions prevail in the CuO tube the helium-oxygen stream was passed from
the thermal conductivity apparatus into a Minoxo unit[13] which measures small
partial pressures of oxygen electrolytically.[14] Experimental oxygen pressures
were in agreement with calculated pressures to $\pm 5\%$.

6
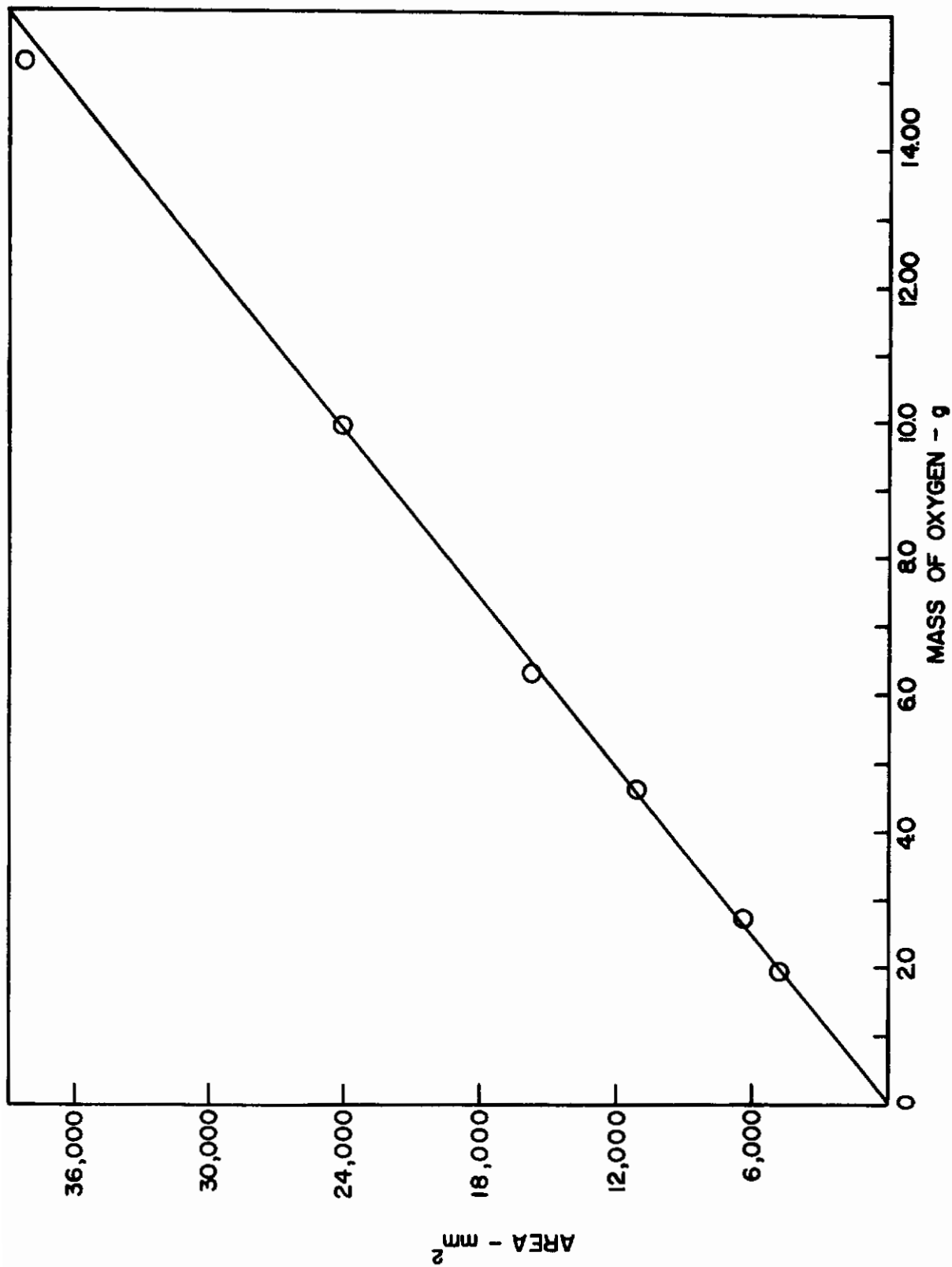
FIGURE I-3   CALIBRATION CURVE FOR A BURRELL 340-148 THERMAL
CONDUCTIVITY CELL

(c) Procedure

Samples are weighed, measured with a micrometer and placed on the refractory fingers. The mounted pellet is positioned for maximum temperature uniformity, so that its upper surface is slightly higher than the top of the concentrator, and so that it rests eccentrically in a quartz tube, close to the concentrator slit. The ground glass joint A' is replaced, and the system evacuated with the mercury diffusion pump, V. When the leak rate in the system is less than 5μ/hour, a flow of pure helium is started. The r.f. power supply is turned on, and the sample pellet is heated, in order to degas it, at a temperature slightly higher than that planned for the oxidation run. The degassing procedure is monitored with the thermal conductivity bridge, and a negative peak generally appears shortly after degassing begins, corresponding to pure helium in the reference cell and released permanent gases in the sampling cell. When degassing has stopped, the signal from the thermal conductivity apparatus drops to zero, and the power supply is turned off to cool the pellet.

The sample is reweighed and remeasured after the degassing procedure, and the apparatus is once again pumped out. The helium flow is started and the stream is diverted through the heated CuO. As the stream containing the helium-oxygen mixture goes through the reference side of the thermal conductivity cell, a peak is seen with a broad plateau, whose height is characteristic of the pressure of oxygen in equilibrium with CuO at the temperature of the copper oxide tube. The peak height serves as a daily check on calibration. When both sides of the thermal conductivity cell become filled with the same helium-oxygen mixture, the signal from the bridge drops to zero, and the oxidation run is started. The sample is heated rapidly by induction to a predetermined temperature, and an unbalance is observed in the thermal conductivity bridge indicative of the rate of oxygen pick-up by the sample. When reaction has proceeded for a definite length of time, the sample is cooled rapidly at room temperature, weighed, measured, and X-rayed. The highest temperature oxidation runs in this laboratory have been made with HfC at 2100°C.

3. ANALYSIS OF THE FLOW SYSTEM

In this section it will be demonstrated semi-empirically that the measured rate of change of oxygen concentration at the detector should indeed be equal to the rate of oxygen pick-up by the sample pellet, to an accuracy of better than 1%, after about 5 minutes, in spite of the spatial separation between reaction and detection sites.

If an oxygen slug spreads mainly by diffusion, and is essentially unaffected by the flow, then the calibration curves of Figure 2 can be fitted approximately by an equation of the form:

$$c = \frac{c_o \, v_o \, \exp(-x^2/Dt)}{\sqrt{4\pi \, Dt}} \qquad\qquad (I-1)$$

and an effective diffusion coefficient D can be calculated from experiment. In equation (1), c_o is the known total mass of oxygen introduced into the system, v_o is the average linear velocity of the gas stream, $x = x' - v_o t$ is a moving distance coordinate, where $x = 0$ ($x' = v_o t$) is the point of maximum oxygen concentration. If the time at which the highest oxygen concentration passes through the first cell is t_1, and through the second cell is t_2, then the effective diffusion coefficient can be calculated from:

$$D(t_2 - t_1) = \frac{c_o^2 \, v_o^2}{4\pi} \left(c_2^{\frac{1}{2}} - c_1^{\frac{1}{2}}\right) \qquad\qquad (I-2)$$

where c_2 and c_1 are the measured amplitudes in g/sec. at t_2 and t_1 respectively. In the experiments reported here, the volume flow rate was maintained at 95 ml/min. in a system constructed primarily of 8 mm tubing; therefore, the average linear velocity v_o is about 3.2 cm/sec. The diffusion coefficient calculated from equation (2), with a number of pulses of varying concentration is 61 ± 3 cm^2/sec.

This diffusion coefficient may be used to compute n', the rate of arrival of oxygen gas at the detector cell, for a given rate of oxygen consumption A (t by the sample pellet. If n_o is the concentration of oxygen in the helium stream prior to reaction with the refractory button, then the signal picked up

9

by the recorder is proportional to $(n_o - n')$. The unreacted oxygen may be looked upon as a continuous series of sharp pulses emitted from the sample region into the flowing stream. A sharp pulse of amplitude $n_1(t_1) = n_o - A(t_1)$ that leaves the vicinity of the pellet at time t_1 will spread out by diffusion, so that its concentration at a later time t at a distance x downstream from the source will be given by:

$$n = \frac{n_1(t_1)}{\sqrt{4\pi\, D(t-t_1)}} \; e^{-(x - v_o t + v_o t_1)^2/4D(t - t_1)} \qquad (I\text{-}3)$$

Since the pulses diffuse into one another, the rate of arrival of oxygen at the detector cell at any time t is the sum of contributions from all pulses that left the pellet region between time zero, when the experiment started and time t,; i.e.

$$n' = \int_{t_1 = 0}^{t} \frac{n_1(t_1)\, e^{-(\ell - v_o t + v_o t_1)^2/4D(t - t_1)}}{\sqrt{4\pi D(t - t_1)}} dt_1 \qquad (I\text{-}4)$$

where ℓ is the distance between pellet and detector. Since the integration in (4) is generally difficult, it is convenient to substitute a square wave for the exponential factor:

$$\frac{e^{-(\ell - v_o t + v_o t_1)^2/4D(t - t_1)}}{\sqrt{4\pi D(t - t_1)}} \approx 0 \text{ for } 0 \le (t - t_1) \le \frac{\ell-\delta}{v_o}$$

$$\approx \frac{v_o}{2\delta} \text{ for } \frac{\ell-\delta}{v_o} \le (t - t_1) \le \frac{\ell+\delta}{v_o} \qquad (I\text{-}5)$$

$$\approx 0 \text{ for } (t - t_1) > \frac{\ell+\delta}{v_o}$$

where $\delta = \sqrt{(4D\ell)/v_o}$. Substituting (5) in (4), the observed signal should be equal to:

10

$$n_o - n' \approx \frac{v_o}{2\delta} \int_{t - (\frac{\ell+\delta}{v_o})}^{t - (\frac{\ell-\delta}{v_o})} A(t_1)dt_1 = \frac{v_o}{2\delta} \int_{-\frac{\delta}{v_o}}^{\frac{\delta}{v_o}} A(t - \frac{\ell}{v_o} - y)dy \quad (I\text{-}6)$$

If $A(t - \frac{\ell}{v_o} - y)$ can be expressed by a Taylor's series expansion in y, then:

$$n_o - n' \approx A(t - \frac{\ell}{v_o}) + \sum_{m=1}^{\infty} \frac{A^{(2m)} (t - \frac{\ell}{v_o})}{(2m + 1)!} (\frac{\delta}{v_o})^{2m} \quad (I\text{-}7)$$

where $A^{(2m)}(t - \ell/v_o)$ denotes the $2m^{th}$ derative of $A (t - \ell/v_o)$ with respect to $(t - \ell/v_o)$. Thus, if the summation in (7) is small, the signal at the detector will be directly proportional to the rate of oxidation of the sample pellet, but will be retarded by the time ℓ/v_o that it takes a slug of gas to travel from pellet to detector.

If the sample oxidizes according to a simple rate law, (7) can be used to estimate the magnitude of the experimental error in the detector signal. For example, if $A(t)$ = constant, (linear oxidation), all of the derivatives in (7) vanish and the correct oxidation rate should be observed. If the sample oxidizes parabolically, $A(t) = k_p/t^{\frac{1}{2}}$, where k_p is the parabolic rate constant, then (7) becomes:

$$n_o - n' \approx k_p/(t - \frac{\ell}{v_o})^{\frac{1}{2}} + \sum_{m=1}^{\infty} \frac{(4m-1)(4m-3)\ldots(1)k_p}{2^{2m}(2m+1)!(t - \frac{\ell}{v_o})^{4m+1/2}} (\frac{\delta}{v_o})^{2m} \quad (I\text{-}8)$$

The error will be less than 1% of the signal at times $(t - \frac{\ell}{v_o})$ that satisfy the relation:

$$\sum_{m-1}^{\infty} \frac{(4m-1)(4m-3)\ldots(1)k_p}{2^{2m}(2m+1)!(t - \frac{\ell}{v_o})^{(4m+1)/2}} (\frac{\delta}{v_o})^{2m} < 0.01 \, k_p/(t - \frac{\ell}{v_o})^{\frac{1}{2}} \quad (I\text{-}9)$$

11

or

$$\sum_{m=1}^{\infty} \frac{(4m-1)(4m-3)\ldots(1)}{2^{2m} (2m+1)! (t - \frac{\ell}{v_o})^{2m}} (\frac{\delta}{v_o})^{2m} < 0.01 \qquad \text{(I-10)}$$

Since the coefficients in (10) are all less than or equal to 1/8:

$$\sum_{m=1}^{\infty} \frac{(4m-1)(4m-3)\ldots(1)}{2^{2m} (2m+1)! (t - \frac{\ell}{v_o})^{2m}} (\frac{\delta}{v_o})^{2m} < \sum_{m=1}^{\infty} 1/8 (\frac{\delta}{v_o})^{2m}/(t - \frac{\ell}{v_o})^{2m} < 0.01$$

$$\text{(I-11)}$$

The inequality in (11) will be valid at times $(t - \frac{\ell}{v_o})$ for which:

$$\left[1/8 (\frac{\delta}{v_o})^2/(t - \frac{\ell}{v_o})^2 \right] \left[\frac{1}{1 - (\frac{\delta}{v_o})^2/(t - \frac{\ell}{v_o})^2} \right] < 0.01 \qquad \text{(I-12)}$$

Thus, the signal should give oxidation rate with an accuracy of better than 1% when $(t - \ell/v_o) > 4(\delta/v_o)$. For the experimental apparatus described in this paper $4(\delta/v_o)$ is less than 3 minutes. Similar results are obtained if the rate equation is logarithmic. Thus, if the data of the first 5 minutes are disregarded, the observed oxidation rates are equal to the true rates, and are essentially unaffected by the physical separation between reaction zone and detector.

4. OXIDATION OF COPPER

The lack of precise oxidation measurements on simply behaved, well-characterized systems above 1000°C makes a detailed quantitative comparison of our results with those of other workers difficult. Copper was selected as the most satisfactory standard material.

The oxidation of copper between 900° and 1000°C at oxygen partial pressures of 5-95 mm Hg was studied by Baur, Bridges, and Fassell,[15] who used a spring system to follow the reaction. Their determination agreed

12

satisfactorily with previous studies.[16,17] In our experiments, rates of oxygen pick-up are measured directly, and hence the integral under the thermal conductivity curve from time zero up to time t is proportional to the total oxygen consumed up to that point. The results of thermal conductivity measurements of the kinetics of oxidation of pure copper between 977°C and 1044°C at oxygen partial pressures between 1.7 and 10 mm, are plotted in Figure 4 as total oxygen consumption vs time. Included in the same figure are weight change data of Baur, Bridges, and Fassel (BBF), Grünewald and Wagner (GW), and Feitknecht (F), who worked in the same temperature and pressure range. For the oxidation of copper, rate of change in weight is precisely equivalent to rate of oxygen consumption, since neither CuO nor Cu_2O is volatile at the temperatures of interest. Our results at 1044°C and an oxygen partial pressure of 10 mm are in good agreement with those of (F) at 1020°C and 7.6 mm. Our results at 990°C and 10 mm are very close to the (BBF) results at 1000°C and 10 mm. Our results at 977°C and 3.0 mm are similar to the findings of (GW) at a higher temperature 1000°C and lower pressure, 0.23 mm, and both lie above our results at 990°C and 1.7 mm. If errors in weighing, in the determination of the zero of time, and in the measurement of temperature and pressure are taken into account, as well as the average precision of results from a given laboratory of $\pm$ 10%, agreement in the experimental data from the four groups can be considered very good. The data suggest that the rate of oxidation of copper increases with both increasing temperature and increasing pressure.

According to Jost, "If copper is oxidized at oxygen pressures below the equilibrium pressure for the formation of CuO a uniform film of Cu_2O is formed, its rate of growth obeying the quadratic law except for the very early stages of reaction." The equilibrium oxygen pressure for dissociation of CuO is 10.86 mm at 900°C, 34.2 mm at 950°C, and 92 mm at 1000°C. Therefore, all of the experiments listed in Figure 4 were performed under conditions where Cu_2O should be the sole oxidation product. If the rate of growth of Cu_2O obeys the quadratic law,[18] then:
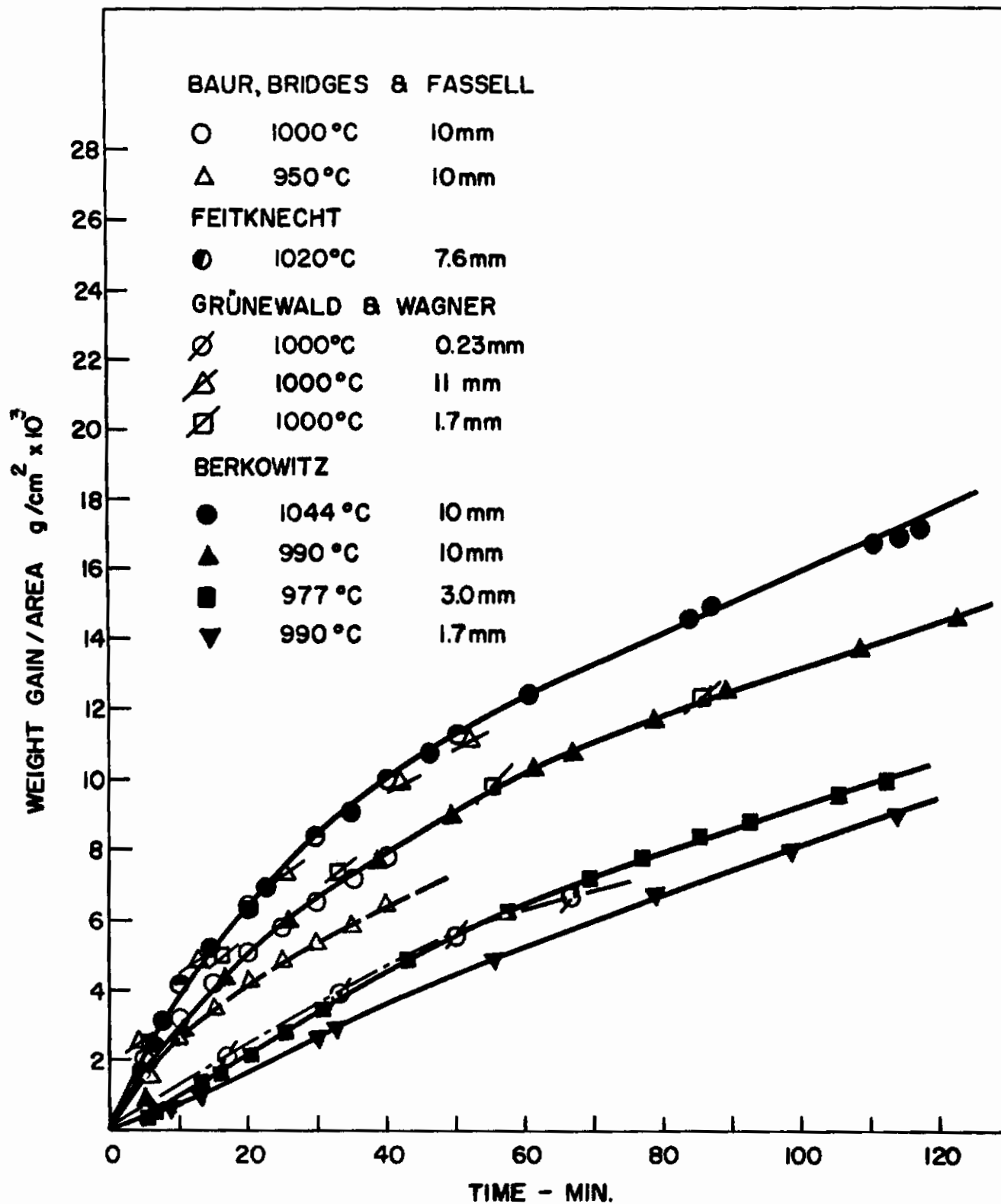
FIGURE I-4   TOTAL OXYGEN CONSUMPTION versus TIME
                FOR Cu

14

$$\frac{d(\frac{\Delta m}{A})}{dt} = k_p/2(\frac{\Delta m}{A}) \tag{I-13}$$

where Δm is measured weight change, A is specimen surface area, t is time, and k_p is a temperature dependent proportionality constant (parabolic rate constant). In general, equation (13) should hold if the rate determining step in the oxidation of copper is diffusion of copper or oxygen through a $Cu_2O(s)$ layer, and if Fick's first law describes the diffusion process.[19] It is clear that at time zero, when the metal is devoid of an oxide layer, solid-phase diffusion cannot be the rate controlling step. Therefore, equation (13) is not expected to apply in the earliest stages of oxidation. However, it might be applicable after a time t_o when the oxide layer has built up to a thickness ξ_o, corresponding to a weight gain per unit area $(\frac{\Delta m}{A})_o$. Integrating (13) between limits $(t_o, (\frac{\Delta m}{A})_o)$ and $(t, \frac{\Delta m}{A})$, one finds:

$$(\frac{\Delta m}{A})^2 = k_p t + \left[(\frac{\Delta m}{A})_o^2 - k_p t_o \right] \tag{I-14}$$

It must be remembered that equation (14) holds only for times $t > t_o$; the fitting of data from time zero to an equation of the form $(\frac{\Delta m}{A})^2 = k_p t + B$, where B is an empirically determined constant,[18] is not justified on the basis of the quadratic rate equation. However, if the quadratic rate law is obeyed once a suitable thickness of oxide has been built up on the surface of the metal, then a plot of $(\frac{\Delta m}{A})^2$ vs t should be a straight line provided $(\frac{\Delta m}{A})^2 > (\frac{\Delta m}{A})_o^2$ and $t > t_o$, but nothing can be said about the form of the $(\frac{\Delta m}{A})^2$ vs t plot up to time t_o. The data in Figure 4 are replotted as $(\frac{\Delta m}{A})^2$ vs t in Figure 5, and it seems that they fit well to straight lines after times that vary between 10 and 60 minutes, depending upon the temperature and pressure. Table 1 lists approximate values of t_o, $(\frac{\Delta m}{A})_o$, ξ_o, and k_p computed by least squaring the data in Figure 5 for the last 15 minutes of each run, and adding points up to the time that the computed slope differs from the final slope by 1%. The last point added was taken as $(t_o, (\frac{\Delta m}{A})_o)$, and k_p was taken as the average of the computed slopes back to that point. It is seen that a layer of $Cu_2O(s)$, 50,000-100,000 Å thick, must be built up during the oxidation

15
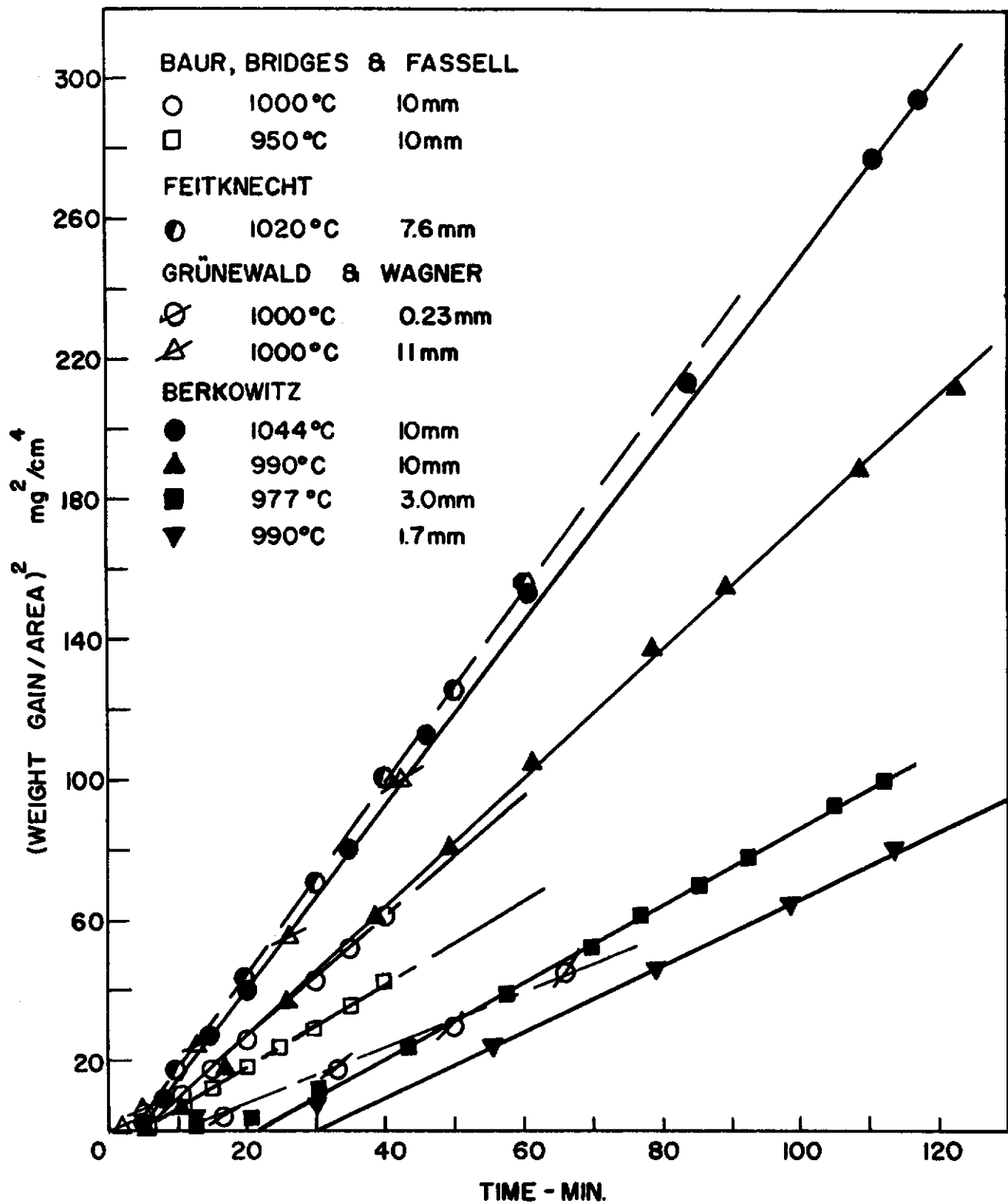
FIGURE I-5   PARABOLIC PLOT FOR THE OXIDATION OF Cu,

$$\left(\frac{\Delta M}{A}\right)^2 \quad \text{versus} \quad t$$

16

TABLE 1

THICKNESS OF OXIDE THAT MUST FORM ON Cu
BEFORE PARABOLIC RATE LAW IS FOLLOWED

Reference	T, °C	P_{O_2}, mm	t_o, min	$\left(\frac{\Delta m}{A}\right)_o$, mg/cm²	ξ_o, Å	k_p, mg²/cm⁴-sec
(F)	1020	7.6	20.0	6.6	110,000	169.7
This work	1044	10	7.9	3.08	51,000	156.0
(GW)	1000	11	26.0	7.5	125,000	159.4
(GW)	1000	1.71	16.67	5.0	83,400	114.8
This work	990	10	10.6	2.85	47,500	110.4
(BBF)	1000	10	25.0	5.84	97,400	106.7
(BBF)	950	10	30.0	5.41	90,300	76.2
This work	977	1.5	30.4	3.42	57,000	66.0
This work	990	0.87	92.3	7.66	128,000	64.0
(GW)	1000	0.23	41.6	4.875	81,200	53.6

17

of copper before the true parabolic rate law (13) is followed.

Wagner[20] derived the rate equation (13) and expressed the parabolic rate constant k_p in terms of the specific conductivity of the oxide film, the transport number of cations, anions, and electrons, and the free energy of the net oxidation reaction. However, in comparing k_p for the oxidation of copper, as measured in a direct oxidation experiment, with k_p computed from the above independently measured quantities, Wagner did not use the integrated equation (14), or the rate constants listed in Table 1. Instead, Wagner and Grünewald fitted their data to an equation of the form:

$$\frac{1}{k_p}\left(\frac{\Delta m}{A}\right)^2 + \frac{1}{K}\left(\frac{\Delta m}{A}\right) = t \qquad \text{(I-15)}$$

corresponding to a differential equation:

$$\frac{d\left(\frac{\Delta m}{A}\right)}{dt} = \frac{1}{\frac{1}{K} + \frac{2}{k_p}\left(\frac{\Delta m}{A}\right)} \qquad \text{(I-16)}$$

which has never been put on a firm theoretical foundation.[18,19] The rationale behind (16) is that diffusion is not the sole rate controlling process, but that a phase boundary reaction at the Cu/Cu_2O interface also influences the over-all reaction rate. Grünewald and Wagner[16] plotted $t/\left(\frac{\Delta m}{A}\right)$ vs $\frac{\Delta m}{A}$, which, if equation (15) is valid, should yield a straight line. The curves are not straight lines for the data obtained at 1000°C and pressures of 0.23 and 1.71 mm,[21,16] but become linear after a weight of oxide of 2.5-5 mg/cm^2 has been built up. Approximately linear behavior is observed, however, for the 1000°C data at 11 mm and 63 mm. It is the reciprocals of the slopes of the linear portions of the $t/\left(\frac{\Delta m}{A}\right)$ vs $\left(\frac{\Delta m}{A}\right)$ curves that (GW) associate with the theoretically derived k_p. The available experimental data has been plotted in this form, and results are listed in column 4 of Table 2. In column 5, the parabolic rate constants derived from equation (14) are listed. In Figure 6, it is seen that plots of $\left(\frac{\Delta m}{A}\right)$ vs $\sqrt{t}$ are also linear to a good approximation, after an initial period, and in Table 2, column 6, the squares

TABLE 2

VALUES OF THE PARABOLIC RATE CONSTANT, k_p (mg^2/cm^4-hr)

Reference	T, °C	P_{O_2}, mm	$\frac{1}{k_p}\left(\frac{\Delta m}{A}\right) + \frac{1}{k} = t/\left(\frac{\Delta m}{A}\right)$	$\left(\frac{\Delta m}{A}\right)^2 = k_p t + \text{Const.}$	$\frac{\Delta m}{A} = \sqrt{k_p t} + \text{Const.}$	Calculated
(F)	1020	7.6	–	169.7 ± 17.0	196.8	132.4
This work	1044	10	158.9	156.0 ± 15.6	161.6	144.8
(GW)	1000	11	178.0	159.4 ± 15.9	179.4	134.0
(GW)	1000	1.71	122.8	114.8 ± 11.5	127.8	93.6
This work	990	10	123.0	110.4 ± 11.0	122.4	127.0
(BBF)	1000	10	142.8	106.7 ± 10.7	127.8	130.8
(BBF)	950	10	81.5	76.2 ± 7.6	83.4	102.3
This work	977	1.5	104.9	66.0 ± 6.6	99.6	84.3
This work	990	0.87	131.8	64.0 ± 6.4	92.4	80.0
(GW)	1000	0.23	79.1	53.6 ± 5.4	72.6	62.9

19
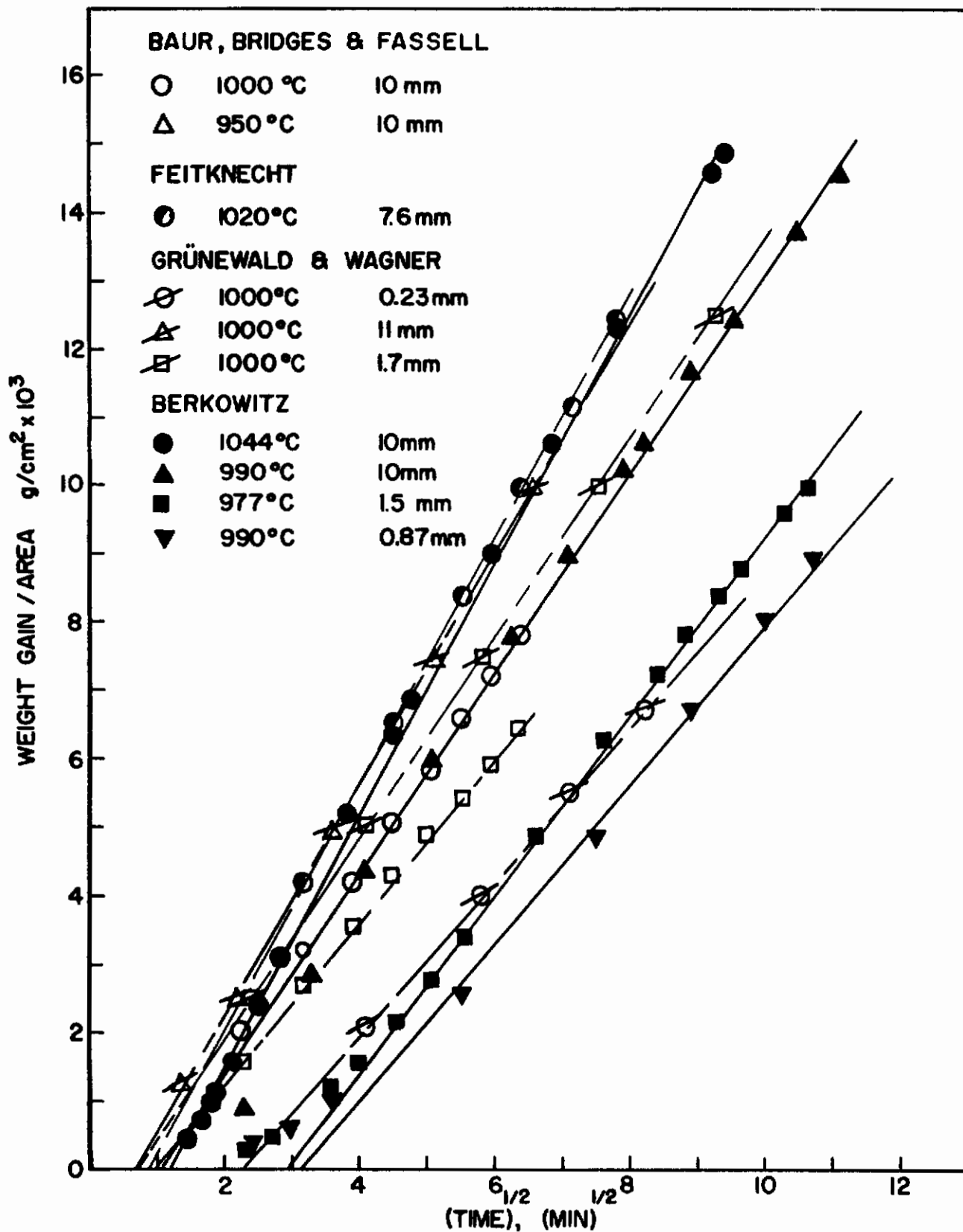
FIGURE I-6   PLOT OF $\left(\frac{\Delta M}{A}\right)$ versus $\sqrt{t}$ FOR OXIDATION OF Cu

20

of the slopes of these lines are listed. In column 7, parabolic rate constants calculated from the theoretical equation:[21]

$$k_p = 2\Omega(\frac{kT}{e^2})\ \sigma_o\ t_i\ [p^{1/8}\ (O_2/X) - p^{1/8}\ (O_2/O)]\qquad\text{(I-17)}$$

In (17), Ω is the volume of Cu_2O per copper ion, σ_o is the electrical conductivity of Cu_2O at an oxygen pressure of one atmosphere, t_i is the transport number of cations in Cu_2O at the experimental temperature, $p(O_2/X)$ is the ambient oxygen pressure, $p(O_2/O)$ is the oxygen pressure calculated from the equilibrium $2Cu + 1/2O_2 \rightleftharpoons Cu_2O$ at the absolute temperature T, k is the gas constant, and e is the charge on the electron. If m-k-s units are used for all quantities, and p is in atmospheres, then k_p is given in m^2/sec of Cu_2O. Calculated values of k_p converted to mg^2/cm^4-sec of oxygen are listed in column 7 of Table 2. The conductivity values were taken from Dünwald and Wagner,[22]; other values in the literature are as much as a factor of two higher.[23] However, the spread among single crystal samples found by O'Keefe and Moore is also of the order of a factor of two. Dünwald and Wagner[22] measured the transference number of Cu^+ in Cu_2O at 1000°C and obtained values between 4 and 5 x 10^{-4}. The lower value was used for the calculation reported here. Thus, the theoretical values in column 7 can be considered minimum values; true values might be as much as 100% higher. If errors in the experimental oxidation rates are taken into account, as well as errors in the conductivity data needed to compute rates from equation (17), agreement between calculated and experimental rates is fair. It must be emphasized that the parabolic rate law is described by the differential equation (13), and only by that equation, or by equations derived directly from it. In the derivation of equation (17), it is assumed that phase boundary reactions have proceeded to equilibrium, and it is shown that equation (13) is followed. Therefore, it is columns 5 and 7 of Table 2 that must be compared to test the validity of the theoretical model, in spite of the fact that the agreement might be slightly better if experimental results were taken from column 4 or 6.

21

Equation (17) predicts that at constant temperature, k_p should be a linear function of $p^{1/8}(O_2/X)$, with $k_p = 0$ when $p^{1/8}(O_2/X) = p^{1/8}(O_2/0)$. The original (GW) k_p data, listed in column 4 showed a perfect linear dependence on $p^{1/7}(O_2/X)$ with intercept at $p^{1/7}(O_2/0)$. This was considered, at the time, adequate agreement with the theoretical prediction. However, (BBF) failed to confirm the 1/7 power dependence, as seen in Figure 7, where both sets of data are plotted. In point of fact, probable experimental errors of $\pm 10\%$ effectively mask differences in pressure dependence between $p^{1/4}(O_2/X)$ and $p^{1/8}(O_2/X)$ at the present time.

5. CONCLUSIONS

The thermal conductivity detector provides a convenient method for monitoring oxidation reactions in a constant pressure flow system. It is particularly well suited for continuous measurement of rates of oxygen consumption by inductively heated samples, since the reaction zone can be maintained at temperatures between 1000° and 2100°C, while the remainder of the apparatus is kept at low temperatures.

In cases where both volatile and non-volatile products form during oxidation, a single measurement of weight change or oxygen consumption does not suffice to define the reaction completely. For such systems, microbalance and thermal conductivity techniques should provide supplementary data.

22
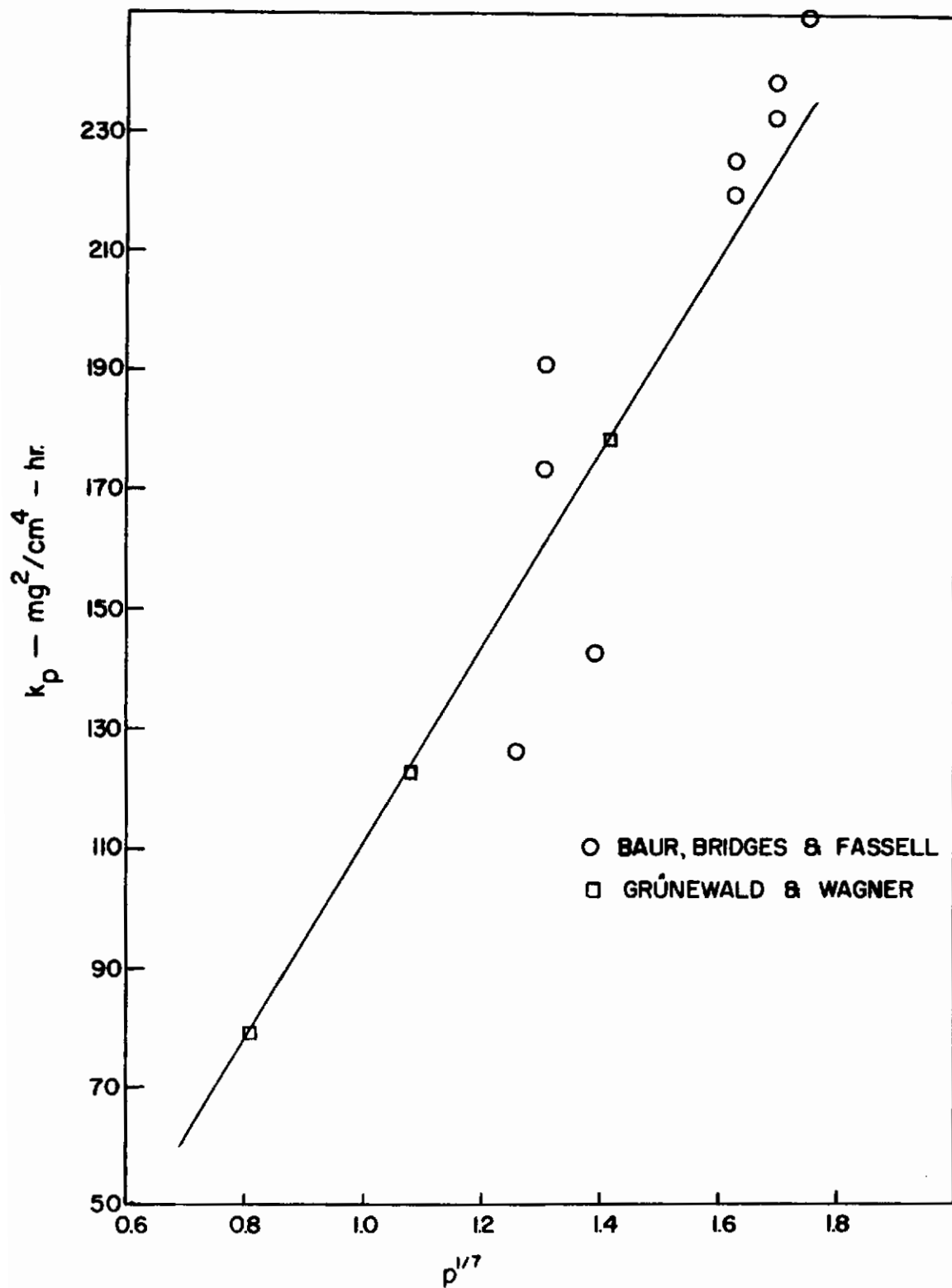
FIGURE I-7   PRESSURE DEPENDENCE OF RATES OF
OXIDATION OF Cu

23

SECTION I - REFERENCES

(1) C. Wagner, Z. Phys. Chem. (B) 21, 25 (1933).

(2) E. A. Gulbransen, Trans. Electrochem. Soc. 81, 327 (1942).

(3) N. F. Mott, Trans. Faraday Soc. 43, 429 (1947).

(4) E. R. Weaver in W. G. Berl, "Physical Methods in Chemical Analysis," Vol. II, p. 387, Academic Press, N. Y. (1951).

(5) F. M. Nelsen and F. T. Eggertsen, Anal. Chem. 30, 1387 (1958).

(6) H. P. Burchfield and E. E. Storrs, "Biochemical Applications of Gas Chromatography," Academic Press, N. Y. (1962), p. 53.

(7) Am. Institute of Physics Handbook, Table 6g-8, p. 6-75, McGraw-Hill, N. Y. (1957).

(8) G. W. Smith, Ind. Eng. Chem., Anal. Ed. 4, 244 (1932).

(9) C. Littman and J. B. Berkowitz-Mattuck, Rev. Sci. Inst. 32, 1154 (1961).

(10) Burrell Corporation, Pittsburgh, Pa.

(11) Gow-Mac, 100 Kings Road, Madison, New Jersey.

(12) O. Kubaschewski and E. Ll. Evans, "Metallurgical Thermochemistry," Pergamon Press, N. Y. (1958).

(13) Baker Company, New Jersey.

(14) P. Hersch, Dechema Monographien, 27, 299 (1956).

(15) J. P. Baur, D. W. Bridges, and W. M. Fassell, Jr., J. Electrochem. Soc. 103, 273 (1956).

(16) C. Wagner and K. Grünewald, Z. Phys. Chem. (B) 40, 455 (1938).

(17) W. Feitknecht, Z. Electrochem. 35, 152 (1929).

(18) O. Kubaschewski and B. E. Hopkins, "Oxidation of Metals and Alloys," Academic Press, N. Y. (1962).

(19) C. Wagner, "Kinetics in Metallurgy," M.I.T. Course 3.63 (M.I.T., Spring (1955)).

(20) C. Wagner, Z. Phys. Chem. (B) 32, 447 (1936).

(21) T. B. Grimley, Ch. 14 in W. E. Garner, "Chemistry of the Solid State," Academic Press, N. Y. (1956).

(22) H. Dünwald and C. Wagner, Z. Phys. Chem. (B) 22, 212 (1933).

(23) M. O'Keeffe and W. J. Moore, J. Chem. Phys. 35, 1324 (1961).

KINETICS OF OXIDATION OF REFRACTORY METALS AND ALLOYS
AT 1000°-2000°C

SECTION II - OXIDATION OF CARBIDES

1. INTRODUCTION

The high melting points of the carbides of groups IV-A, V-A, and VI-A of the periodic table make these materials potentially attractive for high temperature structural applications. The practical usefulness of the carbides, however, depends to a large extent upon their stability in oxygen-containing atmospheres. A valuable thermodynamic basis for selection of carbides with the greatest promise for good oxidation resistance was published by Webb, Norton, and Wagner in 1956. In the present report, the Webb, Norton, Wagner criteria are applied to a prediction of the behavior of the carbides of groups IV-A (TiC, ZrC, and HfC), V-A (VC, NbC, and TaC), and VI-A (Cr_3C_2, MoC, and WC) in oxygen atmospheres at temperatures between 1000° and 2000°K. The available experimental evidence is presented, and discussed in the light of the theoretical considerations.

2. THE THEORY OF WEBB, NORTON, and WAGNER (WNW)[1]

In general, a metal carbide will show good oxidation resistance only if a dense adherent oxide film forms on the carbide surface and acts to restrict oxygen access to the alloy. Since the oxides of carbon are permanent gases, it is clear that protection can only be afforded by the formation of an oxide of the metallic element. Webb, Norton, and Wagner, therefore, consider the system of a metal carbide MeC_x in contact with metal oxide MeO_y, in the presence of oxygen:
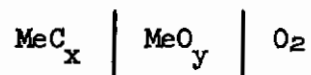
$$MeC_x \quad \Big| \quad MeO_y \quad \Big| \quad O_2$$

If the metallic oxide reacts with the carbide to form $CO(g)$ or $CO_2(g)$ at the MeC_x/MeO_y phase boundary, and if the resultant gas pressure is sufficiently high, then the oxide may be ruptured and thereby lose its effectiveness as a barrier to further oxidation of the alloy. At high temperatures, equilibrium might be expected to be attained rapidly at the alloy/oxide interface, and in

26

this case, the $CO(g)$ and $CO_2(g)$ pressures, p_{CO} and p_{CO_2}, can be computed from the standard free energies $\Delta F^\circ{}_{(1)}$ and $\Delta F^\circ{}_{(2)}$ of the reactions:

$$C\ (alloy) + \frac{1}{y}\ MeO_y(s) = CO(g)\ + \frac{1}{y}\ Me\ (alloy) \qquad (II\text{-}1)$$

$$C\ (alloy) + \frac{2}{y}\ MeO_y(s) = CO_2(g) + \frac{2}{y}\ Me\ (alloy) \qquad (II\text{-}2)$$
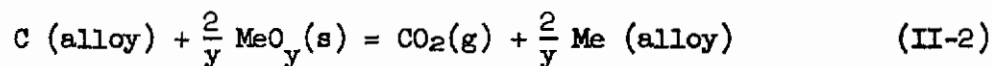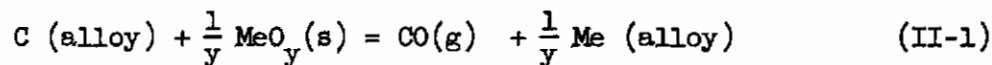
Thus,

$$\Delta F^\circ{}_{(1)} = -RT\ \ln \frac{p_{CO}\ a_{Me}{}^{1/y}}{a_C} \qquad (II\text{-}3)$$

$$\Delta F^\circ{}_{(2)} = -RT\ \ln \frac{p_{CO_2}\ a_{Me}{}^{2/y}}{a_C}$$

where a_{Me} and a_C are metal and carbon activities respectively at the alloy/ oxide interface.

The position of equilibrium will obviously depend upon the relative stabilities of the solid metallic oxide and the gaseous carbon oxides. If $CO(g)$ and $CO_2(g)$ are very much more stable than $MeO_y(s)$, so that the sum of the equilibrium pressures, $(p_{CO} + p_{CO_2})$, is higher than the ambient pressure, then the outburst of $CO(g)$ and $CO_2(g)$ is very likely to rupture the oxide film. If this happens, oxidation of the carbide is likely to proceed more rapidly than oxidation of the corresponding pure metal.

If the metallic oxide is very much more stable than the carbon oxides, then reactions (1) and (2) will not proceed to the right to any large extent. In this case, the carbide may be oxidized more or less rapidly than the corresponding metal depending upon the specific oxidation mechanism. If the metallic element in the alloy is oxidized preferentially, then the activity of carbon at the alloy/oxide interface may become higher than the activity of carbon in the bulk alloy. The resultant activity gradient may provide the driving force for diffusion of carbon backward into the bulk alloy, possibly with the formation of new carbide phases. The net oxidation rate should not be very different in this case from the oxidation rate of the pure metal, except for a small effect due to lowered metal activity, provided, of course, that the cohesion between oxide and substrate is equally good for metal and

27

carbide. If unreacted carbon remains at the oxide/alloy interface, then its activity may increase sufficiently with time to shift the equilibria in (1) and (2) towards the right. In fact, rupture of the oxide film might even occur after a time. The evolution of $CO(g)$ and $CO_2(g)$ might stop, however, as the carbon activity was lowered once again. If carbon is soluble in the oxide lattice, then carbon at the oxide/alloy interface might migrate across the oxide layer, and evolution of $CO(g)$ or $CO_2(g)$ could occur at the oxide/ oxygen interface without destruction of the protective oxide film adjacent to the alloy. The effect of carbon on the defect concentration in the oxide would determine whether the observed oxidation rate would be greater or less than that for the pure metal.

3. APPLICATION OF THE WNW TREATMENT TO THE HIGH TEMPERATURE OXIDATION OF CARBIDES OF GROUPS IV-A, V-A, and VI-A

Equations (1) and (2) are difficult to apply precisely due to the lack of experimental data for the activities of metal and carbon across the homogeneity range of the carbide phases. It is therefore assumed in the calculations that the carbide composition is that of the alloy in equilibrium with pure graphite. The carbon activity in the original alloy may therefore be taken as unity. The pressures of $CO(g)$ and $CO_2(g)$ calculated from equations (3) and (4) on this assumption are therefore maximum permanent gas pressures. If the actual carbon activity in the alloy is less than one, then it becomes more probable that the carbide will show a degree of oxidation resistance. The metal activity is given by the ratio p_{Me}/p°_{Me}, where p_{Me} is the vapor pressure of metal over the MeC-C two phase region, i.e. the equilibrium metal pressure calculated from the equation:

$$MeC(s) \rightarrow Me(g) + C(s) \tag{II-5}$$

and p°_{Me} is the vapor pressure of metal over pure metal at the same temperature:

$$Me(s) \rightarrow Me(g) \tag{II-6}$$

The standard free energies of reactions (5) and (6) are therefore given respectively by:

28

$$\Delta F^{\circ}{}_{(5)} = -RT \ln p_{Me} \tag{II-7}$$

$$\Delta F^{\circ}{}_{(6)} = -RT \ln p^{\circ}{}_{Me} \tag{II-8}$$

Therefore:

$$\Delta F^{\circ}{}_{(5)} - \Delta F^{\circ}{}_{(6)} = -\Delta F^{\circ}{}_{f,MeC} = -RT \ln a_{Me} \tag{II-9}$$

where $\Delta F^{\circ}{}_{f,MeC}$ is the integral free energy of formation of the metal carbide.

(a) Titanium Carbide, TiC

The free energy of formation of TiC, as given by Kubaschewski and Evans,[2] and the activity of titanium over the TiC-C two phase region calculated from equation (9), is tabulated as a function of temperature in columns 2 and 3 of Table 1. Columns 4, 5, and 6 give free energies of formation of $CO(g)$,[3] $CO_2(g)$[3] and $TiO_2(s)$,[4] while columns 7 and 8 give the equilibrium pressures of $CO(g)$ and $CO_2(g)$ calculated from equations (3) and (4) with $MeO_y(s) = TiO_2$ (rut.), and $a_C = 1$. It is clear that if a dense coherent rutile film forms on the surface of TiC, it will not be ruptured by evolution of $CO(g)$ and $CO_2(g)$ up to about 1500°K.

Quantitative experimental data is available only up to 1000°C (1273°K). However, there is general agreement[5,6,7] that the oxidation of TiC is parabolic, to a good approximation, above 700°C, and that the rate is controlled by diffusion of oxygen across a layer of TiO_2 of the rutile structure. It is extremely interesting that although the formation of $CO(g)$ or $CO_2(g)$ at the oxide/metal interface is thermodynamically unfavorable, carbon is consumed at the same rate as titanium.[1] It was suggested by Webb, Norton, and Wagner[1] that carbon from the alloy dissolves in the oxide at the TiC/TiO$_2$ interface, diffuses through the TiO$_2$, and is oxidized at the TiO$_2$/O$_2$ interface. Since $TiO_2(s)$ is an oxygen deficient semi-conductor,[8] and TiC and TiO are known to be mutually soluble, it was not unreasonable to postulate some carbon solubility in the TiO$_2$ lattice. By chemical analysis of the oxide film formed on TiC at 1000°C in pure oxygen at 760 Torr, Nikolaiski[5] showed the presence of about 0.16% C in the TiO$_2$ layer.

29

TABLE 1

ACTIVITY OF Ti OVER TiC-C AND THERMODYNAMIC DATA FOR TiC-TiO₂

$T, °K$	$\Delta F_{f,TiC}$	a_{Ti}	$\Delta F_{f,CO}$	$\Delta F_{f,CO_2}$	$\Delta F_{f,TiO_2}$	p_{CO}	p_{CO_2}
1000	-41,440	8.953×10^{-10}	-47,859	-94,628	-182,960	9.995×10^{-6}	1.343×10^{-6}
1100	-41,124	6.567×10^{-9}	-49,962	-94,658	-177,675	2.368×10^{-4}	5.064×10^{-9}
1200	-40,808	3.758×10^{-8}	-52,049	-94,681	-173,458	2.529×10^{-3}	1.234×10^{-7}
1300	-40,492	1.582×10^{-7}	-54,126	-94,701	-169,220	3.120×10^{-2}	1.928×10^{-6}
1400	-40,176	5.423×10^{-7}	-56,189	-94,716	-165,022	1.069×10^{-1}	2.000×10^{-5}
1500	-39,860	1.577×10^{-6}	-58,241	-94,728	-160,915	4.646×10^{-1}	1.471×10^{-4}
1600	-39,544	4.015×10^{-6}	-60,284	-94,739	-156,610	1.733	8.981×10^{-4}
1700	-39,228	9.177×10^{-6}	-62,315	-94,746	-152,422	5.424	4.273×10^{-3}
1800	-38,912	1.905×10^{-5}	-64,335	-94,750	-148,192	14.99	1.728×10^{-2}
1900	-38,596	3.670×10^{-5}	-66,349	-94,751	-144,025	36.92	5.933×10^{-2}
2000	-38,280	6.622×10^{-5}	-68,353	-94,752	-139,950	81.75	2.212×10^{-1}

30

However, a complete study of the diffusion of carbon through TiO$_2$ remains to be done. The most direct method to demonstrate the significance of carbon diffusion in the oxidation process would be to oxidize a sample of C^{14} enriched TiC. An autoradiograph of the oxidized surface would indicate whether diffusion of carbon occurs primarily by grain boundary or bulk diffusion, while a stripping and counting procedure could be developed for quantitative measurements.

Oxidation isotherms obtained in a number of laboratories are plotted in Figures 1 and 2, as weight gain per unit area squared vs time. Results obtained by three investigators in times less than seven hours are shown in Figure 1. The excellent agreement between Münster[6] and Nikolaiski[5] may be due in part to the fact that both sets of measurements were done in the same laboratory. Samsonov and Golubeva[7] reported their data in terms of thickness of the solid oxide film. This was converted into (weight gain/area)^2 prior to plotting in Figure 1 by multiplying the density of rutile. Agreement among the three workers is good at 900°C. At 800°C, Samsonov's measured rate of oxidation is lower than that found by Nikolaiski and Münster; at 1000°C, Samsonov's rate is also well below the rate measured by Münster or Nikolaiski at even lower temperatures, 925° and 950°C. In spite of the discrepancies in the quantitative rates, there is concurrence that the oxidation of TiC(s) is parabolic between 800° and 1000°C at times up to 7 hours. The parabolic rate constants derived from the slopes of the lines in Figure 1 are plotted against the reciprocal of absolute temperature in Figure 3. The activation energy for oxidation calculated from all of the points of this Arrhenius plot is 58.6 kcal/mole. The smaller activation energy (46.1 kcal/mole) reported in Nikolaiski's paper is the result of including points taken at 600° and 650°C.

In Figure 2 are plotted the results of experiments that extended to times of 10-300 hours. At the longer times, significant departures from parabolic behavior are in evidence. Nikolaiski's data have been transferred from Figure 1 to Figure 2 and extrapolated as straight lines for purpose of comparison. There is good agreement between Nikolaiski[5] and Macdonald and Ransley[9] and between Nikolaiski[5] and Webb, Norton, and Wagner[1] at 900°C, up to about 4000 minutes. There is considerable disagreement, however, between the last two groups and Macdonald and Ransley[9] on the rate of oxidation at 900°C. The weight changes found by Macdonald and Ransley at 900°C exceed those measured by Nikolaiski at 925°C.

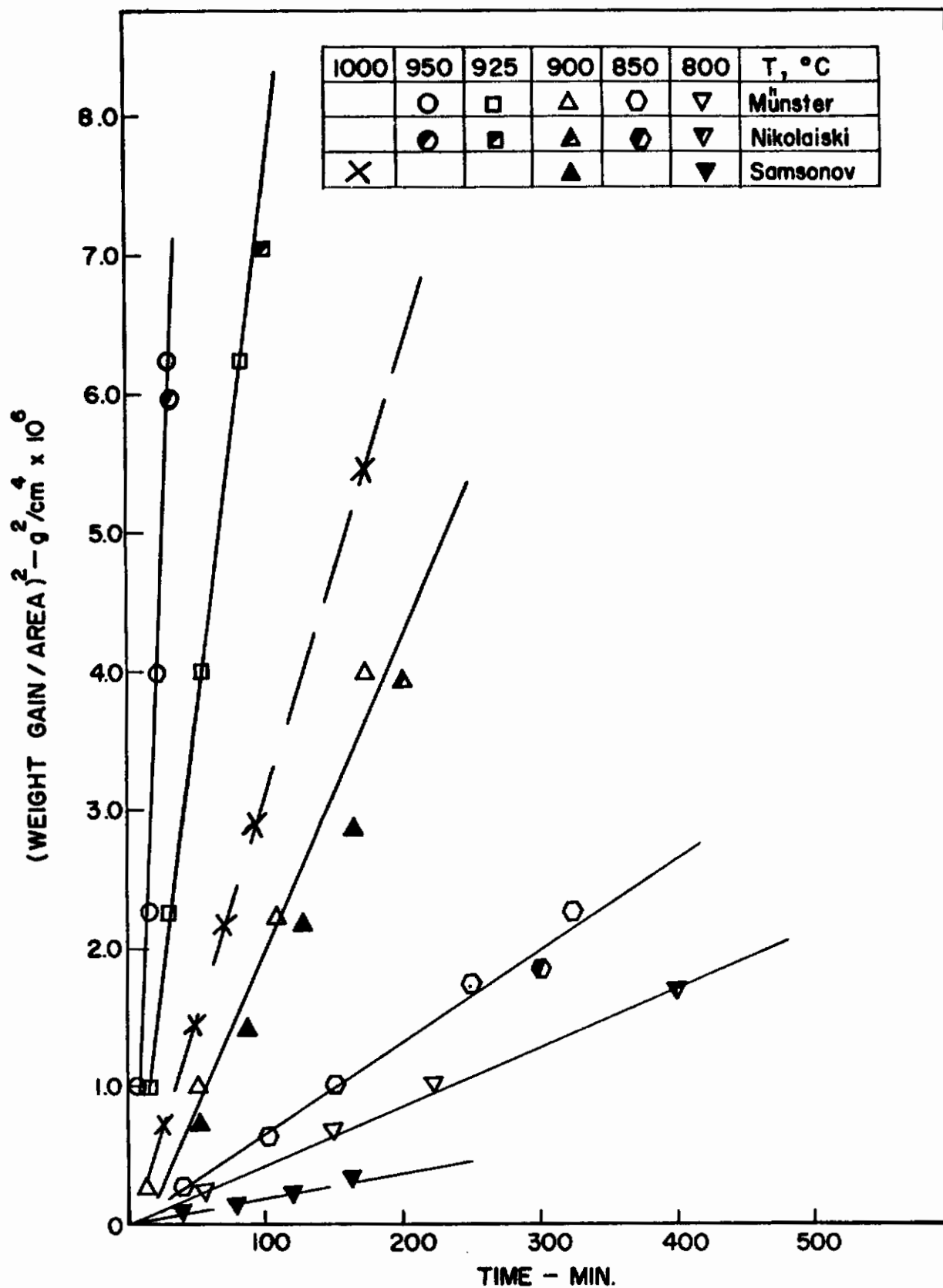|	1000	950	925	900	850	800	T, °C
		○	□	△	⬡	▽	Münster
		◑	◪	▲	⬢	▼	Nikolaiski
	✕			▲		▼	Samsonov

FIGURE II-1 OXIDATION OF TiC

32
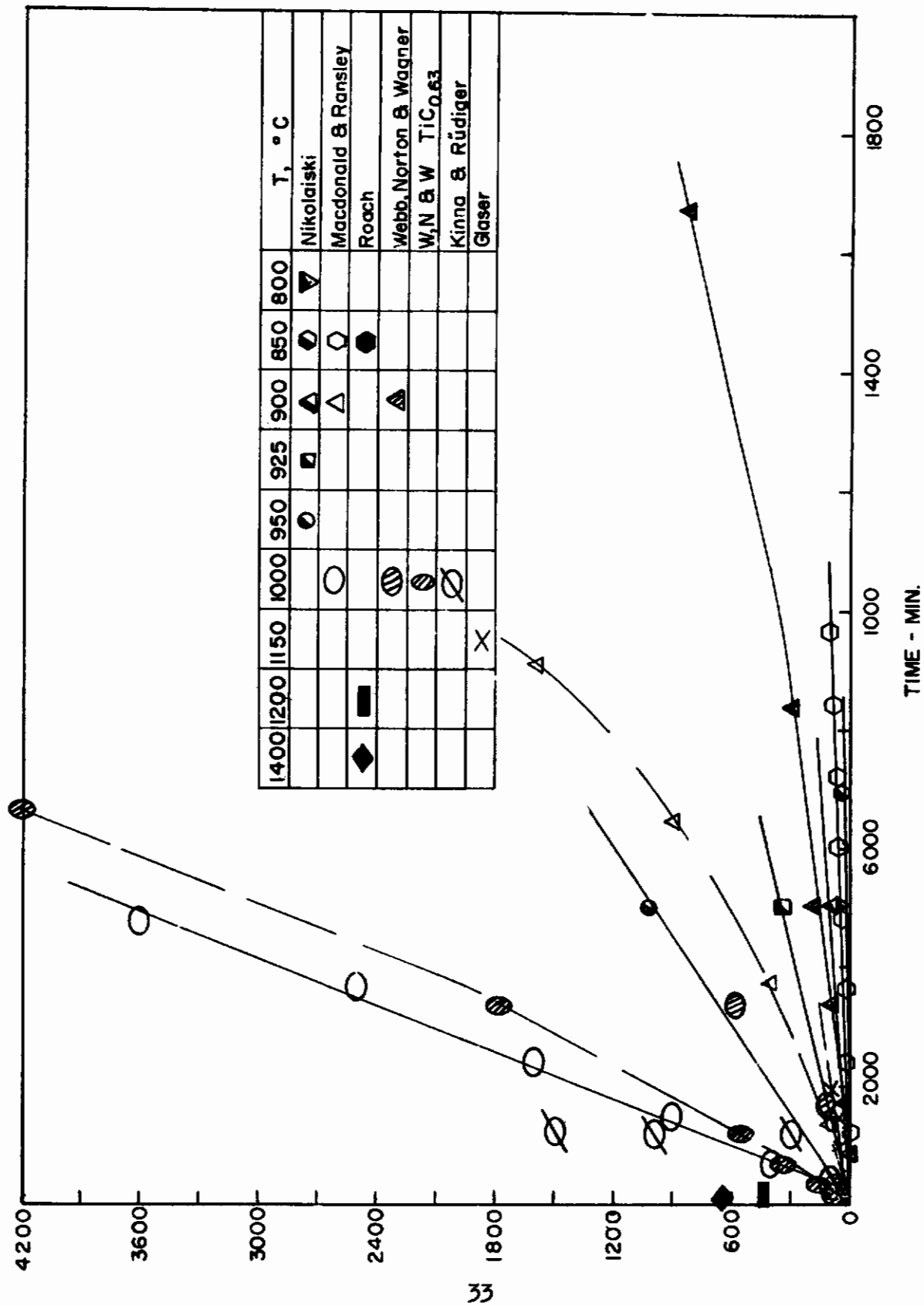
FIGURE II - 2   OXIDATION OF TiC

33

At 1000°C, agreement between Macdonald and Ransley and Webb, Norton, and Wagner is good, although the latter group used a $TiC_{0.63}$ composition and the former group presumably used a starting material closer to stoichiometric TiC. The (WNW) data for stoichiometric TiC at 1000°C seem anomalous in view of the fact that the observed rate is initially lower than that reported by Nikolaiski at 950°C. Furthermore, it is not clear why the rate of oxidation of the carbon rich TiC should be lower than that for the carbon deficient $TiC_{0.63}$. The oxidation rate of the pure metal (carbon free) is about the same as that of the $TiC_{0.63}$ carbide at 1000°C.[1] The values of k_p for pure titanium are included on the Arrhenius plot in Figure 3. The upper curve was constructed from the data of Kinna and Knorr,[10] taken in pure oxygen at 760 Torr. The lower curve is that of Jenkins[11] at an oxygen pressure of 3 Torr. Although k_p in g^2/cm^4-min is somewhat smaller for the carbide than for the pure metal, it must be remembered that the net weight gain of $TiC(s)$ is compounded of a weight loss due to evolution of $CO(g)$ and $CO_2(g)$ as well as a weight gain due to formation of $TiO_2(s)$. Only the latter process occurs in the oxidation of the pure metal. Therefore, the total number of moles per unit area of metal or alloy consumed per unit time is very similar for both $Ti(s)$ and $TiC(s)$. The similar temperature dependence of the parabolic rate constants for oxidation of $Ti(s)$ and $TiC(s)$ suggests a similar rate controlling step for the oxidation of metal and carbide, probably diffusion of oxygen through TiO_2 (rut.).

(b) Zirconium Carbide, ZrC

Columns 2 and 3 of Table 2 give the activities of carbon and zirconium over ZrC as a function of temperature, computed from extrapolation of the vapor pressure data of Coffman, Kibler, and Riethof[12] on ZrC, combined with data for the pure elements from Stull and Sinke.[13] The free energies of formation of $CO(g)$ and $CO_2(g)$ are listed in columns 4 and 5.[3] The free energy of formation of ZrO_2, computed from the data given by Kubaschewski and Evans,[2] is given in column 6. In column 7 are tabulated the equilibrium pressures of $CO(g)$ and $CO_2(g)$ at the ZrC/ZrO_2 phase boundary, calculated from equations (3) and (4) with the Zr activity given in column 3 and a carbon activity of one. Up to 2000°K, a $ZrO_2(s)$ film formed on the surface of ZrC

34
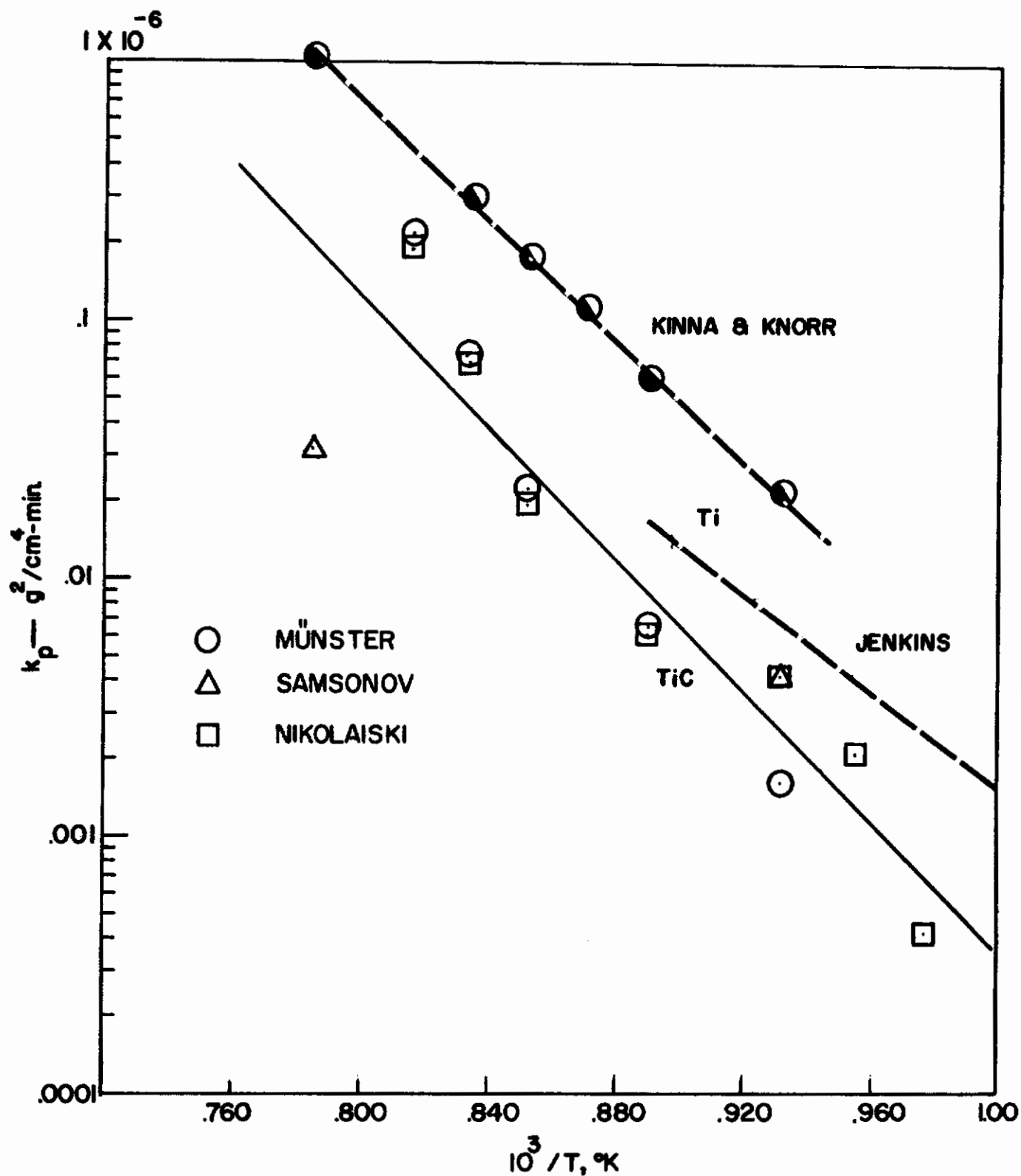
FIGURE II-3   ARRHENIUS PLOT OF PARABOLIC RATE
CONSTANTS FOR TiC & Ti

35

TABLE 2

ACTIVITY OF Zr OVER ZrC-C AND THERMODYNAMIC DATA FOR ZrC-ZrO$_2$

T,°K	a_C	a_{Zr}	$\Delta F_{f,CO}$	$\Delta F_{f,CO_2}$	$\Delta F_{f,ZrO_2}$	p_{CO}	p_{CO_2}
1000	8.128×10^{-3}	4.207×10^{-7}	$-47,859$	$-94,628$	$-213,530$	2.105×10^{-10}	2.601×10^{-20}
1100	1.021×10^{-2}	1.747×10^{-6}	$-49,962$	$-94,658$	$-209,156$	1.089×10^{-8}	1.071×10^{-17}
1200	1.241×10^{-2}	5.970×10^{-6}	$-52,049$	$-94,681$	$-204,808$	2.818×10^{-7}	1.535×10^{-15}
1300	1.462×10^{-2}	1.698×10^{-5}	$-54,126$	$-94,701$	$-200,483$	4.365×10^{-6}	1.007×10^{-13}
1400	1.674×10^{-2}	4.140×10^{-5}	$-56,189$	$-94,716$	$-196,179$	4.529×10^{-5}	3.622×10^{-12}
1500	1.905×10^{-2}	8.995×10^{-5}	$-58,241$	$-94,728$	$-191,896$	3.420×10^{-4}	7.980×10^{-11}
1600	2.118×10^{-2}	1.774×10^{-4}	$-60,284$	$-94,739$	$-187,631$	1.990×10^{-3}	1.189×10^{-9}
1700	2.344×10^{-2}	3.228×10^{-4}	$-62,315$	$-94,746$	$-183,385$	9.375×10^{-3}	1.279×10^{-8}
1800	2.558×10^{-2}	5.520×10^{-4}	$-64,335$	$-94,750$	$-179,153$	3.775×10^{-2}	1.047×10^{-7}
1900	2.782×10^{-2}	8.974×10^{-4}	$-66,349$	$-94,751$	$-174,680$	1.292×10^{-1}	7.447×10^{-7}
2000	2.992×10^{-2}	1.383×10^{-3}	$-68,353$	$-94,752$	$-170,737$	3.732×10^{-1}	3.664×10^{-6}

36

would not be ruptured by evolution of $CO(g)$ or $CO_2(g)$ at the alloy-oxide interface.

The experimental results on the oxidation of ZrC unfortunately indicate that a compact adherent film of ZrO_2 is not formed on the surface of the alloy, and that the oxidation is therefore not diffusion controlled. The rate of oxidation of ZrC powders was measured as a function of oxygen pressure and temperature as part of a doctoral dissertation of R.W. Bartlett.[14] Above 450°C, the oxidation rates were found to be linear, with an activation energy of 45.7 kcal/mole. The principal solid oxidation product was cubic ZrO_2, although minor amounts of the monoclinic phase were found as well. Nothing is said in the abstract about the rate of carbon loss during oxidation, and the thesis, although ordered, has not yet arrived.

Watt, Cockett, and Hall[20] made a single weight change measurement of 49.8 mg/cm^2 on a solid sample of ZrC of density 6.20 g/cc and 4.8% porosity exposed to a stream of dry air flowing at 5.3 cm/sec, for 30 minutes at 800°C. No conclusions could be drawn with respect to oxidation mechanism.

In the course of the present contract, the oxidation of ZrC was studied at temperatures between 1126 and 2200°K at oxygen partial pressures in helium of 2 to 26 Torr. The cylindrical samples, 0.8 cm in diameter and 0.3 cm in height, were fabricated from the elements by a process of sintering and zone melting.[15] The material had a density, measured from total mass and geometric volume, of 6.0 $\pm$ 0.4, compared to a theoretical X-ray density of 6.44 g/cc.[16]

The experimental apparatus used for oxidation studies at high temperatures in this laboratory has been described in detail in Part I of this report. However, modifications were required for the study of refractory carbides. Normally, the stream of helium and oxygen is passed through the reference side of a thermal conductivity cell, over the hot refractory pellet, where some of the oxygen is removed by reaction, and through the sampling side of the thermal conductivity cell. The signal is thus proportional to the rate of oxidation of the sample pellet. In the case of carbides, not only is the stream that emerges from the reaction zone depleted in oxygen; it

37

is also enriched in CO(g) and CO₂(g), both of which will contribute to the bridge signal. A weighed Ascarite trap for the removal of CO₂(g) was interposed between the reaction site and the sampling side of the thermal conductivity bridge. Thus, a mixture of CO(g) and O₂(g) entered the thermal conductivity cell, and the signal from the bridge was proportional to the rate of oxygen consumption minus the rate of evolution of CO(g). (The signal is called positive when the concentration of gas is higher in the reference cell than in the sampling cell, and negative when the situation is reversed.) The exit stream from the thermal conductivity cell was passed over CuO turnings at 700°C to oxidize the CO(g) to CO₂(g), and the CO₂(g) so produced was adsorbed in a weighed Ascarite bulb. Finally, additional information was obtained by weighing the pellets before and after oxidation.

The data obtained is summarized in Table 3. The first column identifies each sample pellet. The second column gives the weight of each pellet after it had been degassed at 2200°K in pure helium until the signal from the thermal conductivity cell indicated that no permanent gases were being evolved. The third column gives geometric surface areas, calculated from micrometer measurements of the height and diameter of the cylindrical pellets. The fourth column records sample densities, computed from weights after degassing and pellet dimensions. Columns 5, 6, and 7 record the pellet temperature, assuming an emissivity of 0.7, oxygen partial pressure, and carrier gas flow rate, respectively, for each oxidation run. The duration of the experiment is given in column 11, and the net weight change, total CO(g) produced, and total CO₂(g) produced in this time are given in columns 8, 9 and 10, respectively.

From the measured quantities in columns 8-10, the derived quantities, total carbon consumed and total zirconium consumed, in columns 12-14 can be computed, if the nature of the oxidation products is assumed. From the observed weight changes in the Ascarite bulbs, it is known that both CO(g) and CO₂(g) form during oxidation. In addition, a white nonadherent oxide, with X-ray pattern of monoclinic ZrO₂, is visible on the surface of the sample pellets after reaction. If it is assumed that the only oxidation products are CO₂(g), CO(g), and ZrO₂(s), then the total carbon consumed, c, is calculated from the measured weights w_{CO_2} and w_{CO} of CO₂(g) and CO(g), respectively.

TABLE 3

SUMMARY OF RESULTS ON ZrC

Pellet	Weight after degassing, g	Surface area, cm²	Density, g/cc	Temp., °K	Oxygen pressure, Torr	Flow rate, cc/min	Wt. change, $g(w_o)$	CO formed, $g(w_{CO_2})$	CO₂ formed, $g(w_{CO_2})$	Time, min.	C consumed, g (c)	Zr consumed, g (z)	$\frac{Zr}{C}$	Wt. change, g/cm²-min x 10⁻⁴
XII-8	0.4446	1.1031	5.72	1126	22.9	58.6	-	0.0001	0.0611	51	-	-	-	-
XII-5	0.5645	1.3942	5.29	1259	20.4	58.6	-	-	0.0709	128	-	-	-	-
XII-3	0.6963	1.4926	5.89	1559	21.2	58.6	-	0.0289	0.0399	62	-	-	-	-
X-31	0.5864	1.310	5.89	1857	9.1	58.6	0.0402	0.0438	0.0220	129	0.0248	0.1852	7.47	2.38
X-29	0.7073	1.450	6.19	1944	8.1	58.6	0.0366	0.0405	0.0145	120	0.0214	0.1652	7.72	2.10
XII-1	0.7051	1.500	5.05	1969	25.9	58.6	0.0851	0.0968	0.0356	112	0.0510	0.388	7.60	5.06
X-27	0.6361	1.252	6.71	2066	8.5	58.6	0.0389	0.0464	0.0175	124	0.0236	0.1780	7.55	2.50
X-16	0.6840	1.388	6.33	2066	8.5	58.6	0.0402	0.0540	0.0073	119	0.0252	0.1862	7.39	2.44
VII-37	0.6643	1.528	5.41	2098	3.0	51.5	0.0207	0.0242	0.0079	180	0.0126	0.0904	7.54	0.754
X-25	0.6812	1.371	6.40	2165	8.9	58.6	0.0356	0.0523	0.0072	120	0.1710	0.0244	7.01	2.16

$$c = \frac{[C]}{[CO_2]} \; w_{CO_2} + \frac{[C]}{[CO]} \; w_{CO} \qquad \text{(II-10)}$$

where the symbols in brackets represent molecular weights. The total weight of zirconium, z, that has been converted to oxide is calculated from the measured weight change, w_o, and the derived carbon consumption:

$$z = \frac{[Zr]}{2[O]} \; [w_o + c] \qquad \text{(II-11)}$$

The ratio of the number of grams of zirconium consumed to the number of grams of carbon consumed during oxidation is given in column 14 of table 3. The ratio is seen to have an approximately constant value of 7.5 ± 0.2. Since the corresponding ratio in the ZrC starting material is 7.6, it would appear that the oxidation of ZrC is stoichiometric and non-preferential. That is, for each zirconium atom converted to oxide, a single carbon atom is also converted to oxide. In column 15, the rate of oxidation is seen to be highest for pellet XII-1. In all of the other runs where weight data is given, more than 90% of the oxygen passed over the refractory pellet reacted with it, and the reaction was probably controlled, therefore, by the rate of arrival of oxygen gas at the sample surface. For XII-1, the supply of oxygen was sufficient to permit a significant determination of oxidation rate.

Weight change data is not given for pellets XII-8, XII-5, and XII-3 because at the relatively low temperatures of these experiments the pellets were broken apart by the oxidation process. At the end of each experiment, the grain boundaries of ZrC were seen to be outlined by a white material, probably ZrO_2. The growth of the oxide in pre-existing cracks and grain boundaries of ZrC undoubtedly creates enough stress to fracture the carbide. Bartlett[14] indicates that oxygen diffuses substitutionally for carbon in the ZrC lattice. The oxygen may then segregate to grain boundaries and precipitate as $ZrO_2(s)$.

Typical curves of extent of oxidation vs time constructed from the thermal conductivity data are reproduced in Figures 4-7. The ordinate in each case is proportional to the number of grams of oxygen consumed to form $CO(g)$, $CO_2(g)$, and $ZrO_2(s)$ minus the number of grams of $CO(g)$ produced at the same
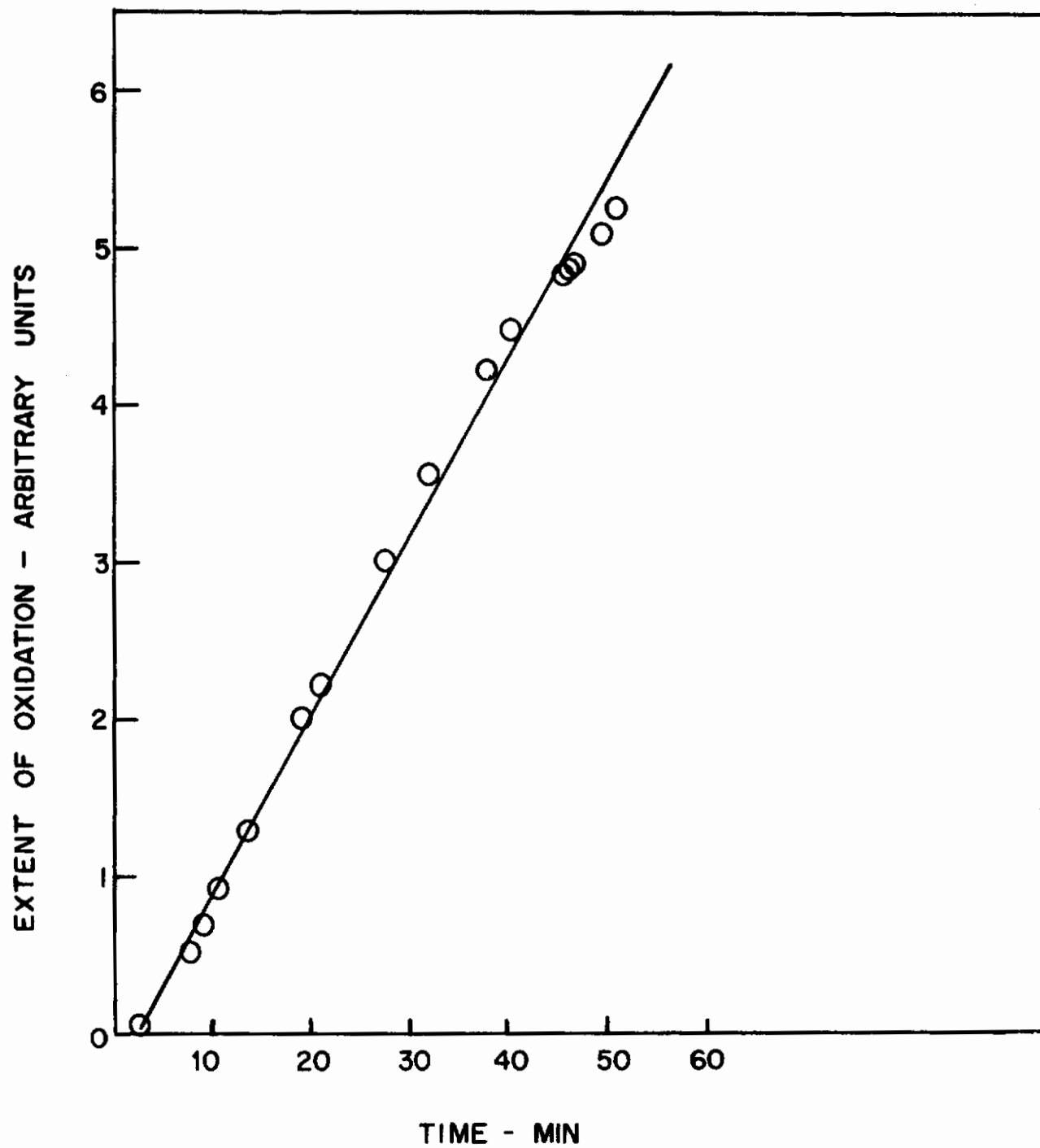
40

FIGURE II - 4   OXIDATION OF ZrC, AT 1126 °K,
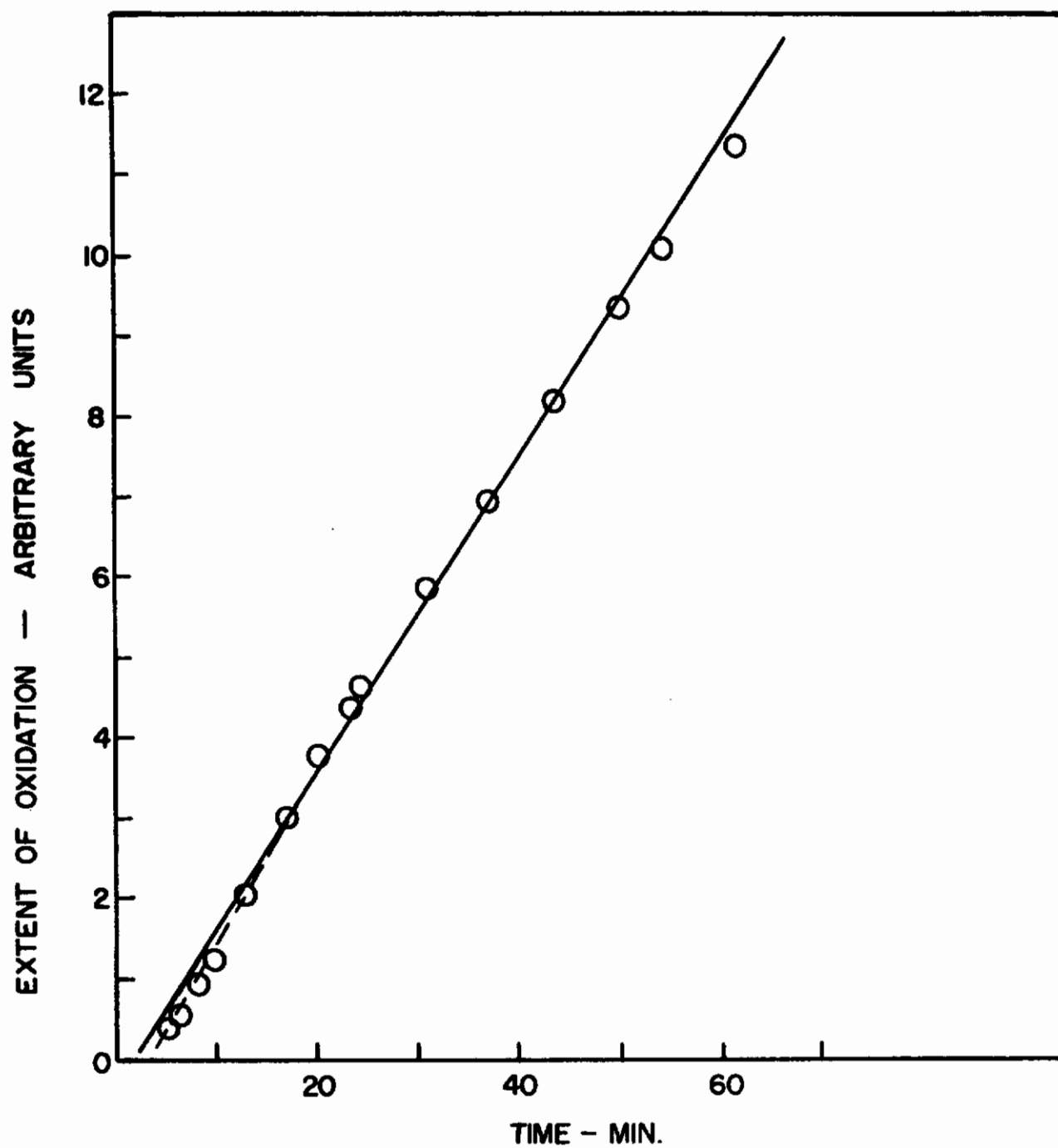
p_{O_2} 22.9 TORR

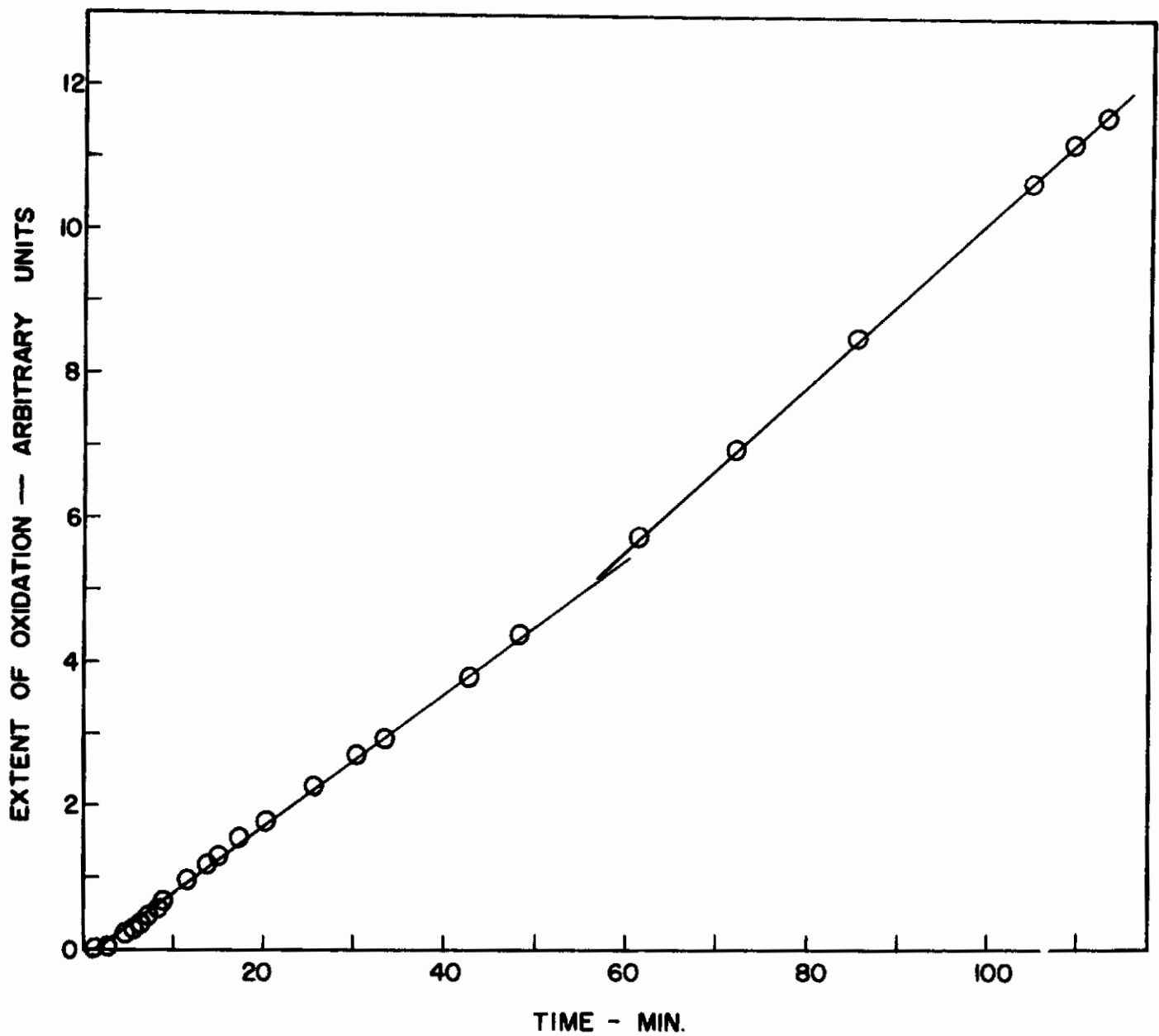FIGURE II-5   OXIDATION OF ZrC, AT 1559 °K,

p_{O_2} 21.2 TORR

FIGURE II-6   OXIDATION OF ZrC, AT 1969 °K, P_{O_2} 25.9 TORR
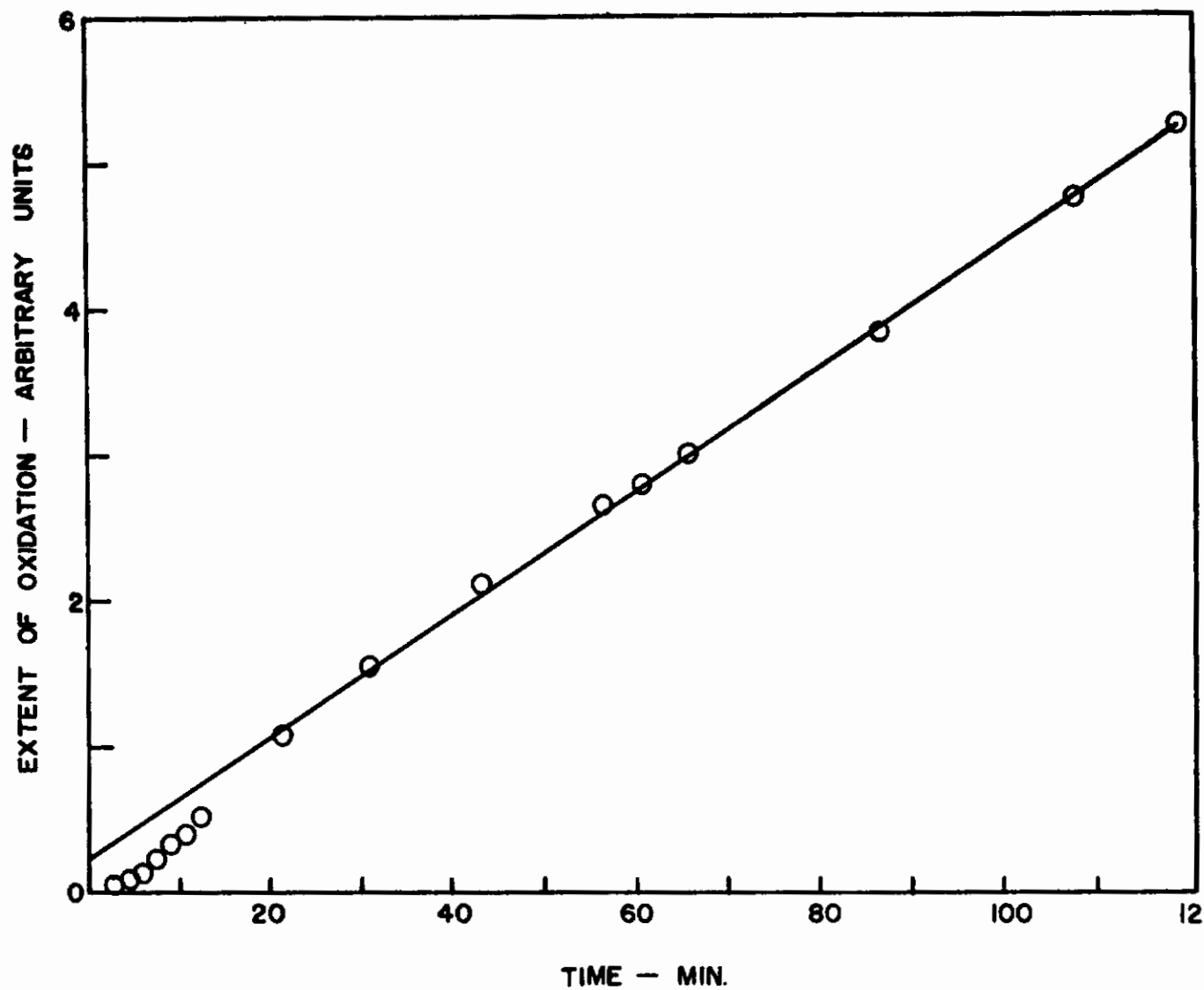
43

FIGURE II – 7   OXIDATION OF ZrC, AT 2165°K, P_{O_2} 8.9 TORR

44

time. Since neither zirconium nor carbon appears to be oxidized preferentially, the rate of formation of $ZrO_2(s)$ must be equal to the sum of the rates of formation of $CO(g)$ and $CO_2(g)$. If, in addition, the ratio of $CO(g)$ to $CO_2(g)$ in the product gas stream is independent of time, then the ordinate will be proportional to the number of grams of oxygen consumed or to the number of grams of $ZrO_2(s)$ or $CO(g)$ or $CO_2(g)$ produced. In any case, a linear rate law appears to be followed under the conditions of the present experiments. The lack of oxidation resistance of ZrC is due, not to the rupture of a protective film by the evolution of $CO(g)$ or $CO_2(g)$, but to the failure of a dense, coherent, protective film to form at all.

The oxidation of pure metallic zirconium is described by a cubic equation between 575° and 950°C, at an oxygen pressure of 760 Torr, while the oxidation of ZrC seems to be linear under similar conditions.[14] Furthermore, the oxidation product on Zr is monoclinic ZrO_2,[17] while on ZrC, the cubic modification of the oxide is formed.[14] In 30 minutes at 800°C, metallic zirconium would be expected to show a weight gain of 1.75 mg/cm^2, compared to the weight gain of 49.8 mg/cm^2 observed for ZrC.[20] At 1126°K, the oxidation of ZrC, as shown in Figure 4 is linear; the oxidation of Zr is cubic.

(c) Hafnium Carbide, HfC

The general similarity between hafnium and zirconium might be expected to extend to the behavior of the respective carbides in oxygen at high temperatures.

The free energy of formation of HfC(s) and the activity of hafnium over the HfC-C two phase region is given in columns 2 and 3 respectively of Table 4. The thermodynamic data for HfC were estimated by Thomas and Hayes,[18] and the activity of hafnium was computed from equation (9). The free energy of formation of $HfO_2(s)$, also estimated by Thomas and Hayes,[18] is tabulated in column 6, and the calculated equilibrium pressures of $CO(g)$ and $CO_2(g)$ at a HfC/HfO_2 phase boundary are given in columns 7 and 8 respectively. Again, as in the case of the other group IV-A carbides, TiC and ZrC, a film of HfO_2 would be thermodynamically stable over HfC well above 1000°K. However, a

45

TABLE 4

ACTIVITY OF Hf OVER HfC-C AND THERMODYNAMIC DATA FOR HfC-HfO$_2$

T, °K	$\Delta F_{f,HfC}$	a_{Hf}	$\Delta F_{f,CO(g)}$	$\Delta F_{f,CO_2}$	$\Delta F_{f,HfO_2}$	p_{CO}	p_{CO_2}
1000	-43,400	3.342×10^{-10}	-47,859	-94,628	-221,700	9.660×10^{-10}	5.382×10^{-19}
1100	-43,300	2.543×10^{-9}	-49,962	-94,658	-217,500	4.250×10^{-8}	1.628×10^{-16}
1200	-43,100	1.438×10^{-8}	-52,049	-94,681	-213,400	9.490×10^{-7}	1.742×10^{-14}
1300	-43,000	5.998×10^{-8}	-54,126	-94,701	-209,200	1.360×10^{-5}	9.804×10^{-13}
1400	-42,800	2.113×10^{-7}	-56,189	-94,716	-205,200	1.257×10^{-4}	2.781×10^{-11}
1500	-42,600	6.296×10^{-7}	-58,241	-94,728	-201,100	8.748×10^{-4}	5.214×10^{-10}
1600	-42,500	1.586×10^{-6}	-60,284	-94,739	-197,100	4.764×10^{-3}	6.781×10^{-9}
1700	-42,300	3.691×10^{-6}	-62,315	-94,746	-193,100	2.087×10^{-2}	6.320×10^{-8}
1800	-42,100	7.822×10^{-6}	-64,337	-94,750	-189,100	1.292×10^{-2}	4.593×10^{-7}
1900	-42,000	1.491×10^{-5}	-66,349	-94,751	-185,100	2.525×10^{-1}	3.147×10^{-6}
2000	-41,800	2.733×10^{-5}	-68,353	-94,752	-181,200	7.117×10^{-1}	1.336×10^{-5}

sufficient $CO(g)$ pressure to rupture the oxide film might be generated at the HfC/HfO_2 interface at temperatures around 2000°K.

Data on the oxidation of $HfC(s)$ are extremely sparse. In the course of the present program, a single run was made at 2305°K at an oxygen partial pressure of 4.2 Torr in helium, with a total pressure of 760 Torr. The reaction was monitored with the thermal conductivity bridge, but no attempt was made to determine separately the oxides of carbon in the product gas stream. A net weight gain of 0.0189 g was observed in a period of 98 minutes, for a sample with a geometric surface area of 1.850 cm^2. In Figures 8 and 9, the abscissa is proportional to the total number of grams of oxygen consumed in the formation of $HfO_2(s)$, $CO(g)$, and $CO_2(g)$, minus the number of grams of $CO(g)$ and $CO_2(g)$ evolved. The ordinate is time in Figure 8 and $\sqrt{t}$ in Figure 9. If the rate of oxidation of hafnium from the alloy is equal to the rate of oxidation of carbon from the alloy, and if the ratio of $CO(g)$ to $CO_2(g)$ is constant with time at a given temperature of oxidation, then the abscissa in the figures is proportional to the rate of conversion of the alloy to the oxides of the constituents. The oxidation rate appears to be parabolic, although it may prove to be linear if carried to longer times. Further work with HfC was postponed because the available commercial samples were porous and contaminated from the start with HfO_2, while at the same time, a synthesis program begun in this laboratory[15] promises to provide better specimens in the near future.

(d) Vanadium Carbide, VC

Columns 2 and 3 of Table 5 give the free energy of formation of $VC(s)$ and the activity of vanadium over carbon rich VC. For $VC(s)$, $\Delta H_{f,298}$ and S_{298} were taken from Kubaschewski and Evans;[2] heat capacity data were taken from Kelley.[19] For the elements, Stull and Sinke's tables were used.[13] Column 6 of Table 4 gives the free energy of formation of $V_2O_3(s)$, as calculated from Kubaschewski and Evans' tables,[2] and columns 7 and 8 give the equilibrium pressures of $CO(g)$ and $CO_2(g)$ at an assumed VC/V_2O_3 phase boundary. It is clear that above 1500°K, V_2O_3 in contact with VC is unstable with respect to decomposition to $V(s)$ and $CO(g)$, and rupture of a dense film of $V_2O_3(s)$, if it formed, would be likely to occur as a result of interaction.
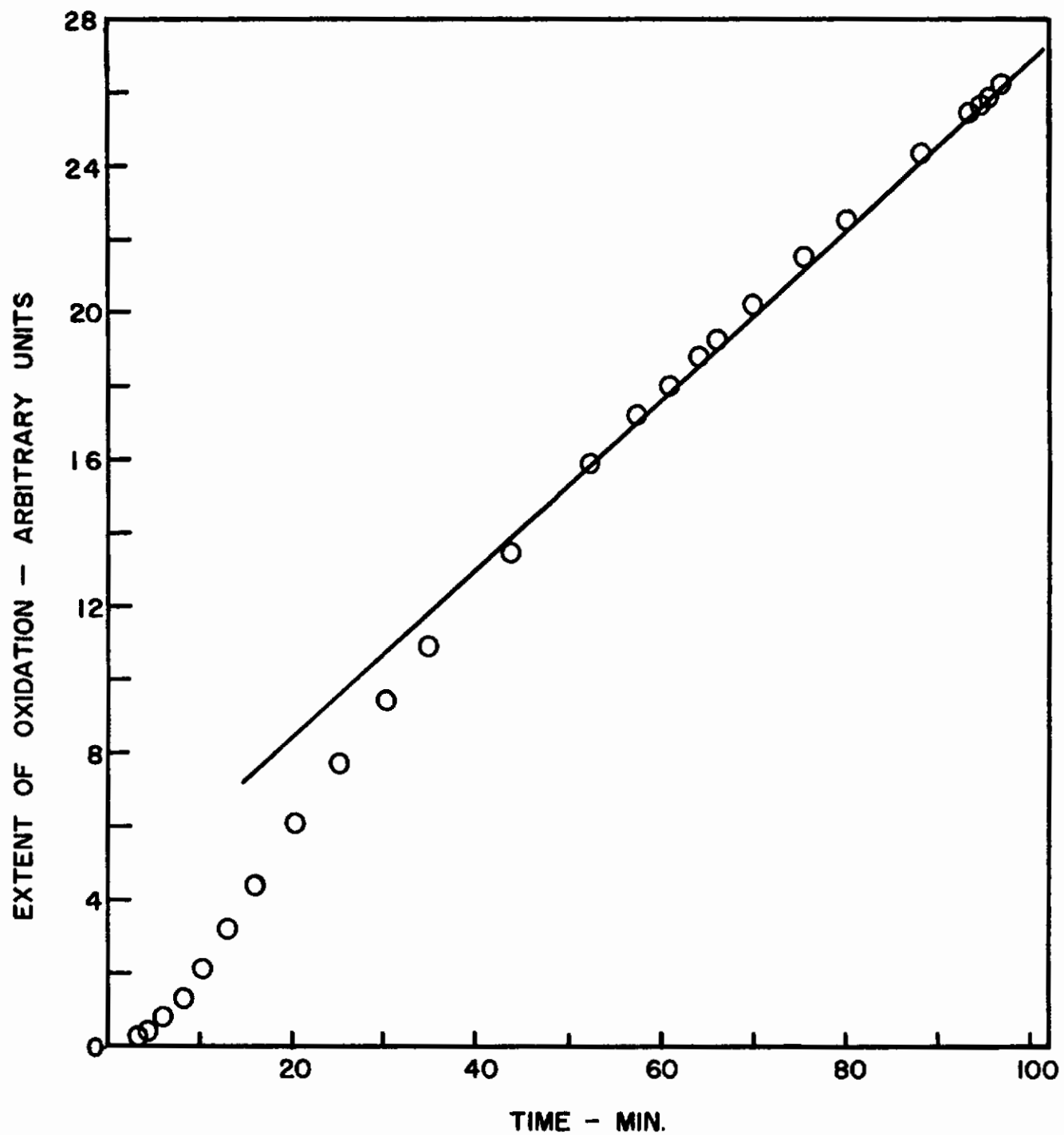
47

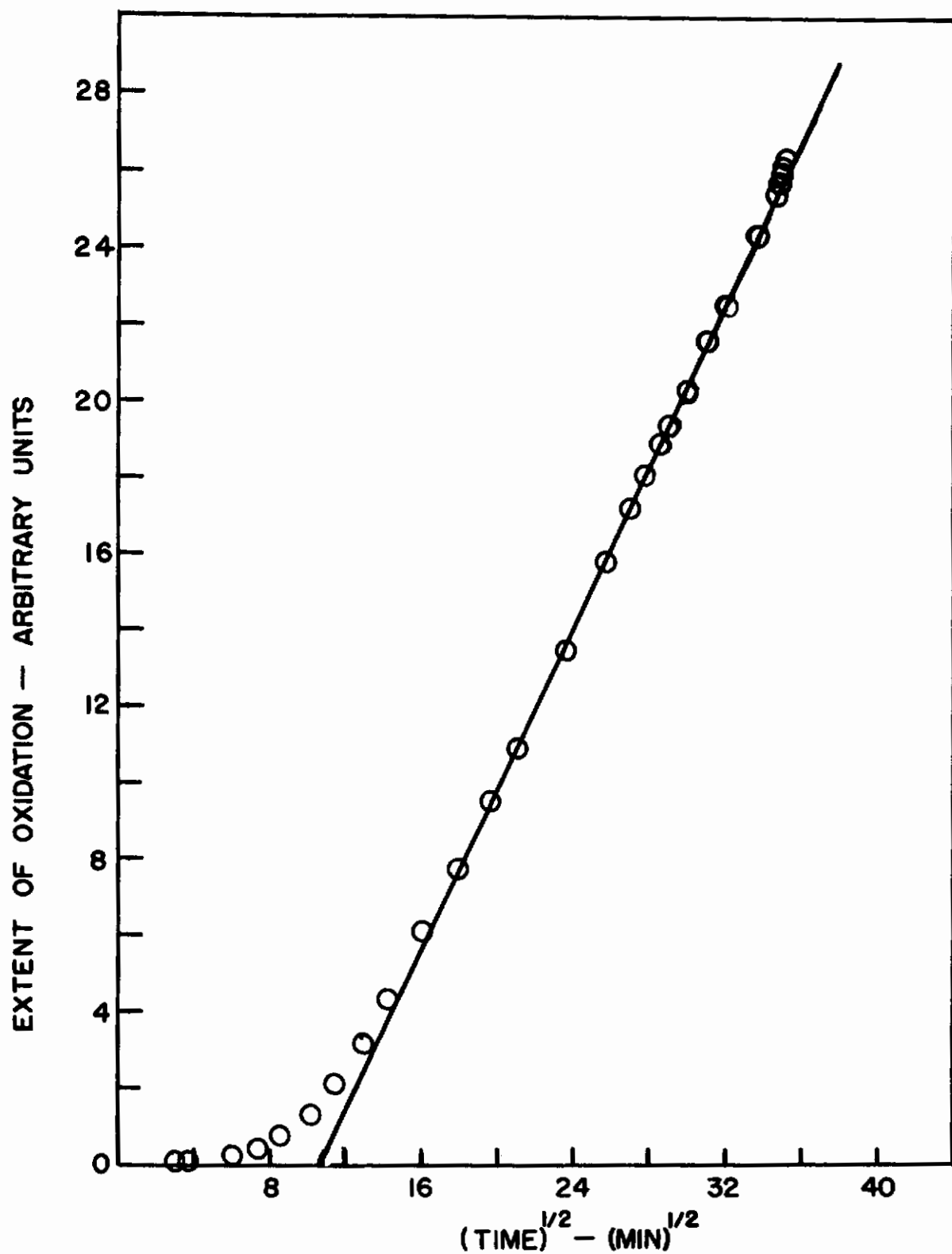FIGURE II — 8 OXIDATION OF HfC, AT 2305 °K, P_{O_2} 4.2 TORR

FIGURE II-9   OXIDATION OF HfC, AT 2305 °K,

p_{O_2} 4.2 TORR

49

TABLE 5

ACTIVITY OF V OVER VC-C AND THERMODYNAMIC DATA FOR VC-V₂O₃

$T, °K$	$\Delta F_{f,VC}$	a_V	$\Delta F_{f,CO}$	$\Delta F_{f,CO_2}$	$\Delta F_{f,V_2O_3}$	p_{CO}	p_{CO_2}
1000	-13,243	1.285×10^{-3}	-47,859	-94,628	-237,400	1.257×10^{-5}	9.119×10^{-11}
1100	-13,093	2.519×10^{-3}	-49,962	-94,658	-231,785	2.060×10^{-4}	4.309×10^{-9}
1200	-12,908	4.481×10^{-3}	-52,049	-94,681	-226,170	2.084×10^{-3}	8.398×10^{-8}
1300	-12,730	7.277×10^{-3}	-54,126	-94,701	-220,555	1.474×10^{-2}	1.150×10^{-6}
1400	-12,550	1.103×10^{-2}	-56,189	-94,716	-214,940	7.823×10^{-2}	1.080×10^{-5}
1500	-12,357	1.589×10^{-2}	-58,241	-94,728	-209,325	3.314×10^{-1}	7.480×10^{-5}
1600	-12,200	2.164×10^{-2}	-60,284	-94,739	-203,710	1.162	4.126×10^{-4}
1700	-12,000	2.876×10^{-2}	-62,315	-94,746	-198,095	3.549	1.828×10^{-3}
1800	-11,786	3.719×10^{-2}	-64,337	-94,750	-192,480	14.71	6.824×10^{-3}
1900	-11,585	4.663×10^{-2}	-66,349	-94,751	-186,865	22.60	2.227×10^{-2}
2000	-11,340	5.781×10^{-2}	-68,353	-94,752	-181,250	49.16	6.357×10^{-2}

The available datum is semi-quantitative in nature,[20] and con-
sists of a single measurement of the weight change of a VC(s) specimen after
one-half hour in flowing dry air at 1073°K. The sample was prepared in the
form of a cylinder, 0.64 cm in diameter and about equally long, by hot
pressing. The material contained 13.5-14% total carbon, of which about 1%
was free carbon, compared to a theoretical weight percentage of 19.05% carbon
for stoichiometric VC(s). The hot pressed material had a density of 5.04 g/cc,
a 6.2% porosity, and a surface area of 1.76 cm². The specimen was heated at
1073°K in a quartz tube in a stream of dry air flowing with a linear velocity
of 5.3 cm/sec. The observed weight gain after 30 minutes was 41.7 mg/cm².
The authors do not indicate whether $CO(g)$ or $CO_2(g)$ was evolved, or whether
a dense solid oxide formed on the surface of the sample. The net weight
change, however, was approximately the same as that observed by the authors
for ZrC(s) exposed under similar conditions.

The oxidation of pure vanadium metal has only been investigated
between 400° and 600°C. If the data[17] is extrapolated to 800°C, a weight
gain of 1.1 mg/cm² is predicted in a period of 30 minutes. The carbide thus
appears to be oxidized more rapidly than the corresponding metal, although an
extrapolation over 200°C must be accepted only with greatest reservation.

(e) Niobium Carbide, NbC

Free energy of formation and activity data for NbC(s) are given in
columns 2 and 3 of Table 6. Column 6 gives the free energy of formation of
$NbO_2(s)$, and columns 7 and 8 give the equilibrium $CO(g)$ and $CO_2(g)$ pressures
for reactions (1) and (2) with $MeO_y = NbO_2$. Thermodynamic data for NbC and
NbO_2 were taken from Kubaschewski and Evans.[2] A diffusion barrier of $NbO_2(s)$
might be built up on a surface of NbC at temperatures up to 1100°K, but above
this temperature, rupture of the $NbO_2(s)$ film would destroy its effectiveness
in reducing the rate of oxidation of carbide.

Again, the only available experimental datum is that of Watt,
Cockett, and Hall,[20] who used a hot pressed sample with a density of
7.51 g/cc and a porosity of 3.9%. The observed net weight change after 30
minutes at 1073°K in dry air, flowing at 5.3 cm/sec, was 56.8 mg/cm². No
conclusions about oxidation mechanism can be drawn from this single measurement.

TABLE 6

ACTIVITY OF Nb OVER NbC-C AND THERMODYNAMIC DATA FOR NbC-NbO$_2$

T,°K	$\Delta F_{f,NbC}$	a_{Nb}	$\Delta F_{f,CO}$	$\Delta F_{f,CO_2}$	$\Delta F_{f,NbO_2}$	p_{CO}	p_{CO_2}
1000	-39,230	2.720×10^{-9}	-47,859	-94,628	-146,850	5.021×10^{-2}	1.455×10^{-3}
1100	-39,830	1.242×10^{-8}	-49,962	-94,658	-142,780	5.008×10^{-1}	2.260×10^{-1}
1200	-40,455	4.357×10^{-8}	-52,049	-94,681	-138,749	3.273	2.201×10^{-1}
1300	-41,090	1.256×10^{-7}	-54,126	-94,701	-134,733	16.86	1.505
1400	-41,730	3.101×10^{-7}	-56,189	-94,716	-130,738	66.43	7.766
1500	-42,370	6.801×10^{-7}	-58,241	-94,728	-126,763	2.166×10^{2}	31.94
1600	-43,020	1.347×10^{-6}	-60,284	-94,739	-122,805	6.062×10^{2}	1.098×10^{2}
1700	-43,670	2.462×10^{-6}	-62,315	-94,746	-118,864	1.495×10^{3}	3.245×10^{2}
1800	-44,320	4.208×10^{-6}	-64,337	-94,750	-114,939	3.318×10^{3}	8.454×10^{2}
1900	-44,970	6.795×10^{-6}	-66,349	-94,751	-111,029	6.744×10^{3}	1.982×10^{3}
2000	-45,630	1.044×10^{-5}	-68,353	-94,752	-107,132	1.273×10^{4}	4.265×10^{3}

52

However, the pure metal under the same conditions would have shown a weight gain of about 9.9 mg/cm^2.[21] Therefore, the carbide does indeed seem to oxidize more rapidly than the metal.

(f) Tantalum Carbide, TaC

Columns 2, 3, 4, 5, 6, 7, and 8 of Table 7 give, respectively, the free energy of formation of TaC,[2] the activity of Ta over carbon rich TaC, the free energies of formation of $CO(g)$,[3] $CO_2(g)$,[3] and Ta_2O_5,[2] and the equilibrium pressures of $CO(g)$ and $CO_2(g)$ for the interaction between $Ta_2O_5(s)$ and $TaC(s)$. On the basis of the WNW criteria, a film of Ta_2O_5 on TaC would be ruptured by evolution of $CO(g)$ and $CO_2(g)$ at temperatures above 1300°K.

No extensive measurements are available on the kinetics of oxidation of TaC. A single weight change determination at 800°C was made by Watt, Cockett, and Hall[20] in the course of their survey of the oxidation resistance of carbides, and a measurement of weight changes, $CO(g)$, and $CO_2(g)$ evolution at 2159° was made during the course of the present contract.

At 1073°K, on the basis of the WNW criterion, a protective film of $Ta_2O_5(s)$ might be stable on the surface of TaC(s). A hot-pressed TaC sample with a density of 13.10 g/cc and a porosity of 6.8% was heated in a quartz tube at 1073°K in a stream of dry air, flowing at 5.3 cm/sec, for 30 minutes. The net observed weight gain was 103 mg/cm^2, about twice that observed for ZrC, VC, and NbC, exposed under similar conditions. However, it must be remembered that Zr and Nb form dioxides, ZrO_2 and NbO_2, V forms a lower oxide, $VO_{1.5}$, while Ta forms a higher oxide, $TaO_{2.5}$. Therefore, the number of moles of metal consumed per square centimeter during oxidation of the carbides is in the ratio of 4.1:2.8:2.8:2.5 for TaC:VC:NbC:ZrC, assuming similar weight losses due to evolution of $CO(g)$ and $CO_2(g)$ for all four materials. The experimental data does not indicate whether a film of $Ta_2O_5(s)$ was built up on the carbide surface, but the implication is that oxidation was rapid and non-protective. Pure tantalum would have shown a weight change of about 11 mg/cm^2 under the same conditions.[22]

At 2432°K, $Ta_2O_5(s)$ would be expected to undergo extensive reaction with TaC(s) to form $CO(g)$, $CO_2(g)$ and Ta (alloy). A hot pressed TaC(s) pellet,[23] with a density of 11.48 g/cc and a surface area of 1.754 cm^2, was

TABLE 7

ACTIVITY OF Ta OVER TaC-C AND THERMODYNAMIC DATA FOR TaC-Ta$_2$O$_5$

| $T, °K$	$\Delta F_{f,TaC}$	a_{Ta}	$\Delta F_{f,CO}$	$\Delta F_{f,CO_2}$	$\Delta F_{f,Ta_2O_5}$	p_{CO}	p_{CO_2}
1000	-37,983	5.094×10^{-9}	-47,859	-94,628	-385,100	8.912×10^{-4}	4.590×10^{-7}
1100	-37,611	3.427×10^{-8}	-49,962	-94,658	-375,405	1.001×10^{-1}	9.015×10^{-6}
1200	-37,213	1.694×10^{-7}	-54,049	-94,681	-365,785	1.701×10^{-1}	1.049×10^{-4}
1300	-36,794	6.607×10^{-7}	-54,126	-94,701	-356,245	3.944×10^{-1}	8.241×10^{-4}
1400	-36,352	2.142×10^{-6}	-56,189	-94,716	-346,775	1.640	4.731×10^{-3}
1500	-35,891	5.971×10^{-6}	-58,241	-94,728	-337,370	5.571	2.118×10^{-2}
1600	-35,411	1.472×10^{-5}	-60,284	-94,739	-328,020	16.10	7.744×10^{-2}
1700	-34,913	3.248×10^{-5}	-62,315	-94,746	-318,730	40.73	2.409×10^{-1}
1800	-34,397	6.730×10^{-5}	-64,337	-94,750	-309,490	1.242×10^{2}	6.531×10^{-1}
1900	-33,870	1.282×10^{-4}	-66,349	-94,751	-300,305	1.906×10^{2}	1.578
2000	-33,325	2.301×10^{-4}	-68,353	-94,752	-291,160	3.597×10^{2}	3.459

54

heated for 108 minutes at 2432°K in a stream of dried helium and oxygen, at a total pressure of 760 Torr, oxygen partial pressure of 6.8 Torr, and flow rate of 58.6 ml/min. A net weight loss of 0.0399 g/cm^2 was observed, while the amounts of $CO(g)$ and $CO_2(g)$ evolved were 0.659 g/cm^2 and 0.0359 g/cm^2, respectively. The ratio of pressures of $CO(g)$ and $CO_2(g)$ found experimentally was therefore $p_{CO}:p_{CO_2}$ = 28.8:1. The corresponding ratio for $CO(g)$ and $CO_2(g)$ in equilibrium with $TaC(s)$ and $Ta_2O_5(s)$ is larger than 100:1. It therefore seems likely that some oxidation of $CO(g)$ to $CO_2(g)$ occurred in the gas phase. For the equilibrium:

$$CO(g) + \frac{1}{2} O_2(g) = CO_2(g)$$
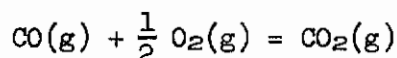
the ratio of $p_{CO}:p_{CO_2}$ at 298°K and an oxygen partial pressure of 6.8 Torr is 10^{-44}, while at 2400°K, the corresponding ratio is 0.2 at equilibrium.

The total carbon loss from the TaC sample due to vaporization of $CO(g)$ and $CO_2(g)$ was 0.0242 g/cm^2, while the net observed weight loss was 0.0399 g/cm^2. Therefore there must have been a minimum tantalum loss of 0.0107 g/cm^2 during the course of oxidation. The vaporization behavior of $Ta_2O_5(s)$ in the presence of oxygen has not been investigated. The vaporization of $TaO(g)$ or $TaO_2(g)$ by reaction of $Ta_2O_5(s)$ with Ta (alloy) or C (alloy) at the alloy/oxide interface would not account for the observed rate of tantalum weight loss. The existence of a $Ta_2O_5(g)$ species in the vapor has not been demonstrated but is certainly possible at high oxygen pressures.

If the oxidation of TaC were non-preferential it could be expressed at any time t by a stoichiometric relationship of the form:

$$TaC + \left(\frac{9}{4} - \frac{b}{2}\right) O_2 \rightarrow \frac{1}{2} Ta_2O_5(s) + bCO(g) + (1 - b) CO_2(g) \qquad \text{(II-12)}$$
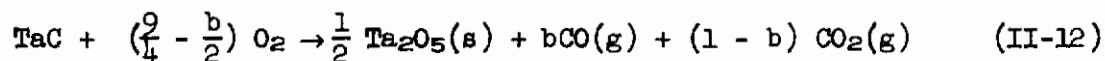
where b is an unknown number of moles. For simplicity, we denote:

y = number of g/cm^2 of $Ta_2O_5(s)$ formed between time zero and time t

z = number of g/cm^2 of $CO(g)$ formed between time zero and time t

x = number of g/cm^2 of $CO_2(g)$ formed between time zero and time t

55

Then, we assume that the rate of formation of $Ta_2O_5(s)$ is governed by a simple law:

$$\frac{dy}{dt} = k \, f(y) \qquad \text{(II-13)}$$

where k is a rate constant, and $f(y)$ is some function of y, commonly a constant (linear growth) or $1/y$ (parabolic growth). Since stoichiometry always obtains, we must have:

$$\frac{dz}{dt} = 2b \, k \, f(y) \, \frac{[CO]}{[Ta_2O_5]} \qquad \text{(II-14)}$$

and

$$\frac{dx}{dt} = 2(1-b) \, k \, f(y) \, \frac{[CO_2]}{[Ta_2O_5]} \qquad \text{(II-15)}$$

where the symbols in brackets are molecular weights.

The signal from the thermal conductivity bridge in the carbide experiments is given by:

$$\text{Signal} = A \left\{ \frac{[5O]}{[Ta_2O_5]} \, \frac{dy}{dt} + \frac{[O]}{[CO]} \, \frac{dz}{dt} + \frac{[2O]}{[CO_2]} \, \frac{dx}{dt} - \frac{dz}{dt} \right\} \qquad \text{(II-16)}$$

where A is a proportionality constant to convert millivolts to g/cm^2-sec, and the instrument sensitivity is assumed equal for $CO(g)$ and $O_2(g)$. Substituting the rate expressions in (13), (14), and (15) into (16), one finds:

$$\text{Signal} = \frac{Akf(y)}{[Ta_2O_5]} \left\{ [5O] + 2b \, [O] + 2(1-b) \, [2O] - 2b \, [CO] \right\} \qquad \text{(II-17)}$$

Introducing molecular weights into (17), the signal is given finally by:

$$\text{Signal} = \frac{Akf(y)}{[Ta_2O_5]} \, [144 - 88b]$$

Since b must be smaller than or equal to one, the signal would have to be positive if the reaction were stoichiometric. Since the signal was negative during the entire experiment, the oxidation of $TaC(s)$ cannot proceed, under

the conditions described, so that the rate of oxidation of tantalum is exactly equal to the rate of oxidation of carbon. There must be preferential oxidation of one component. Free energy considerations suggest that there should be preferential oxidation of carbon. Since TaC has a wide range of homogeneity, extending from $TaC_{0.85}$ to $TaC_{1.0}$[2], diffusion of carbon from the bulk alloy to the alloy oxide interface, under the activity gradient created as the carbon becomes depleted through oxidation, is highly probable.

Figure 10 is a plot of $A\left\{\dfrac{[5O]}{[Ta_2O_5]}y + \dfrac{[O]}{[CO]}x + \dfrac{[2O]}{[CO_2]}z - z\right\}$ vs $\sqrt{t}$. The abscissa are obtained by integration of the signal between times zero and t. After about 25 minutes, the data can be approximated by a straight line, which could indicate that the rates of formation of both $Ta_2O_5(s)$ and the carbon oxides are diffusion controlled, although the net rate of oxidation of carbon is larger than the rate of oxidation of Ta. X-ray analysis of the oxidized pellet surface revealed lines for α- and β- Ta_2O_5, as well as lines for pure Ta metal, serving to confirm the assumption of preferential oxidation of carbon.

(g) Chromium Carbide, Cr_3C_2

Table 8 gives the free energy of formation of Cr_3C_2,[2,19] the activity of Cr over carbon rich Cr_3C_2, the free energies of formation of $CO(g)$,[3] CO_2,[3] and $Cr_2O_3(s)$[2,19] and the equilibrium pressures of $CO(g)$ and $CO_2(g)$, for the interactions between $Cr_2O_3(s)$ and $Cr_3C_2(s)$. At an ambient pressure of one atmosphere, rupture of a potentially protective $Cr_2O_3(s)$ film would be likely at temperatures above $1400°K$.

Kosolapova and Samsonov[24] measured the oxidation rates of powdered and hot-pressed $Cr_3C_2(s)$ in oxygen at temperatures between 400° and 1000°C. For the powdered samples, the rate of oxidation was followed by measuring the amount of $CO_2(g)$ evolved during exposure in a flowing oxygen stream. The rate of gas evolution was approximately parabolic with time. The authors fail to indicate whether $CO(g)$ was also generated, and whether a solid oxide formed as well. Since the surface areas of the powdered specimens are not known, the results on powders cannot be directly compared to results on dense fabricated samples. With hot-pressed cylinders, no weight changes could be detected in two-hour exposures between 800° and 1100°C, but the authors do not state
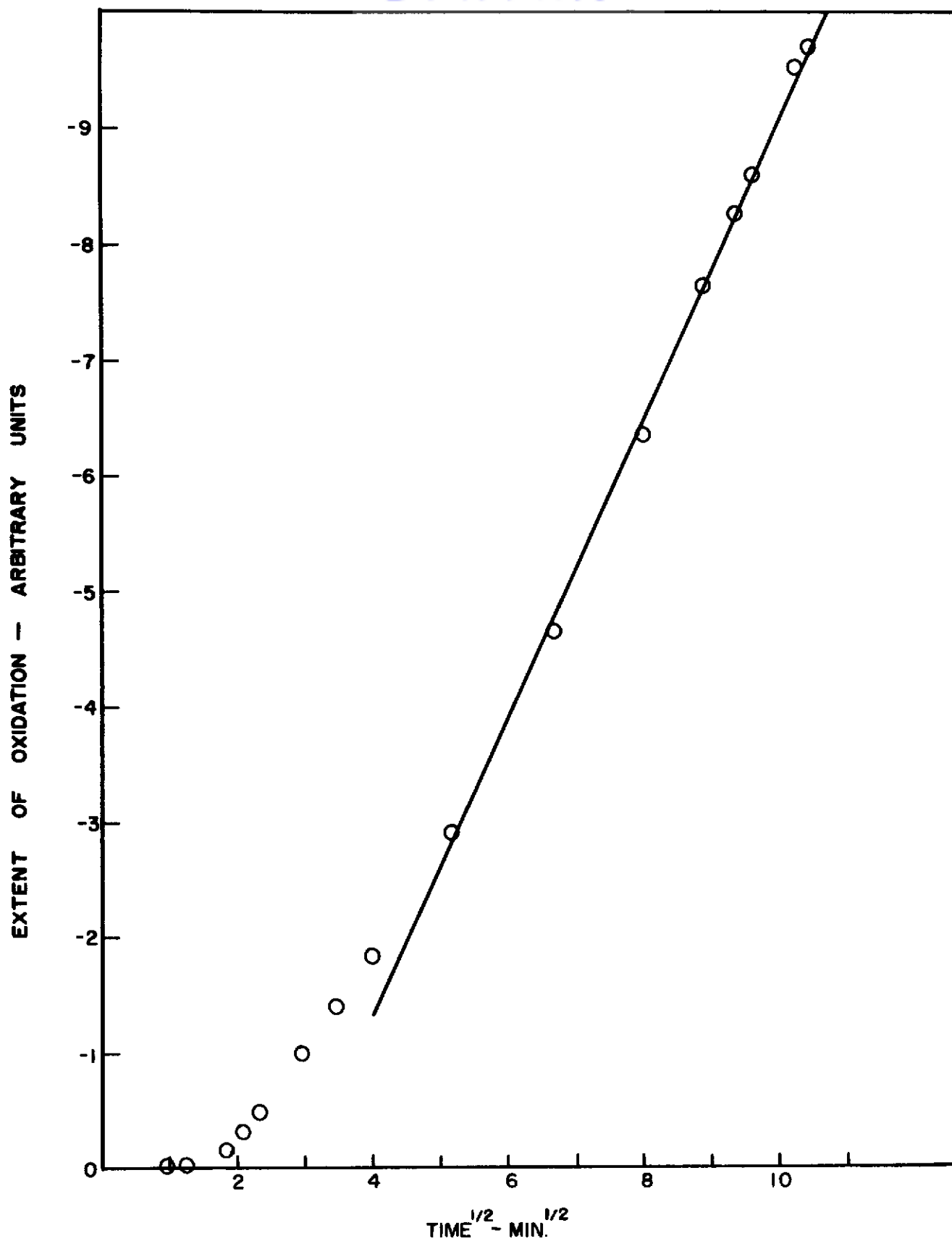
57

FIGURE II – 10   OXIDATION OF TaC, AT 2432°K, P_{O_2} 6.8 TORR

58

TABLE 8

ACTIVITY OF Cr OVER Cr_3C_2-C AND THERMODYNAMIC DATA FOR Cr_3C_2-Cr_2O_3

$T, °K$	$\Delta F_{f,Cr_3C_2}$	a_{Cr}	$\Delta F_{f,CO}$	$\Delta F_{f,CO_2}$	$\Delta F_{f,Cr_2O_3}$	p_{CO}	p_{CO_2}
1000	-19,890	3.570×10^{-2}	-47,859	-94,628	-205,650	2.801×10^{-4}	4.536×10^{-8}
1100	-19,550	5.087×10^{-2}	-49,962	-94,658	-199,440	3.834×10^{-3}	1.324×10^{-6}
1200	-19,048	6.993×10^{-2}	-52,049	-94,681	-193,230	3.321×10^{-2}	2.132×10^{-5}
1300	-18,458	9.259×10^{-2}	-54,126	-94,701	-187,020	2.039×10^{-1}	2.201×10^{-4}
1400	-17,716	1.199×10^{-1}	-56,189	-94,716	-180,810	9.498×10^{-1}	1.587×10^{-3}
1500	-16,890	1.515×10^{-1}	-58,241	-94,728	-174,600	3.567	8.672×10^{-3}
1600	-16,029	1.866×10^{-1}	-60,284	-94,739	-168,120	11.49	4.052×10^{-2}
1700	-15,021	2.274×10^{-1}	-62,315	-94,746	-162,180	30.83	1.380×10^{-1}
1800	-14,912	2.495×10^{-1}	-64,337	-94,750	-155,970	79.34	4.833×10^{-1}
1900	-13,621	3.008×10^{-1}	-66,349	-94,751	-149,760	1.721×10^2	1.291
2000	-12,295	3.569×10^{-1}	-68,353	-94,752	-143,550	3.440×10^2	3.113

59

whether a thin protective film of $Cr_2O_3(s)$ was responsible for the observed behavior. Watt, Cockett, and Hall[20] also failed to detect a weight change in a Cr_3C_2 sample that had been treated for 30 minutes in oxygen at 800°C. However, they do report the formation of a green film of $Cr_2O_3(s)$ on the carbide surface.

Quantitative weight change measurements on hot-pressed samples of Cr_3C_2 at 900° and 1000°C are plotted in Figure 11[20] as (wt. gain/area)^2 vs time. The points are transcribed from a small and sparsely ruled graph. The material used for the experiments contained 13% total carbon and 84-86% chromium, compared to theoretical values of 13.3% and 86.7% Cr. The specimens had a density of 6.31 g/cc and a porosity of 5.4%. The experiment consisted of heating the samples in a quartz tube, and passing dry air over them at a rate of 5.3 cm/sec. Unfortunately, the authors obtained no information on the important question of carbon loss as $CO(g)$ or $CO_2(g)$. Included in Figure 11 are the weight change curves for pure chromium metal under similar conditions. The carbide is seen to show somewhat greater oxidation resistance than the metal, possibly because of the lowered metal activity, possibly because of a better adhesion of the oxide to the substrate.

Above 1100°C, the oxidation resistance of $Cr_3C_2(s)$ is expected to break down due to rupture of the $Cr_2O_3(s)$ film by evolution of $CO(g)$ and $CO_2(g)$. During the present contract, the oxidation of dense samples of Cr_3C_2[25] was studied at temperatures between 1660° and 1900°K and oxygen pressures of 4 to 9 Torr. Results were indeed very different from those at the lower temperatures. A summary of the data obtained is given in Table 9. Column 1 simply identifies the sample, column 2 gives the original weight of the unoxidized pellet after heat treatment at 1870°K for a sufficient time to remove permanent gas impurities; columns 3 and 4 give surface areas and densities of the samples calculated from micrometer dimensions and weights; columns 5 and 6 give the temperature of the pellet (assuming an emissivity of 0.6) and the oxygen partial pressure during the oxidation experiment; column 7 gives the volume flow rate of the helium-oxygen mixture; columns 8, 9, and 10 give the net weight change of the pellet, weight of $CO(g)$ evolved, and weight of $CO_2(g)$ evolved after oxidation for the times listed in column 11. Column 12
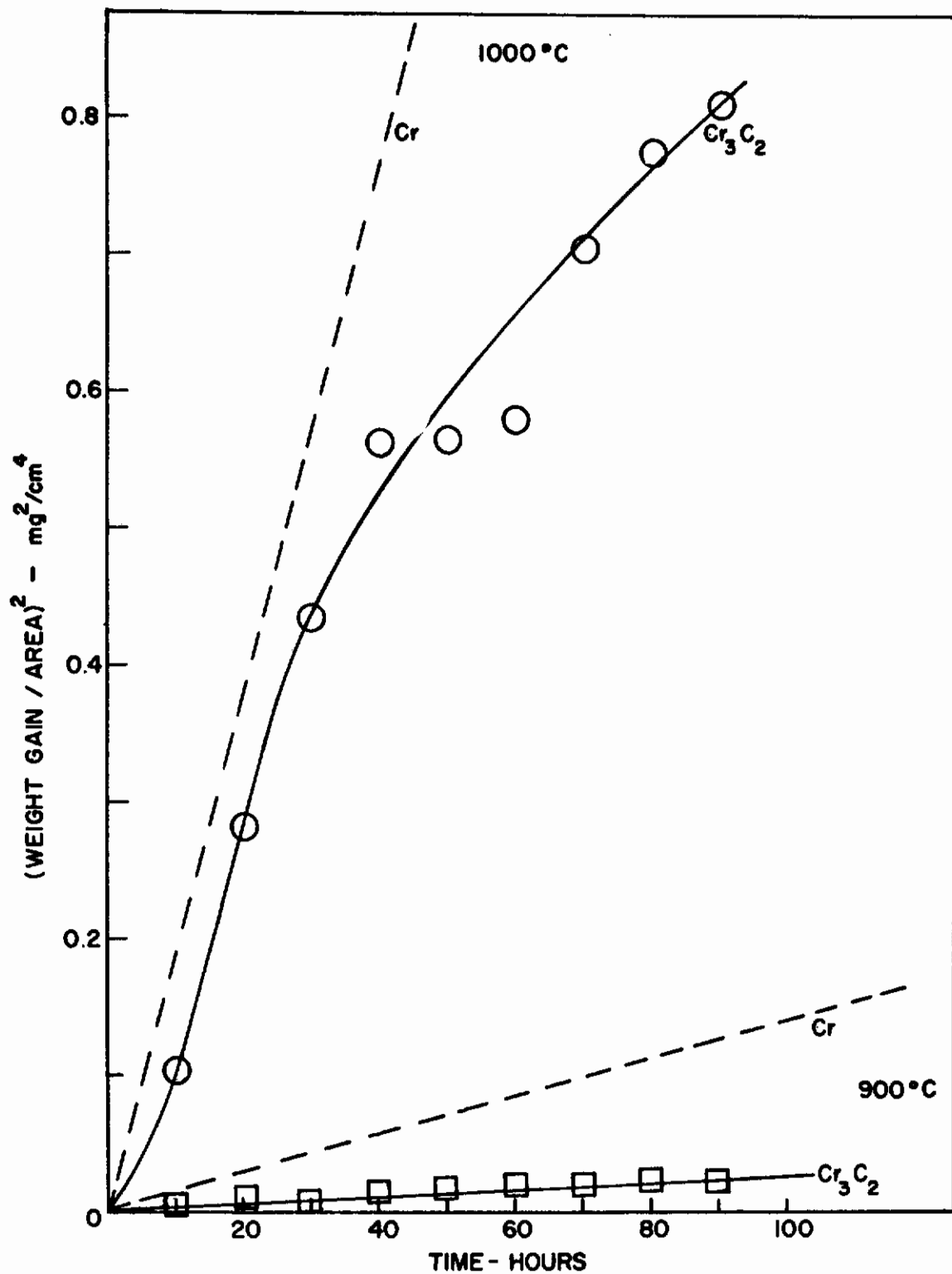
60

FIGURE II-11 PARABOLIC PLOT FOR OXIDATION OF Cr_3C_2 &
Cr IN OXYGEN

61

TABLE 9

SUMMARY OF RESULTS ON Cr_3C_2

Pellet	Original weight after degassing, g	A, cm²	ρ, g/cc	T, °K	P_{O_2}, Torr	Flow rate, cc/min	Weight change, g	CO(g) formed, g	CO_2(g) formed, g	Time, min	C consumed	(CO/CO_2)expt	Weight change, g/cm²-min x 10⁵
X-23	0.5839	1.220	6.40	1662	8.9	58.6	+0.0014	0.0042	0.0030	121	0.0026	1.40	0.949
X-21	0.5819	1.220	6.36	1771	8.7	58.6	-0.0013	0.0013	0.0006	120	0.00072	2.16	-0.887
VII-24	0.5695	1.202	6.44	1776	3.8	51.5	-0.0494	-	-	80	-	-	-51.3
VII-23	0.5851	1.219	6.42	1847	8.5	51.5	-0.0773	-	-	197	-	-	-32.2
X-19	0.5697	1.219	6.24	1869	8.5	58.6	-	-	0.0017	64	-	-	-
VII-34	0.5539	1.218	5.44	1895	4.0	51.5	-0.0623	0.0234	0.0056	120	0.0115	4.18	-42.6

gives the total number of grams of carbon oxidized in each experiment, calculated from the measured weights of $CO(g)$ and $CO_2(g)$.

For pellet X-23, at 1662°K, if we assume that the only products are $CO(g)$, $CO_2(g)$ and $Cr_2O_3(s)$, then the net weight change is given by the number of grams of oxygen picked up to form $Cr_2O_3(s)$ less the number of grams of carbon lost as $CO(g)$ or $CO_2(g)$. From the data, we calculate, then, that 0.0087 of chromium were consumed in experiment X-23. Thus, the chromium to carbon weight ratio in the product oxides is 3.3, compared to a ratio of 6.5 for the chromium to carbon ratio in Cr_3C_2. Thus, carbon appears to be oxidized preferentially in Cr_3C_2 at 1662°K at an oxygen pressure 8.9 Torr. X-ray analysis of the oxidized surface revealed the presence of the lower carbide Cr_7C_3, as well as Cr_2O_3. Above 1770°K, the net weight loss is very much larger than the loss in weight due to vaporization of $CO(g)$ and $CO_2(g)$. Therefore, some chromium must obviously enter the vapor, probably as an oxide, but possibly, to some extent, as the metal, which subsequently becomes oxidized in the gas phase. The experimental CO/CO_2 ratio in the product gas stream is very much smaller than the equilibrium ratio over a Cr_2O_3-Cr_3C_2 mixture. This is probably due to oxidation of $CO(g)$ in the vapor.

(h) Molybdenum Carbide, MoC

Neither thermodynamic data nor kinetic data are available for the monocarbide of molybdenum, and insufficient data is available for calculation of activities over the Mo_2C phase. One might guess that the oxidation behavior of MoC should be very much like that of WC.

(i) Tungsten Carbide, WC

Table 10 gives, in successive columns, the free energy of formation of WC[2], the activity of W over carbon rich WC, the free energies of formation of $CO(g)$,[3] $CO_2(g)$,[3] and $WO_2(s)$,[25] and the equilibrium pressures of $CO(g)$ and $CO_2(g)$ for the interaction between $WO_2(s)$ and $WC(s)$. Even at temperatures as low as 700°C, it is clear that $WO_2(s)$ is not thermodynamically stable in the presence of $WC(s)$, and high pressures of $CO(g)$ and $CO_2(g)$ are expected at the alloy/oxide interface. The same conclusion obtains for $WO_3(s)$ in contact with $WC(s)$.

63

TABLE 10

ACTIVITY OF W OVER WC-C AND THERMODYNAMIC DATA FOR $WC-WO_2$

$T, °K$	$\Delta F_{f,WC}$	a_W	$\Delta F_{f,CO}$	$\Delta F_{f,CO_2}$	$\Delta F_{f,WO_2}$	P_{CO}	P_{CO_2}
1000	-8,700	1.260×10^{-2}	-47,859	-94,628	-97,350	5.904	19.72
1100	-8,660	1.910×10^{-2}	-49,962	-94,658	-93,250	33.25	99.54
1200	-8,620	2.701×10^{-2}	-52,049	-94,681	-89,150	1.393×10^{2}	3.758×10^{2}
1300	-8,580	3.622×10^{-2}	-54,126	-94,701	-85,050	4.666×10^{2}	1.153×10^{3}
1400	-8,540	4.643×10^{-2}	-56,189	-94,716	-81,050	1.285×10^{3}	2.904×10^{3}
1500	-8,500	5.79×10^{-2}	-58,241	-94,728	-77,050	3.083×10^{3}	6.456×10^{3}
1600	-8,460	7.006×10^{-2}	-60,284	-94,739	-73,100	6.546×10^{3}	1.282×10^{4}
1700	-8,420	8.291×10^{-2}	-62,315	-94,746	-69,150	1.270×10^{4}	2.333×10^{4}
1800	-8,380	9.627×10^{-2}	-64,337	-94,750	-65,250	2.259×10^{4}	3.935×10^{4}
1900	-8,340	11.01×10^{-2}	-66,349	-94,751	-61,400	3.758×10^{4}	6.186×10^{4}
2000	-8,300	12.41×10^{-2}	-68,353	-94,752	-57,600	5.902×10^{4}	9.162×10^{4}

64

Data on the oxidation of WC(s) were reported in the original paper of Webb, Norton, and Wagner,[1] and are reproduced in Figure 12. Linear oxidation behavior was found at 700° and 1000°C. A comparison of the observed weight changes with the measured carbon loss as CO(g) or CO_2(g) indicated stoichiometric oxidation behavior (i.e. for every atom of carbon converted to oxide, an atom of tungsten was also converted). The principal tungsten oxide formed seemed to be the yellow WO_3(s). No evidence was found for the presence of WO_2(s), the principal oxide formed on pure tungsten in the same temperature range. The rate of oxidation of the carbide is higher than that for the pure metal under comparable conditions, due, perhaps, to rupture of a potentially protective oxide film by evolution of CO(g) and CO_2(g).

4. CONCLUSIONS

For the highest carbides of the metals of Groups IV-A, V-A, and VI-A of the periodic table, calculations have been made of the pressures of carbon monoxide and carbon dioxide over an equilibrium mixture of metal carbide and the corresponding metal oxide. Table 11 summarizes the practical results. The carbides considered are listed in groups of three in column 1 and their melting points are tabulated in column 2. On the basis of melting point alone, one is justified in considering all of the refractory carbides (except for Cr_3C_2) for applications up to 2500°C. ZrC is potentially useful up to at least 3000°C, NbC and TaC up to 3500°C, and HfC up to at least 3800°C. In the presence of oxygen, however, not a single one of the pure carbides holds any promise of displaying oxidation resistance above 2000°C. In fact, only ZrC and HfC have the potential of sustaining a protective metal oxide film at temperatures above 1250°C.

In column 3 of Table 11, the oxides which commonly form on the surface of the pure metals at high temperatures are listed. If the same oxides were to form on the carbide surfaces, reaction between the oxide and carbon in the alloy substrate might result in the formation of CO(g) and CO_2(g) in sufficient quantities to rupture the oxide film. On the assumption that equilibrium is established in finite time at the carbide/oxide interface, the pressures of CO(g) and CO_2(g) to be expected at the phase boundary can be calculated from known thermodynamic data. In column 4, the temperatures are listed at which
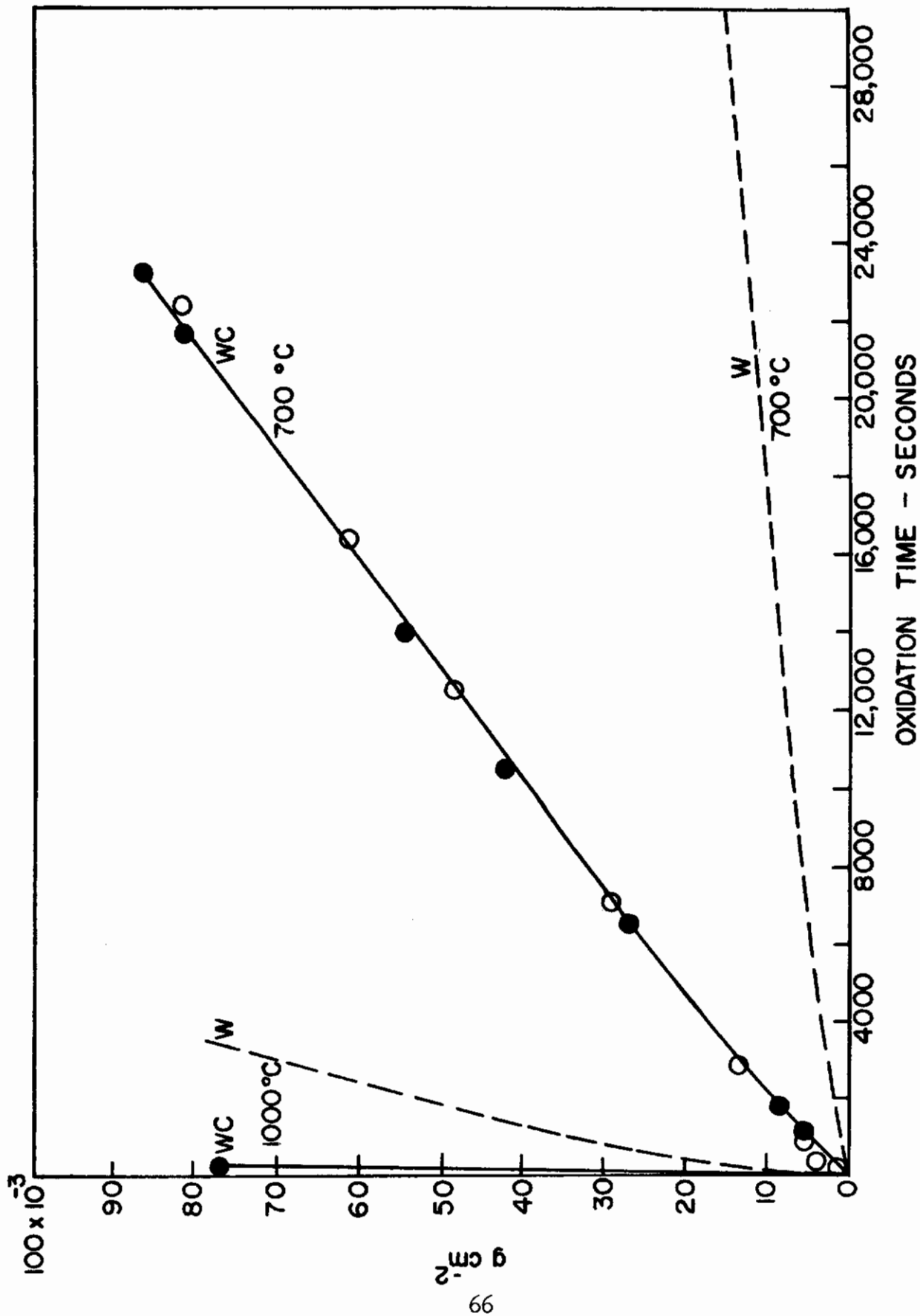
65

FIGURE II-12   LINEAR PLOT FOR OXIDATION OF WC & W IN OXYGEN

TABLE 11

POTENTIALITY OF CARBIDES FOR OXIDATION RESISTANCE

Carbide	Melting Point	Most common oxide formed on the metal during oxidation	Maximum temperature of stability of oxide on carbide, °C
IV-A			
TiC	3140	TiO_2 (rut)	1230
ZrC	3540	ZrO_2	>1730
HfC	4160	HfO_2	1730
V-A			
VC	2810	V_2O_3	1230
NbC	ca. 3900	NbO_2	830
TaC	3880	Ta_2O_5	1030
VI-A			
Cr_3C_2	1890	Cr_2O_3	1130
MoC	-	MoO_2	-
WC	2870	WO_2	730

67

the sum of the pressures, $p_{CO} + p_{CO_2}$, for the oxide in column 3 in equilibrium with the carbide of column 1, become approximately equal to one atmosphere. Above these temperatures an oxide film would be ruptured by evolution of $CO(g)$ and $CO_2(g)$ and would therefore not serve as an effective diffusion barrier to protect the carbide surface against rapid oxidation. If equilibrium is established at the carbide/oxide interface, and the chances are good that it will be established rapidly particularly as the temperature of interest increases, then the temperatures in column 4 are really maximum temperatures at which the pure carbide can be used in oxygen-containing atmospheres. Thus, it would be fruitless to try to improve the oxidation resistance of TiC at 2000°, for example, by improving the adhesion between $TiO_2(s)$ and the substrate. For ZrC, on the other hand, it might be worthwhile to learn to grow dense, coherent, non-porous films of ZrO_2, and to bond them in some way to alloy. Such films do not grow naturally on ZrC, but if they could be formed, they should be thermodynamically stable to above 2000°C, and could make it possible to use ZrC in oxidizing atmospheres for high temperature applications.

The extent of reaction between oxide and carbide to form the volatile oxides of carbon defines an upper limit for the usefulness of carbides in oxidizing atmospheres, provided of course, that phase boundary equilibrium is established. If there is a kinetic barrier to the attainment of equilibrium at the carbide/oxide interface, then the carbide may be stable in oxygen at higher temperatures than the ones given in column 4 of Table 11. Interaction between oxide and carbide might be slow, for example, if the metal-carbon or metal-oxygen bonds can be broken only with great difficulty. Alternatively, a slow reaction might be due to a steric barrier at the interface to the formation of the activated complex intermediate between reactants and products.

While failure to reach equilibrium might force an upward revision of some of the temperatures of maximum stability given in column 4, the more usual situation is that, for a number of reasons, the carbides will react rapidly with oxygen at temperatures below the listed ones. The oxidation of TiC can be described by a parabolic rate law up to 1000°C, but it has not been studied above 1230°C where rupture of the rutile surface film should occur. ZrC appears to oxidize according to a linear rate law at temperatures above 450°C.

68

Thus, ZrC displays none of the oxidation resistance that would be predicted on the basis of the thermodynamic stability of $ZrO_2(s)$ over ZrC. The reason is undoubtedly that the $ZrO_2(s)$ film which forms on the surface of ZrC is porous and non-adherent. HfC, on the other hand, should be investigated in further detail, since both the WNW criteria, and the preliminary experimental work that was done in our laboratory suggest that a protective oxide film might be formed up to high temperatures.

All of the Group V-A carbides oxidize more rapidly than the corresponding pure metals, even at temperatures as low as 800°C. This again is probably due more to the morphology of the oxide film than to the rupture of a potentially protective film by gas evolution.

The oxidation behavior of the Group VI-A carbides is substantially as predicted on thermodynamic grounds. Cr_3C_2 shows excellent oxidation resistance up to at least 1000°C, and in fact, oxidizes somewhat less rapidly than pure metallic chromium. Above 1300°C, the green $Cr_2O_3(s)$ no longer protects the carbide surface from oxidation, and $CO(g)$ and $CO_2(g)$ are evolved in substantial quantity. WC oxidizes linearly at 700°C and above, at a rate higher than that for the pure metal.

From the point of view of understanding carbide oxidation, further work is needed on $CO(g)$ and $CO_2(g)$ evolution, as well as net weight change, in the neighborhood of the temperatures of maximum stability given in Table 11. In the temperature range where parabolic behavior is in evidence, oxidation studies should be made on C^{14} enriched carbides to determine whether carbon dissolves in the oxide lattice during the course of oxidation. Better thermodynamic data for the activity of metal and carbon across the homogeneity range of the carbides of interest would permit more accurate calculations and predictions.

From the point of view of application, HfC is the only refractory hard metal carbide that holds any promise in oxygen above 1400°C, where the steels begin to fail. The other carbides would have to be protected with coatings. ZrC might be protected with ZrO_2, if it could be applied satisfactorily, and if the phase transition did not destroy its effectiveness. The other carbides would have to be protected with oxides or mixtures of oxides of foreign

69

elements; VC for example cannot be protected by V_2O_3 at 1500°C, no matter what the morphology of the oxide is. Thus, from thermodynamic considerations, a selection can be made of the useful directions for kinetic and coating studies.

(1) W. W. Webb, J. T. Norton, and C. Wagner, J. Electrochem. Soc. 103, 112 (1956).

(2) O. Kubaschewski and E. Ll. Evans, "Metallurgical Thermochemistry," Pergamon, N. Y. (1958).

(3) JANAF Thermochemical Tables, U.S. AF 33(616)-6149, prepared by D. R. Stull, Project Director for Dow Chemical Co., Midland, Michigan.

(4) G. N. Lewis and M. Randall, "Thermodynamics," revised by K. S. Pitzer and L. Brewer, McGraw-Hill, N. Y. (1961).

(5) E. Nikolaiski, Z. Physik. Chem. (Frankfort), 24, 405 (1960).

(6) A. Münster, Z. für Elektrochemie 63, 807 (1959).

(7) G. V. Samsonov and N. K. Golubeva, Zhurnal Fizicheskoi Khimii 30, 1258 (1956).

(8) W. Kinna and O. Rüdiger, Archiv. für das Eisenhütten 24, 535 (1953).

(9) N. F. Macdonald and C. E. Ransley, Powder Metallurgy (London) 3, 172 (1959).

(10) W. Kinna and W. Knorr, Z. Metallk. 47, 594 (1956).

(11) A. E. Jenkins, J. Inst. of Metals, 84, 1 (1955).

(12) J. A. Coffman, G. M. Kibler, and T. R. Riethof, NP-9791 (1960).

(13) D. R. Stull and G. C. Sinke, "Thermodynamic Properties of the Elements," American Chemical Society, Washington, D. C. (1956).

(14) R. W. Bartlett (Univ. of Utah, 1961), Dissertation Abstr. 22 (11), 3973 (1961-62).

15) G. Feick, Technical Documentary Report No. ASD-TDR-62-204 Part I, Aeronautical Systems Division, Wright-Patterson Air Force Base, Ohio, April, 1962.

(16) P. Schwarzkopf and R. Kieffer, "Refractory Hard Metals," Macmillan Co., N. Y. (1953).

(17) O. Kubaschewski and B. E. Hopkins, "Oxidation of Metals and Alloys," Academic Press, N. Y. (1962).

(18) D. E. Thomas and E. T. Hayes, "The Metallurgy of Hafnium," U.S. At. En. Comm.

(19) K. K. Kelley, Contributions to the Data on Theoretical Metallurgy, Bureau of Mines Bulletin 584 (1960).

(20) W. Watt, G. H. Cockett, and A. R. Hall, Metaux 28, 222 (1953).

(21) W. D. Klopp, C. T. Sims, and R. I. Jaffee, Trans. Amer. Soc. Metals 51, 282 (1959).

(22) G. L. Miller, "Tantalum and Niobium," Academic Press, N. Y. (1959).

(23) Supplied by Technical Research Group, Yonkers, N. Y.

(24) T. Ya. Kosolapova and G. V. Samsonov, Russian J. of Phys. Chem. 35, 175 (1961) English Translation.

(25) E. G. King, W. W. Weller, and A. U. Christensen, Thermodynamics of Some Oxides of Molybdenum and Tungsten, Bureau of Mines Report of Investigations, R. I. 5664 (1960).

KINETICS OF OXIDATION OF REFRACTORY METALS AND ALLOYS
AT 1000°-2000°C

SECTION III - OXIDATION OF MOLYBDENUM SILICIDES

1. INTRODUCTION

A summary of the experimental work on the oxidation of molybdenum silicides completed under the present contract and reported in ASD-TDR-62-203[1] and in our Quarterly Report No. 8[2] is included in this section. Misprints and errata that have been found in the latter report are corrected in this one.

2. ISOTHERMAL MEASUREMENTS OF EXTENT OF OXIDATION vs TIME

Curves of total oxygen consumption per unit initial sample surface area at temperatures between 1300° and 2100°K are given for Mo_3Si, Mo_5Si_3 and $MoSi_2$ in Figures 1, 2, and 3, respectively. The curves can be fitted approximately by an equation of the form:

$$Q = Q_o (1 - e^{-\alpha t})$$

where Q is total oxygen consumption per unit area up to time t, and Q_o and α are temperature and composition dependent parameters. Values of Q_o and α calculated from the experimental data are given in Table 1 for each of the molybdenum silicides. The initial oxidation rate is given by $(Q_o \alpha)$, since for short times t, $Q \approx Q_o \alpha t$. The maximum oxygen pick-up after infinite time is Q_o. From the point of view of experimental measurement, the larger the value of α, the more rapidly is the limiting rate approached.

For each of the silicides, Q_o decreases with increasing temperature between 1300° and 2000°K, and α increases. That is, the higher the temperature, the more rapidly is a protective glass built up on the silicide surface, and the lower are both the net weight loss and the total oxygen consumed. Although the final limiting rates are as low for Mo_3Si and for Mo_5Si_3 as for $MoSi_2$ at the highest temperatures the net extent of oxidation prior to formation of a

73
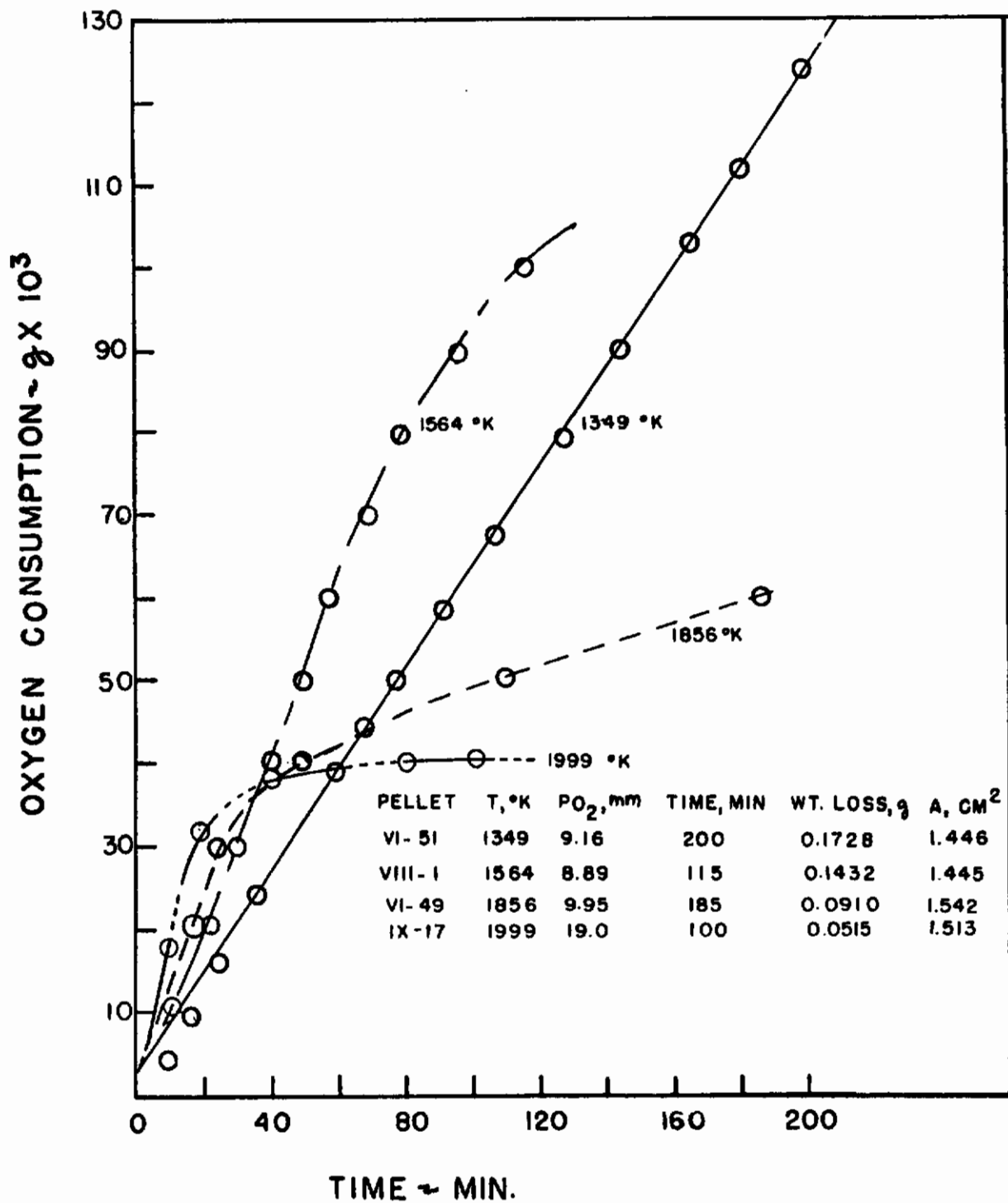
FIGURE III – I   OXIDATION OF Mo_3Si AS A

FUNCTION OF TEMPERATURE

74
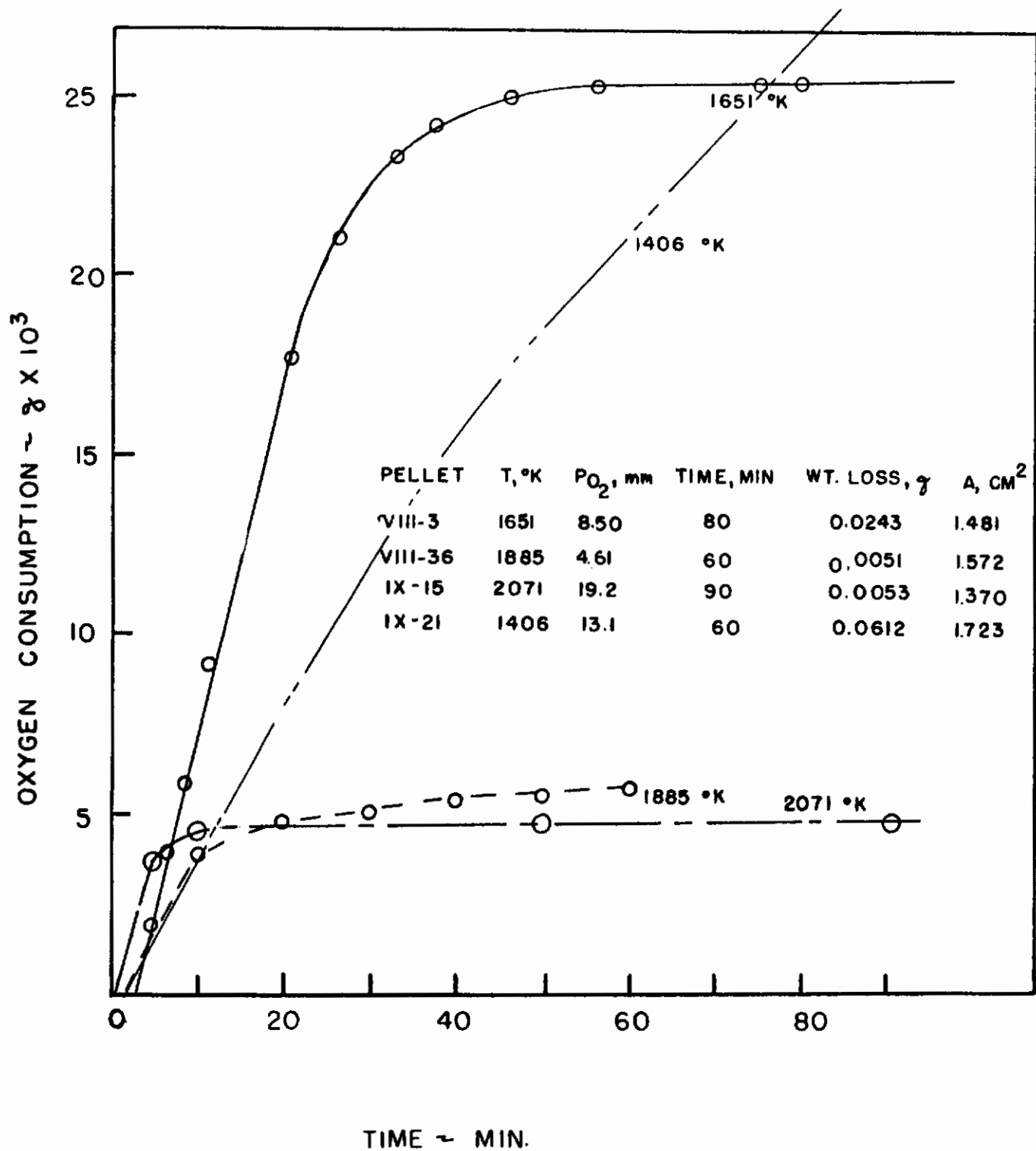
FIGURE III – 2   OXIDATION OF Mo_5Si_3

75

PELLET	T, °K	P_{O_2}, mm	TIME, MIN	WT. LOSS, g	A, CM^2
VIII-11	1303	11.58	185	0.0056	1.849
VIII-7	1627	8.08	90	0.0002	1.573
IX-19	1917	15.2	70	0.0003	1.561
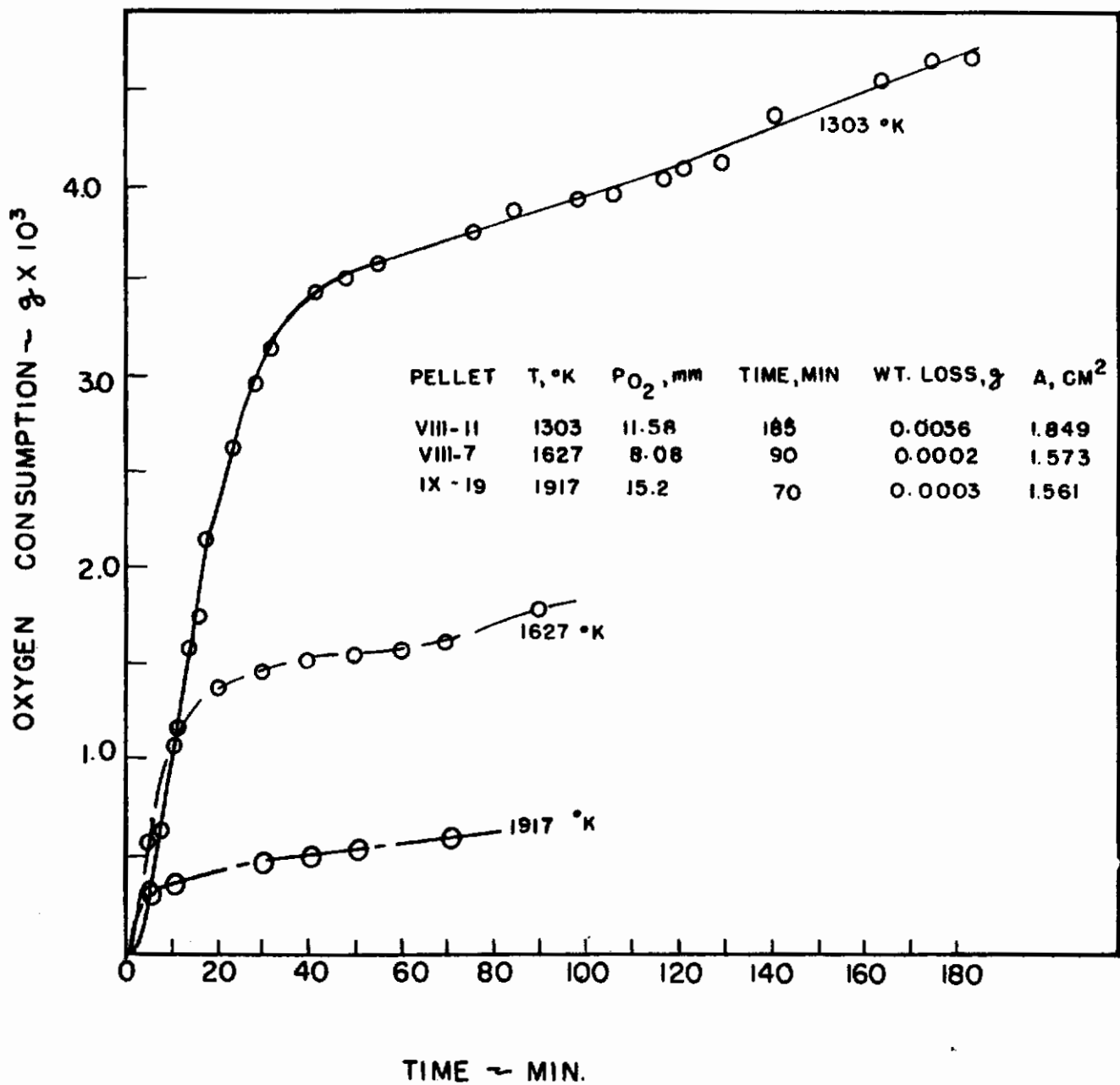
FIGURE III-3   OXIDATION OF MoSi$_2$

76

TABLE 1

EMPIRICAL EQUATION FOR THE OXIDATION OF MOLYBDENUM SILICIDES

$$Q = Q_o (1 - e^{-\alpha t})$$

Material	T, °K	$Q_o \times 10^5$, g/cm^2	α, min^{-1}	$Q_o \alpha \times 10^5$, g/cm^2-min
Mo$_3$Si	1349	-	-	66
	1564	10,000	0.009	90
	1856	4,340	0.036	156
	1999	2,740	0.085	233
Mo$_5$Si$_3$	1406	5,000	0.009	45
	1651	1,740	0.106	184
	1885	370	0.043	16
	2071	348	0.30	104
MoSi$_2$	1303	384	0.019	7.3
	1627	118	0.159	19
	1917	39	0.54	21

protective film is highest for Mo_3Si, less by a factor of about six for Mo_5Si_3, and reduced by another factor of about six for $MoSi_2$.

Figure 4 shows the oxidation of $MoSi_2$ at 2000°K, where the condensed oxide is almost certainly a liquid. A protective oxide layer has indeed formed, but five times more oxide has been consumed prior to the bend than at 1627°K, and the protection does not last. A sudden increase in oxidation rate occurs after about 100 minutes, followed by the re-establishment of a protective layer.

3. PRESSURE DEPENDENCE OF OXIDATION RATE

At sufficiently low oxygen partial pressures, a protective glass will not be stable in contact with the molybdenum silicides due to vaporization of $SiO(g)$ according to the reaction:

$$\tfrac{1}{2} Si(a_{Si}) + \tfrac{1}{2} SiO_2(s) = SiO(g) \tag{III-1}$$
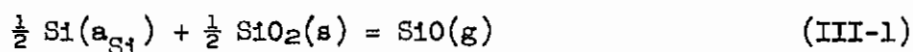
where a_{Si} is the activity of silicon in the silicide alloy. The importance of reaction (1) in the oxidation of silicon alloys was pointed out by Wagner.[3] Oxygen molecules striking a silicide surface are expected to react rapidly, particularly at high temperatures. Therefore, the oxygen pressure at the alloy/gas interface, p_{O_2}, will be very much less than the oxygen pressure in the bulk of the gas phase, $p^\circ_{O_2}$. The rate of transport of oxygen towards the silicon surface, under the concentration gradient created by the reaction, is:

$$j' = 2\, D_{O_2}\, p^\circ_{O_2} / \delta_{O_2}\, RT$$

where D_{O_2} is the diffusion coefficient for oxygen molecules and δ_{O_2} is the effective thickness of the boundary layer for oxygen diffusion. A similar equation obtains for the transport of $SiO(g)$ away from the alloy into the bulk gas. According to Wagner, a steady state will be established in which the transport of oxygen towards the alloy as $O_2(g)$ will exactly balance the transport of oxygen away from the alloy surface as $SiO(g)$. Since the ratio of δ_{SiO} to δ_{O_2} can be expressed in terms of the corresponding gas phase

78
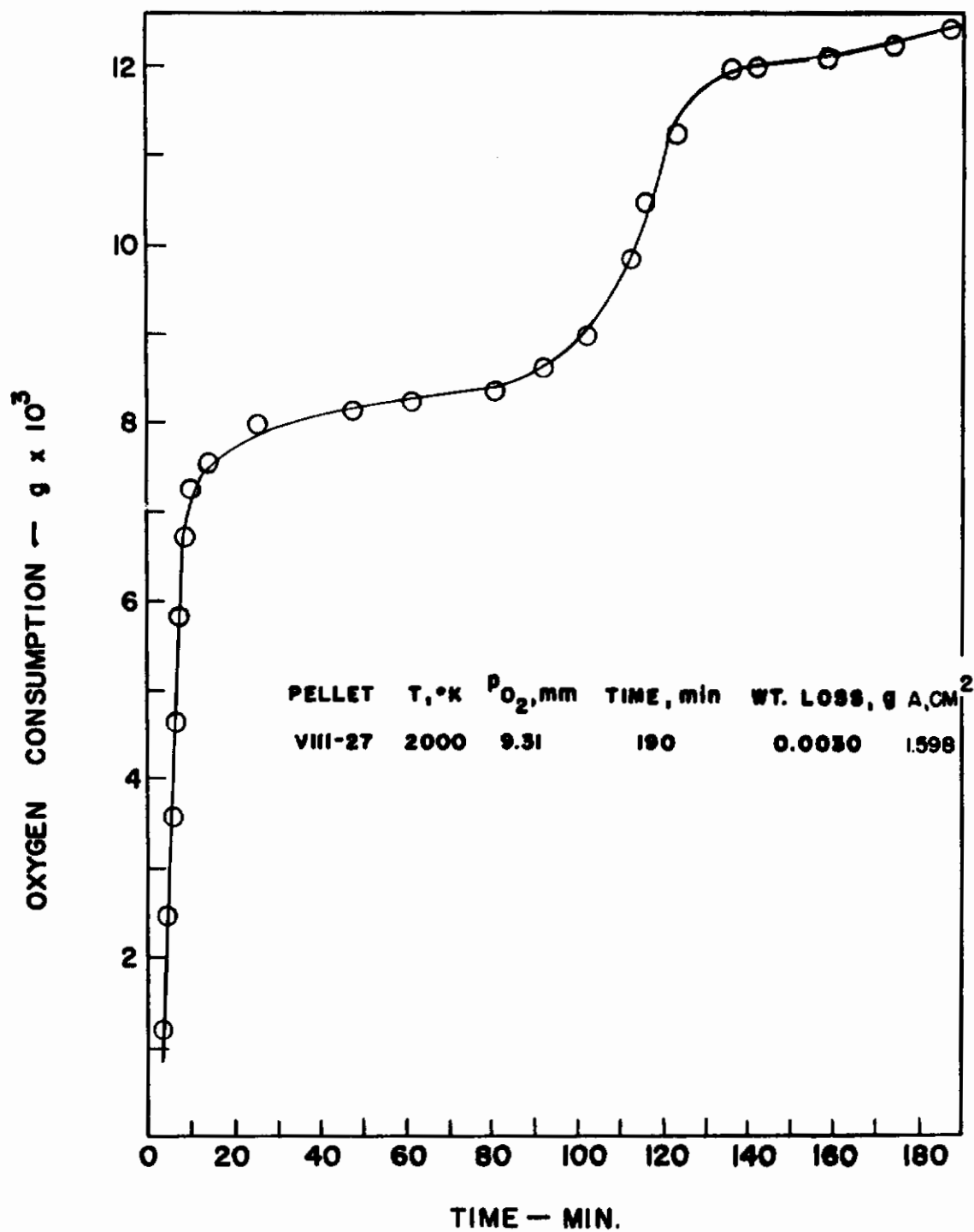
FIGURE III — 4   OXIDATION OF $MoSi_2$ ABOVE THE MELTING POINT OF SILICA

79

diffusion coefficients, one finds a relationship between the $SiO(g)$ pressure at the alloy-gas interface, p_{SiO} and the bulk oxygen pressure, $p_{O_2}^{\circ}$:

$$p_{O_2}^{\circ} = \tfrac{1}{2} \left(\frac{D_{SiO}}{D_{O_2}}\right)^{\frac{1}{2}} p_{SiO} \qquad\qquad (III-2)$$

$SiO_2(s)$ can only form on a silicide surface if p_{SiO} is larger than the equilibrium pressure $p_{SiO(eq.)}$ for reaction (1) at the experimental temperature. Equivalently, from equation (2), $SiO_2(s)$ will be stable on a silicide surface only at ambient oxygen pressures greater than $\tfrac{1}{2}(D_{SiO}/D_{O_2})^{\frac{1}{2}} p_{SiO(eq.)}$. The ratio of diffusion coefficients is approximately 0.64. With a silicon activity of unity at the alloy-gas interface, an ambient oxygen pressure of 4.6 mm should be necessary for formation of an $SiO_2(s)$ layer on the silicide surface at 1400°C. At 1600°C, the calculated oxygen pressure needed for formation of $SiO_2(s)$ is 23 mm. If the silicon activity in the alloy is less than unity (as it generally will be), then the theoretically required oxygen pressures for formation of a protective glass will be lowered correspondingly.

In the course of the present study, an $MoSi_2(s)$ pellet was heated to 1683°C in a flowing stream of helium-oxygen at a total pressure of 760 Torr, oxygen partial pressure of 1.6 Torr. Oxidation was linear over a period of an hour, and there was no evidence for formation of a glassy layer of $SiO_2(s)$ on the silicide surface. The net observed weight loss during the experiment was 0.0116 g, and the total oxygen consumed was 0.00867 g. If the correct oxidation reaction were:

$$MoSi_2(s) + \tfrac{5}{2} O_2(g) \rightarrow MoO_3(g) + 2\ SiO(g)$$
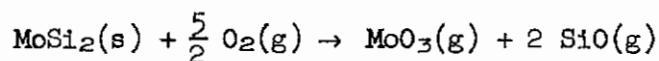
then the ratio of net weight loss to total oxygen consumption would be 1.9. The experimentally measured ratio is 1.3. The discrepancy is probably due to oxidation of $SiO(g)$ in the gas phase to $SiO_2(s)$, which condenses on cool walls in the reaction chamber.

The sharp change in oxidation mechanism at low oxygen pressures was corroborated by Perkins, et. al.,[4] in work on $MoSi_2$ coated molybdenum.

They failed to see a continuous glassy protective oxide at pressures below 5 Torr.

4. METALLOGRAPHIC EXAMINATION OF OXIDE FILMS

(a) Mo_3Si

The surface of an Mo_3Si sample prior to oxidation is shown in Figure 5, and gives evidence for the presence of a second phase, probably the α-solid solution of silicon in molybdenum. Figures 6 and 7 show polished cross-sections of the same sample after oxidation at 1564°K at an oxygen partial pressure of 9 Torr for 115 minutes. In Figure 6a, the second phase is still plainly visible in both substrate and the oxide. The growth of the oxide around the second phase inclusions is clearly seen in Figure 6. This configuration could hardly have been observed unless the oxide grows, at least in part, by diffusion of oxygen inward from the atmosphere towards the oxide-alloy interface. Thus, the α-phase appears to have served as an inert marker during the course of the experiment.

After oxidation, the Mo_3Si pellet was covered with a flaky white oxide, which constituted the bulk of the product. However, the outer scale was not adherent, and much of it was lost during the preparation of the sample for microscopic examination. In Figure 7a, an attempt is made to focus on a portion of the outermost scale separated by a crack from a more adherent oxide. Figure 7c focuses on the subscale once more and indicates the uniform thickness that was obtained over most of the surface of the sample. The clear abrupt break in the oxide layer has not been explained. Figures 7b and 7d, at higher magnification, show the morphology of the subscale -- areas of columnar growth interspersed among apparently amorphous areas. Figure 7e shows a portion of the oxide that has grown into the substrate to a considerable extent.

In Figure 8 photomicrographs of cross-sections of Mo_3Si oxidized at 1856°K are shown. A smooth outer oxide, and an inner columnar one are visible in Figures 8a and 8b. In Figures 8c and 8d, regions of amorphous oxide that have grown around second phase inclusions in the alloy are shown in addition to the smooth and columnar regions.

81
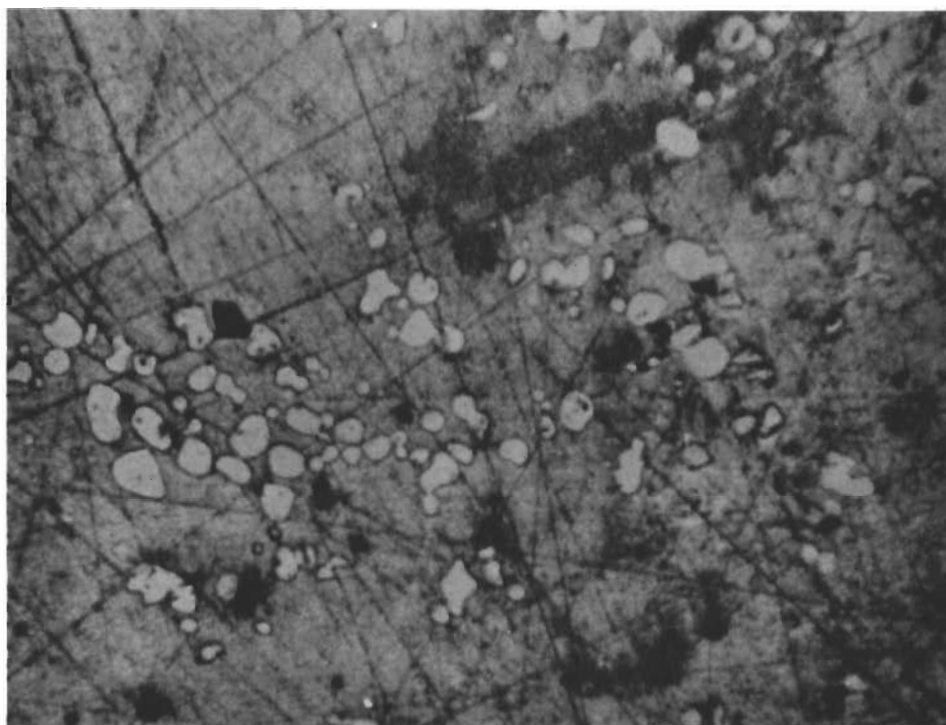
FIGURE III-5   Mo$_3$Si , AS POLISHED, 90X
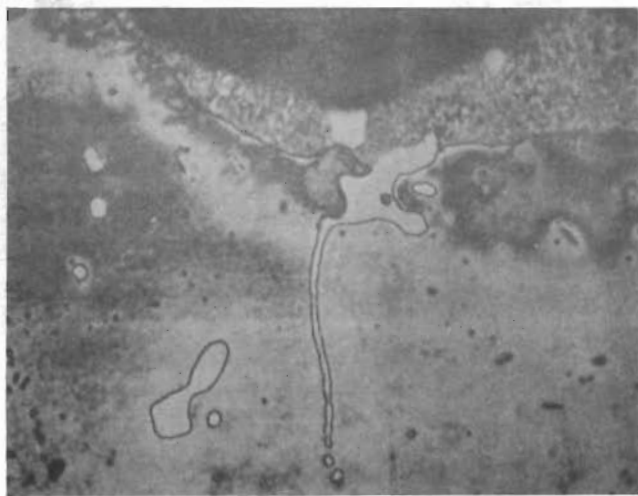
a.
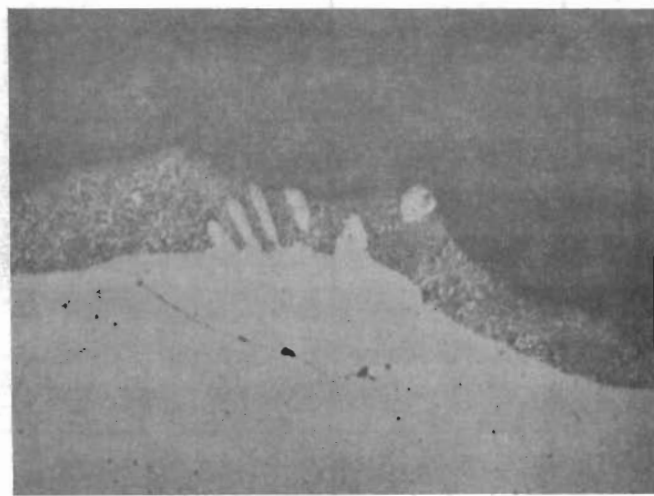
b.
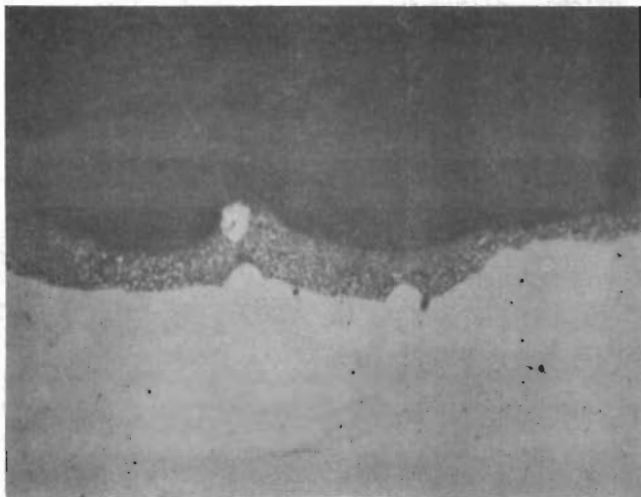
c.
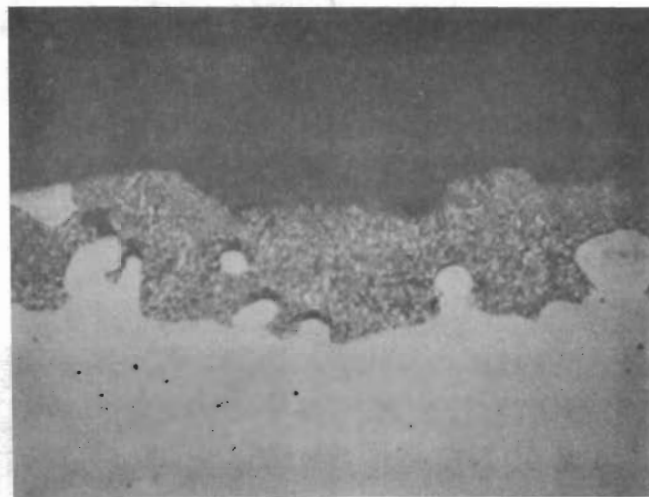
d.

FIGURE III-6   CROSS-SECTIONS OF Mo_3Si OXIDIZED AT 1564°K
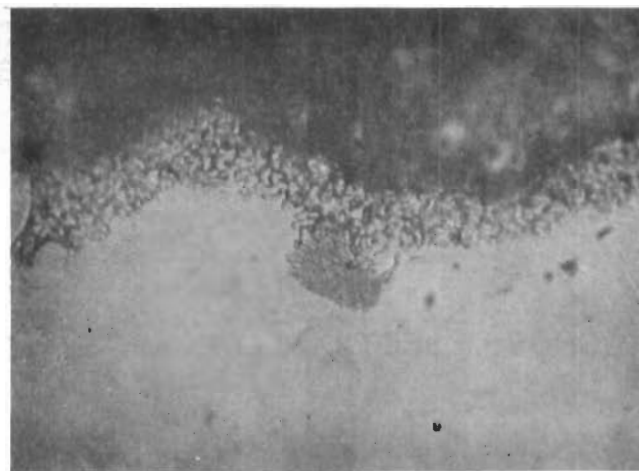   (400X)

83
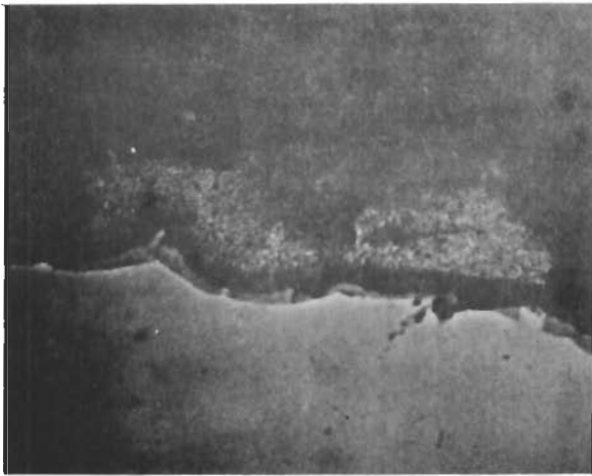
a. 170X
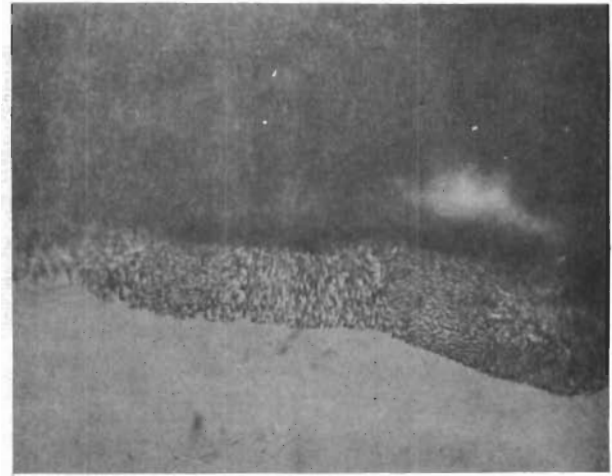
b. 400X

c. 750X
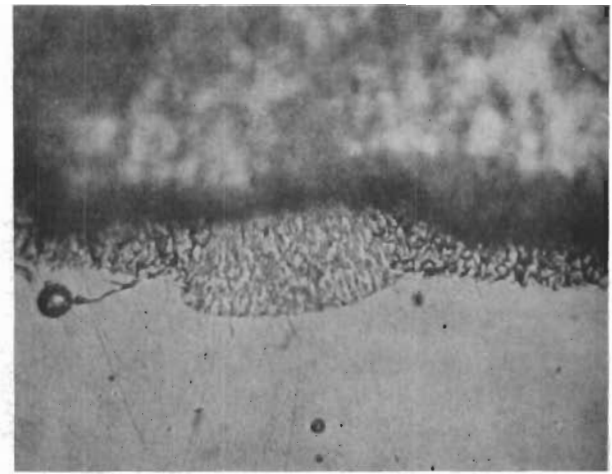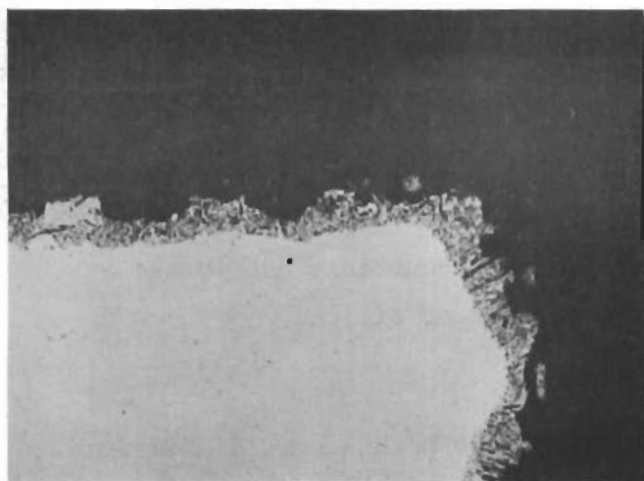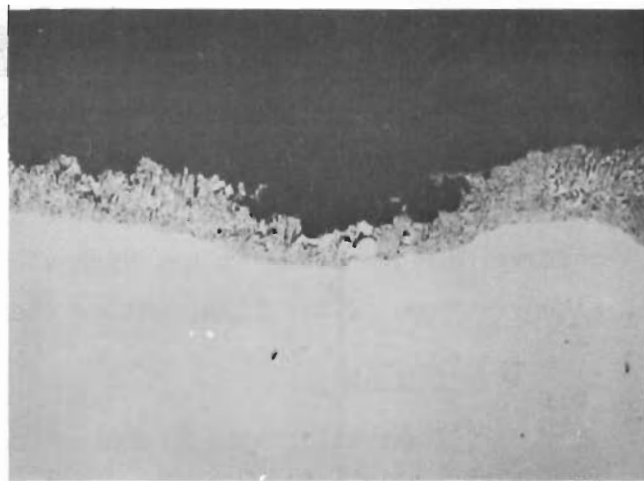

d. 750X

e. 750X
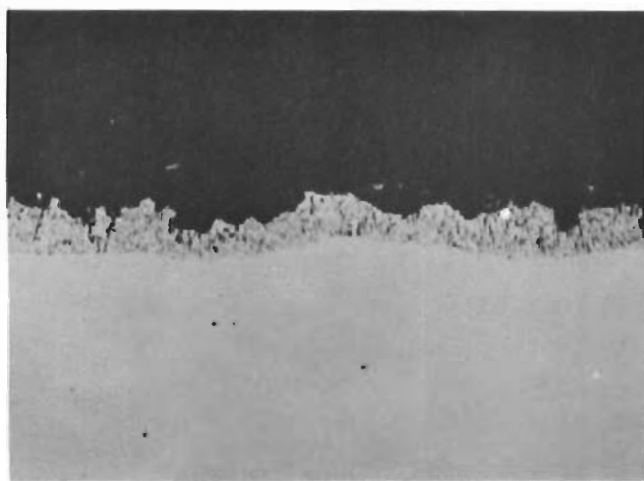
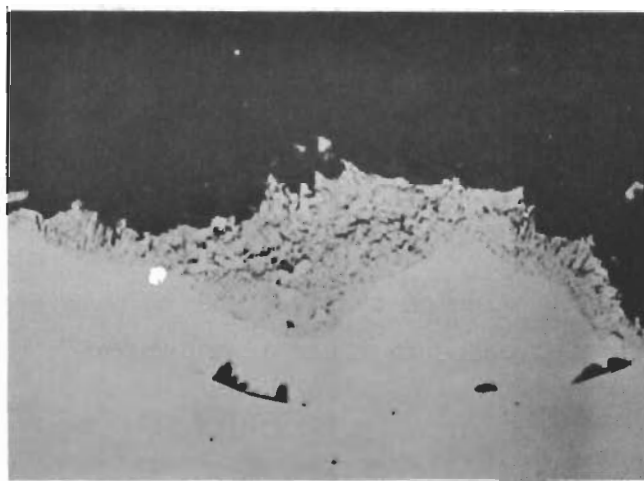FIGURE III - 7   CROSS - SECTIONS OF $Mo_3 Si$ OXIDIZED AT 1564 °K

84

A

C

B

D

FIGURE III — 8   CROSS - SECTIONS   OF   Mo$_3$Si OXIDIZED
AT 1856   °K   (133x)

85

The X-ray patterns of the sample surface after degassing at 1600°C showed lines for molybdenum. After oxidation, the samples exposed at 1349° and 1564°K showed the strongest lines of SiO_2 as well as those of Mo, while the sample exposed at 1856°K showed only the lines for Mo. The failure to observe SiO_2 in X-ray at the highest temperature is undoubtedly due to the glassy nature of the film, rather than to the absence of silica.

(b) Mo_5Si_3

A metallographic examination was made of the Mo_5Si_3 sample oxidized at 1651°K, oxygen pressure of 8.5 Torr. Figure 9a is a view of the sample immediately after sectioning, and before polishing. A thick outer scale and a dense coherent inner one are visible. It is evident that oxidation has been most extensive at the edge of the sample pellet; an originally sharp edge is plainly rounded after reaction. Figure 9b shows the opposite corner, after polishing, at higher magnification. The inner and outer scales are now brought out sharply. The bright layer immediately adjacent to the alloy surface is probably not a separate oxide phase, but belongs to the inner oxide layer. In Figure 9, c and d, both oxide layers can again be seen, and the uniform thickness of the inner scale is striking. The second phase inclusions seem to oxidize at the same rate as the bulk of the sample. It is interesting to note that oxide does not appear to have grown down into all of the cracks in the specimen, even those that intersect the surface.

Photomicrographs of Mo_5Si_3, oxidized at 1885°K are reproduced in Figure 10. Here there appears to be an outer granular oxide, and a layer of smooth oxide growing into the alloy. Figure 10a, particularly interesting, shows the growth of smooth oxide into a crack to a depth identical to that in the surrounding sound alloy.
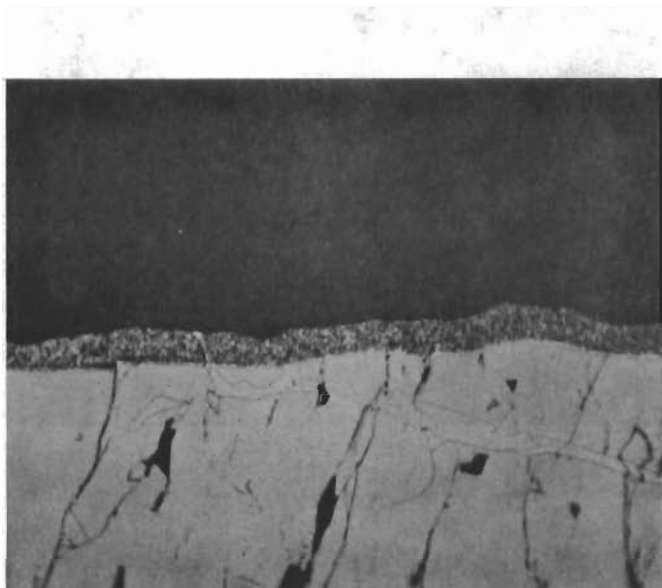
X-ray analysis of the samples after degassing showed the lines for Mo_3Si. After oxidation at 1651°K, a dark glassy layer covered the sample surface, and X-ray lines for SiO_2 and Mo were picked up. At 1885°K, a dark grey glassy layer again covered the surface, and the strongest X-ray lines for Mo, Mo_3Si, and SiO_2 were found.
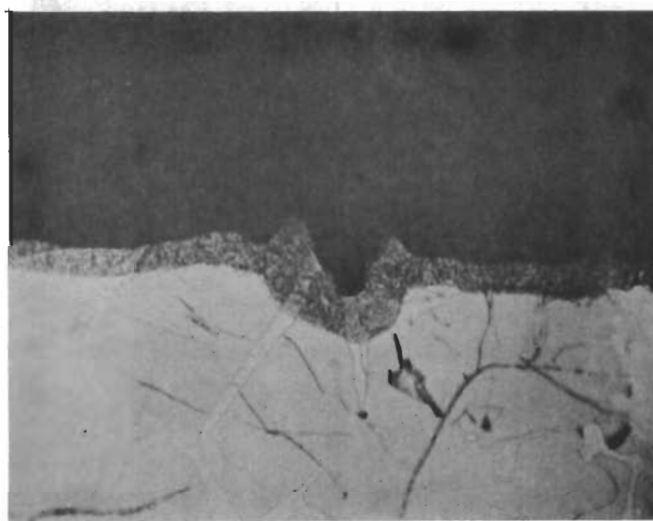
86
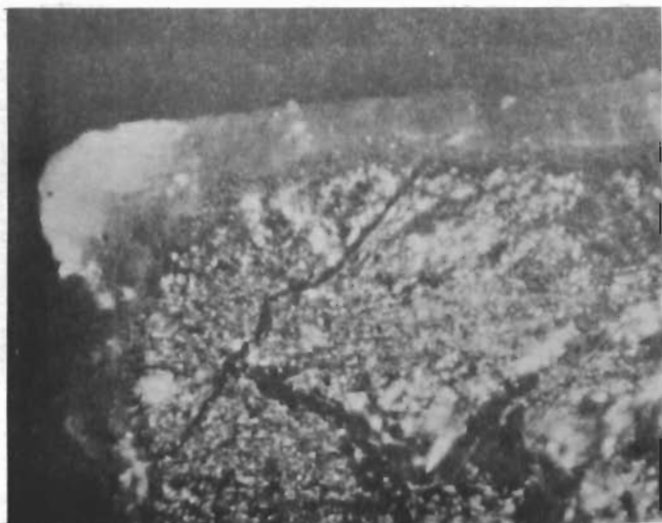
a. 60X
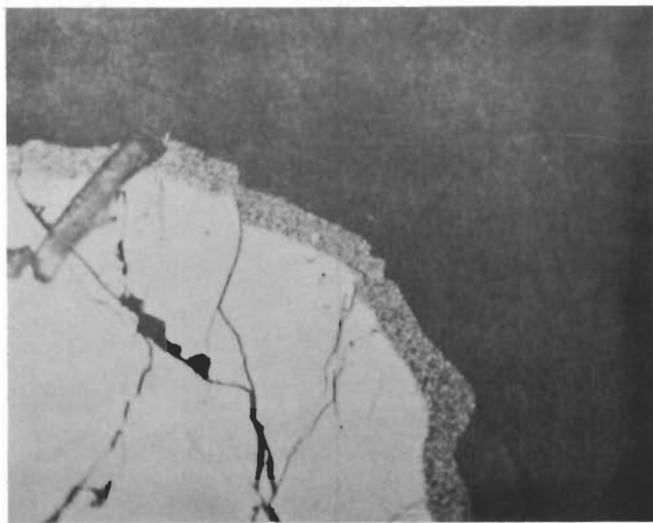
b. 170X
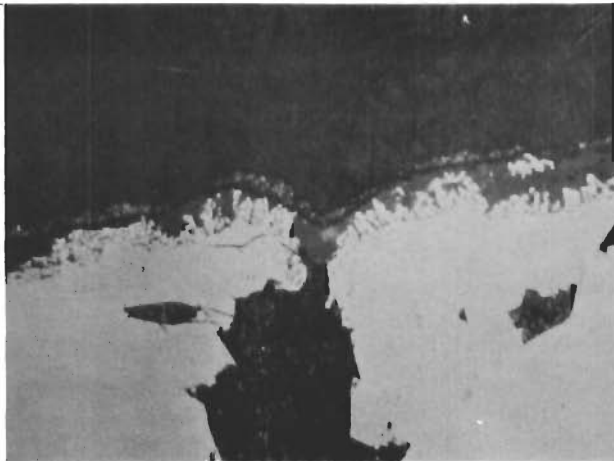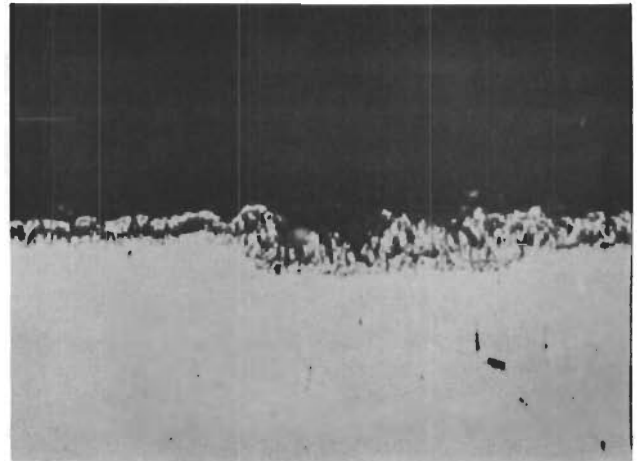

c. 170X

d. 170X

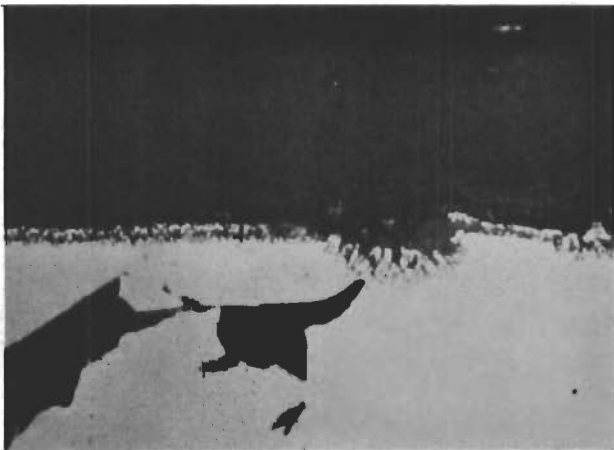FIGURE III- 9   CROSS – SECTIONS OF Mo_5Si_3 OXIDIZED AT 1651°K

87

A   (267x)

C   (267x)

B   (267 x)

D   (800x)

FIGURE III – 10   CROSS-SECTIONS   OF Mo_5Si_3 OXIDIZED
AT   1885   °K

(c) <u>MoSi$_2$</u>

Metallographic examination of the MoSi$_2$ sample oxidized at 1627°K failed to reveal any oxide layer, although the surface of the sample was glassy in appearance, and gave X-ray lines for SiO$_2$, as well as MoSi$_2$ and Mo$_5$Si$_3$. Cross-sections of the oxidized samples are shown in Figure 11. The apparent surface layer does not look like an oxide, and may be a silicon deficient region that develops during degassing. Cracks that seem to intersect the surface show no evidence of having been filled in with oxide.

In Figure 12, photomicrographs of MoSi$_2$ oxidized at 1981°K are shown. In this case, the rate of supply of oxygen was smaller than the reaction rate in the early stages of exposure, and therefore the extent of oxidation prior to formation of a diffusion barrier was higher than usual for this temperature. Regions of smooth oxide and regions of alloy interspersed with oxide grains are seen in both 12a and 12b. In 12b, smooth oxide is seen to partially fill cracks in several places.
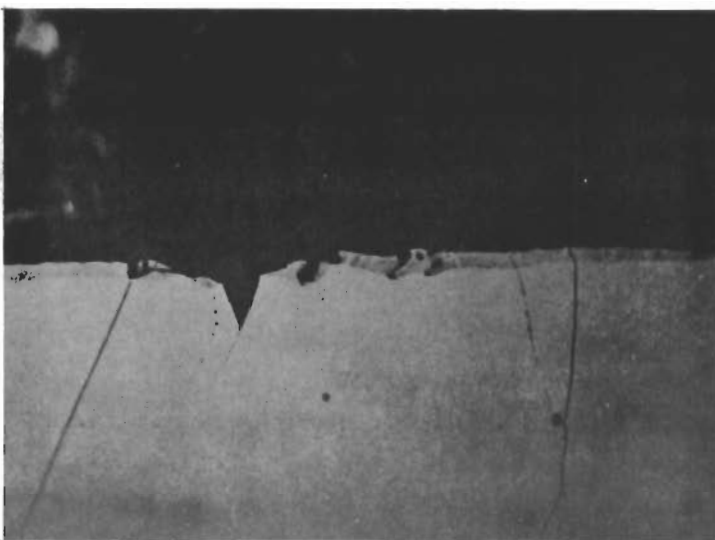
a. 170X

b. 170X

FIGURE III – 11   CROSS–SECTIONS OF MoSi$_2$ OXIDIZED
AT 1627 °K

90

A

B

FIGURE III – 12   CROSS - SECTIONS OF $MoSi_2$ OXIDIZED AT 1981 °K (67x)

91

SECTION III - REFERENCES

(1) J. Berkowitz, Kinetics of Oxidation in the Mo-Si System, Technical
     Documentary Report No. ASD-TDR-62-203 Part I, Aeronautical Systems
     Division, Wright-Patterson Air Force Base, Ohio, May, 1962.

(2) Quarterly Report No. 8, A. D. Little, Inc., to Wright Air Development
     Center, Contract AF 33(616)-6154.

(3) Carl Wagner, J. Electrochem. Soc. 103, 627 (1956).

(4) R. A. Perkins and D. D. Crooks, J. Metals 13, 490 (1961).

KINETICS OF OXIDATION OF REFRACTORY METALS AND ALLOYS
AT 1000°-2000°C

SECTION IV - OXIDATION OF MISCELLANEOUS MATERIALS

1. TUNGSTEN SILICIDES

(a) W_5Si_3

Curves of oxygen consumption vs time for W_5Si_3 at temperatures of 1635°, 1763°, 1871°, and 2001°K are shown in Figures 1-5. At 1635°K, the degree of oxidation was greatest and formation of a protective glass was not apparent. However, since the rate of oxidation did fall from 22.6×10^{-5} g/min-cm^2 after 60 minutes to 12.1×10^{-5} g/min-cm^2 after 120 minutes, a diffusion barrier might be built up in longer exposure times. In Figures 2-5 the oxidation behavior is seen to be approximately independent of temperature. The limiting oxygen pick-up is 4.3 ± 0.9 g/cm^2 in the plateau region. The pattern, familiar from the work on molybdenum silicides, of rapid initial oxidation rate that levels off to an imperceptible value after 40-60 minutes is in evidence. The rates in the final stages are below the limit of detectability of the thermal conductivity method, or less than 10^{-6} g/min.

(b) WSi_2

The oxidation behavior of WSi_2 was studied at 1693°, 1793°, 1902°, and 2030°K with the results shown in Figures 6-9. At the three lower temperatures, curves of the customary form, indicative of protective oxidation, are obtained. Final rates of oxidation were once again too small to be measured. The limiting total oxygen pick-up is 1.1 ± 0.5 g/cm^2. In general, net weight losses and total oxygen consumed were somewhat less for WSi_2 than for W_5Si_3. At 2030°K, the integrated curve of Figure 9 does not show a plateau region. The thermal conductivity curve of oxidation <u>rate</u> vs time at 2030°K clearly shows that the rate of oxidation is initially high, drops rapidly and fluctuates randomly about a low average value. The increases and decreases of oxidation rate in this region may be correlated with a rupture of the glassy film due to evolution of $SiO(g)$, and subsequent repair or
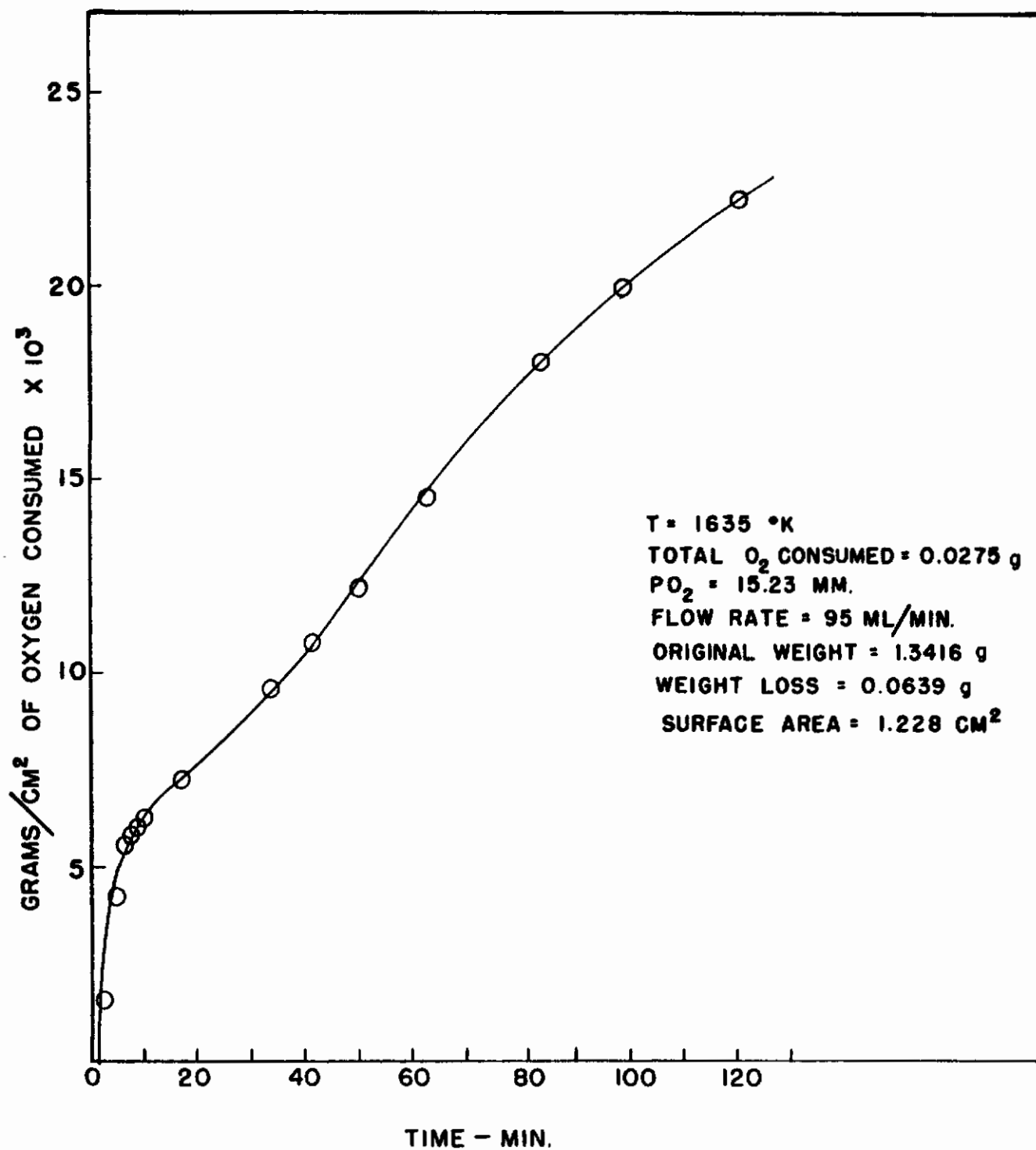
93

FIGURE $\underline{\text{IV}}$ - 1   OXIDATION OF W_5Si_3 (XI-20) AT 1635 °K

94
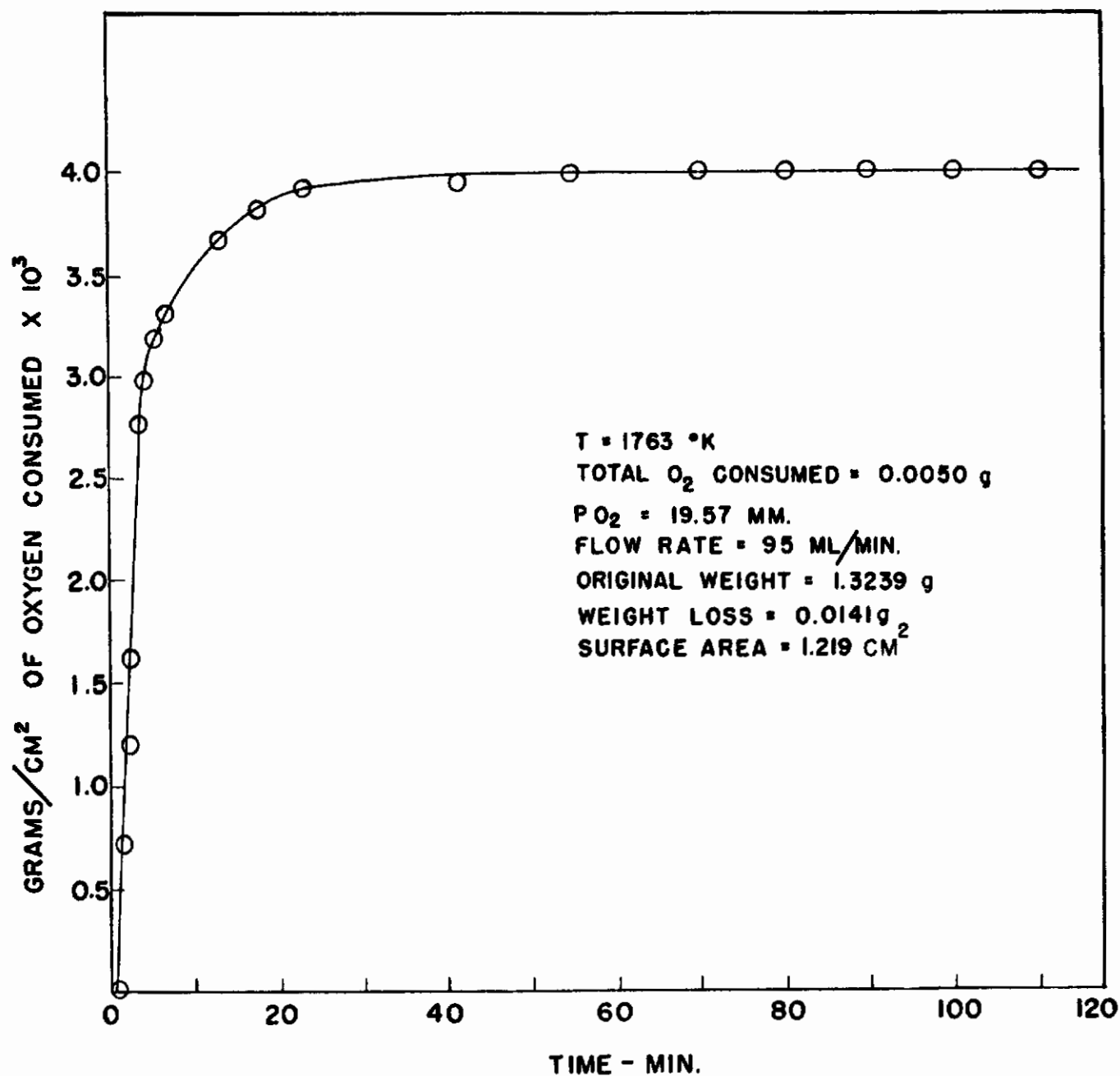
FIGURE IV - 2   OXIDATION OF W_5Si_3 (XI-18) AT 1763 °K

T = 1871 °K
TOTAL O₂ CONSUMED = 0.0091 g
PO₂ = 20 8 MM.
FLOW RATE = 95 ML/MIN.
ORIGINAL WEIGHT = 1.4912 g
WEIGHT LOSS = 0.0163 g
SURFACE AREA = 1.591 CM²
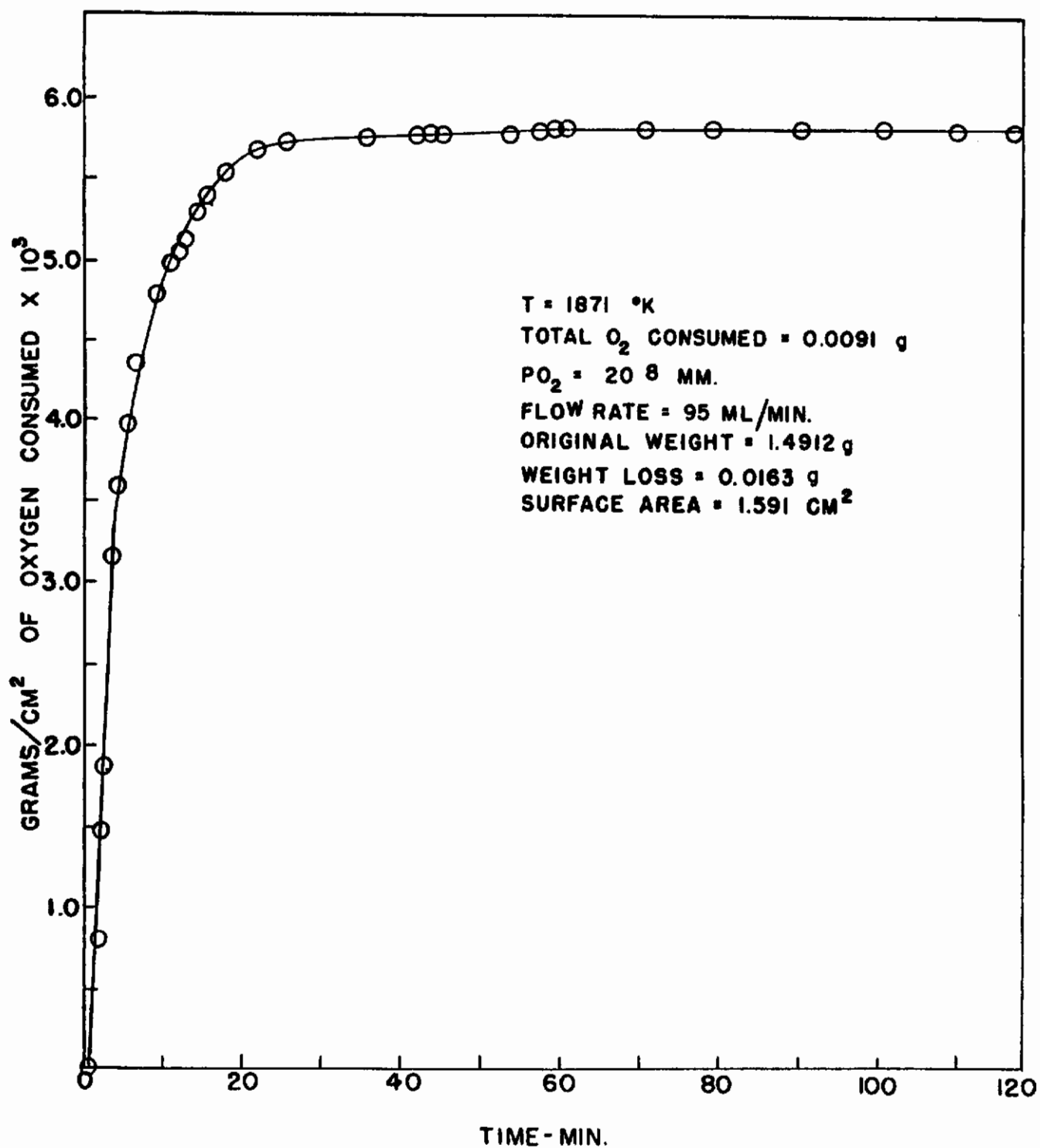
FIGURE IV - 3   OXIDATION OF W₅Si₃ (XI-10) AT 1871 °K

96

T = 1969 °K
TOTAL O_2 CONSUMED = 0.0027 g
PO_2 = 11.8 MM.
FLOW RATE = 95 ML/MIN.
ORIGINAL WEIGHT = 0.9446 g
WEIGHT LOSS = 0.0027 g
SURFACE AREA = 0.974 CM^2
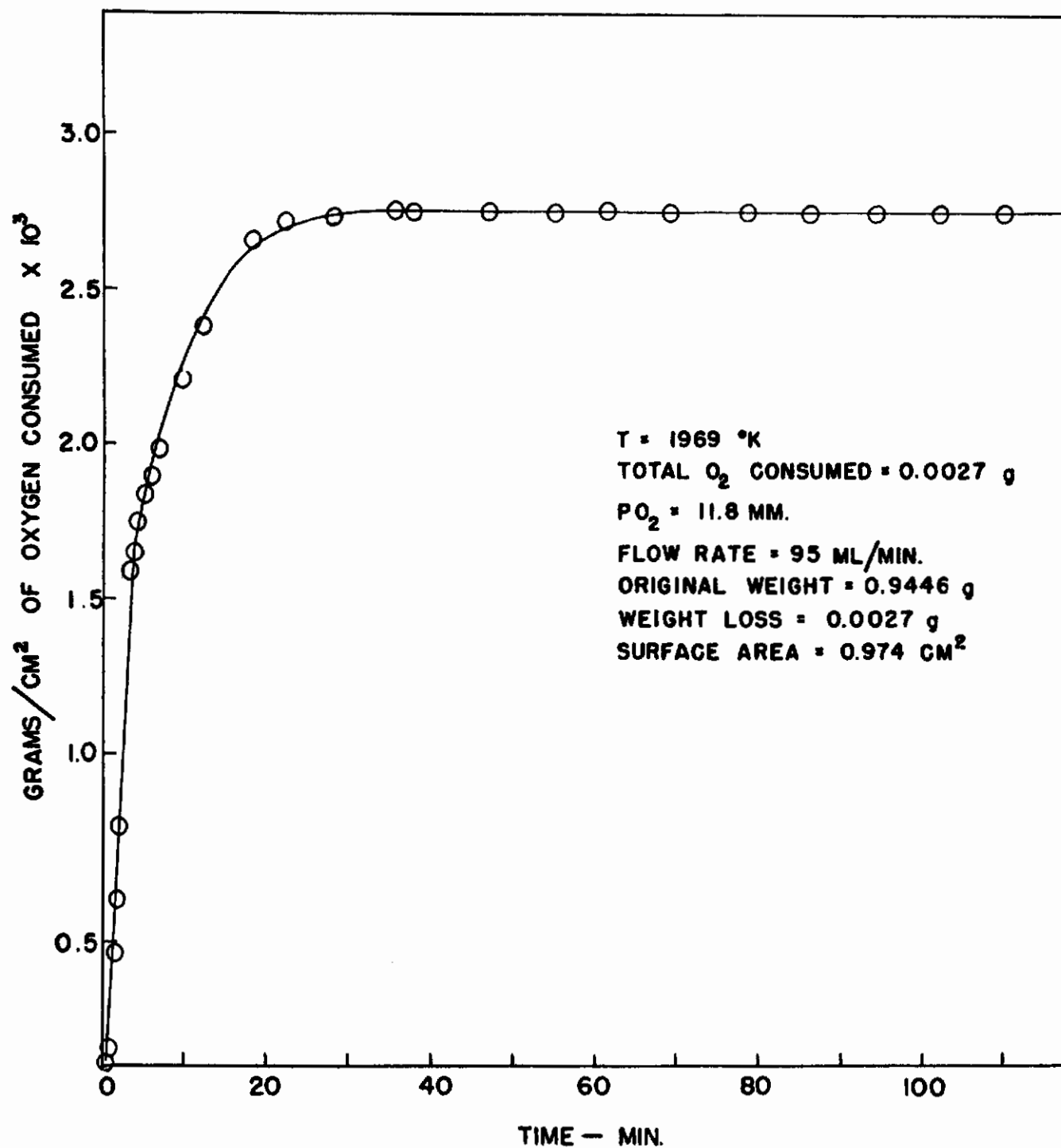
FIGURE IV-4   OXIDATION OF W_5Si_3 (X-32) AT 1969 °K

97

T = 2001 °K

TOTAL O_2 CONSUMED = 0.0065 g

PO_2 = 27.1 MM.

FLOW RATE = 95 ML/MIN.

ORIGINAL WEIGHT = 1.5381 g

WEIGHT LOSS = 0.0166 g

SURFACE AREA = 1.381 CM^2
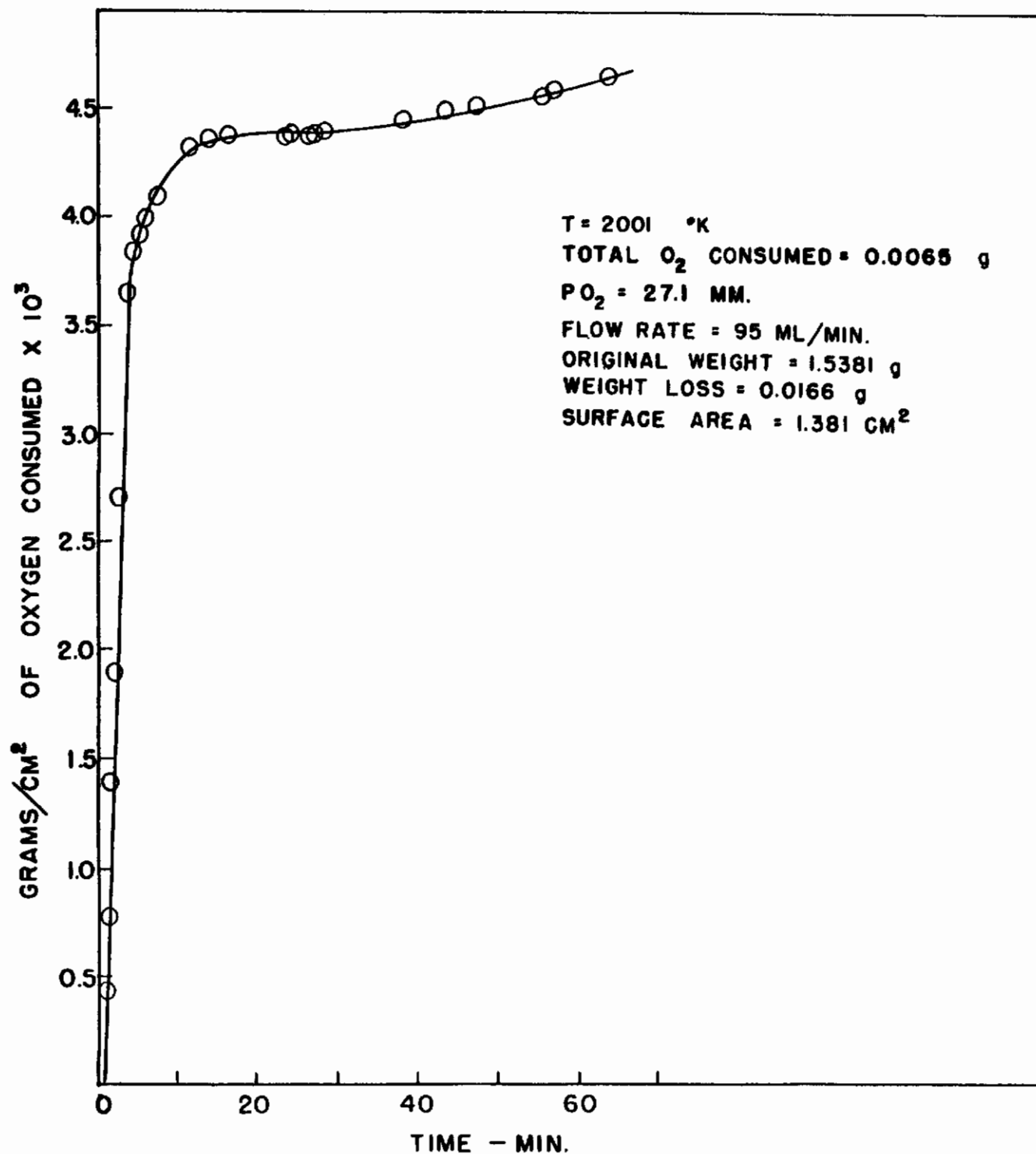
FIGURE Ⅳ-5   OXIDATION OF W_5Si_3 (XI-4) AT 2001 °K

98
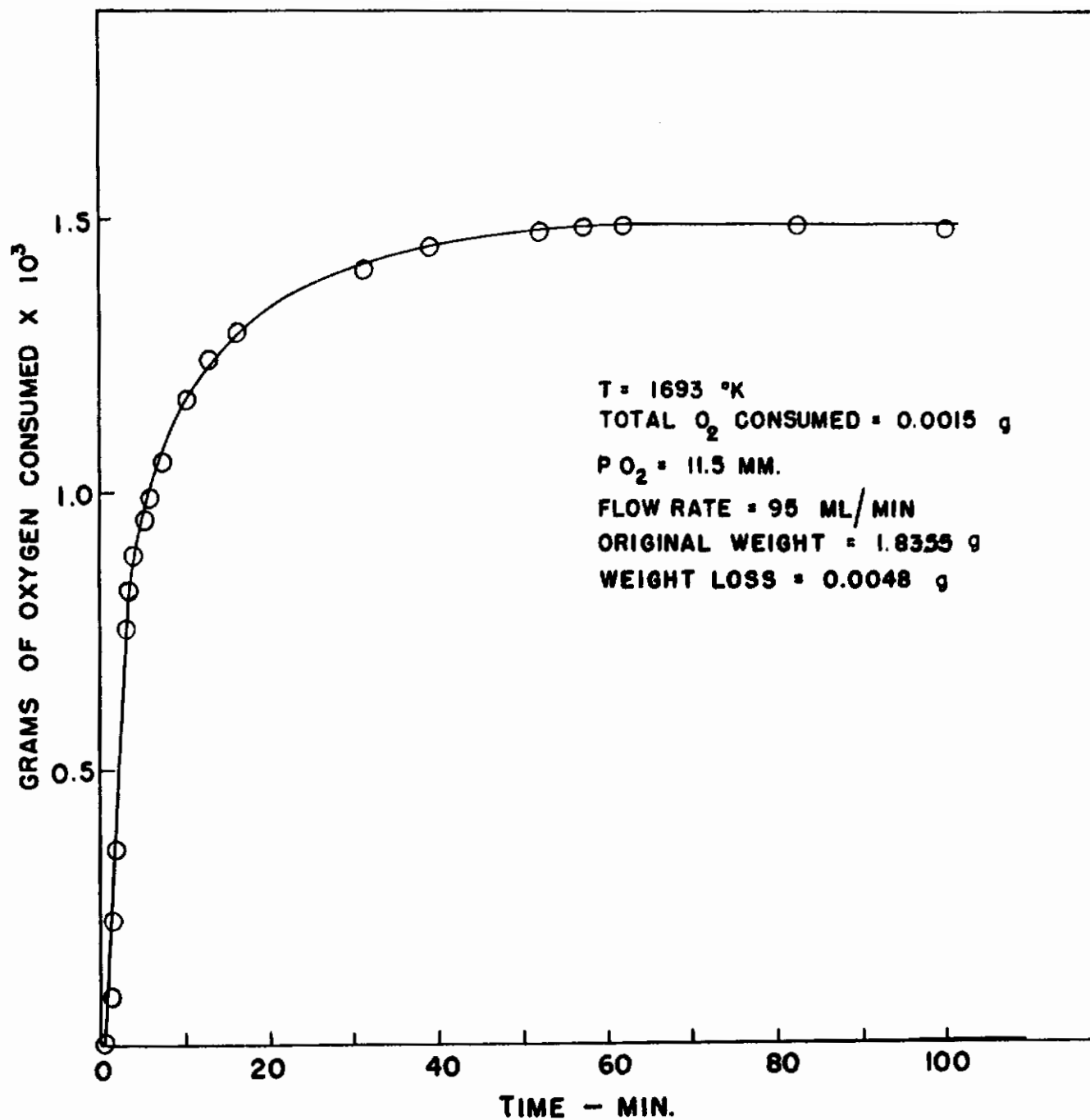
FIGURE Ⅳ-6   OXIDATION OF WSi$_2$ (XI-30) AT 1693 °K

99

T = 1793 °K
TOTAL O_2 CONSUMED = 0.0004 g
PO_2 = 10.4 MM.
FLOW RATE = 95 ML/MIN.
ORIGINAL WEIGHT = 1.0138 g
WEIGHT LOSS = 0.0017 g
SURFACE AREA = 1.309 CM^2
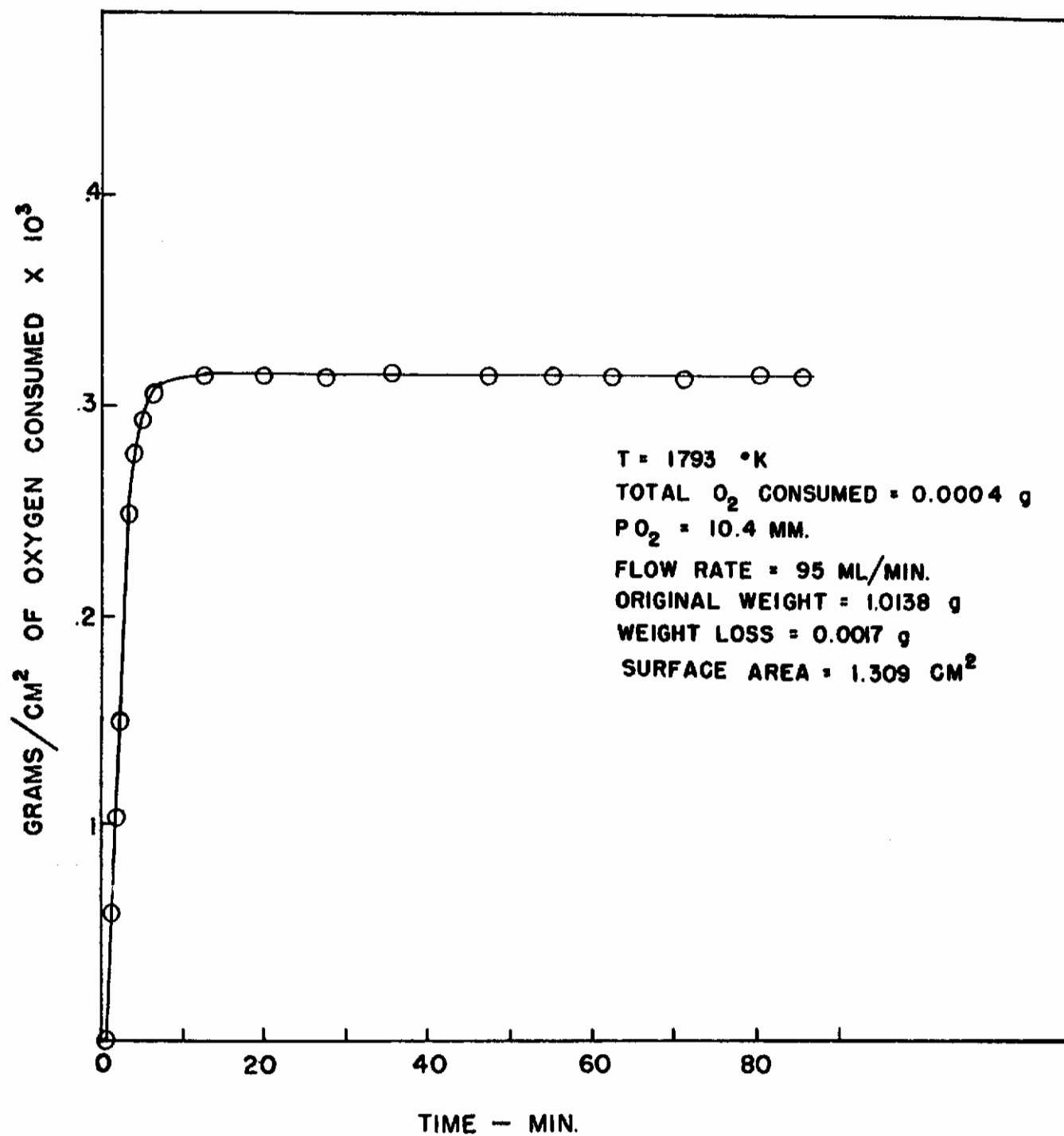
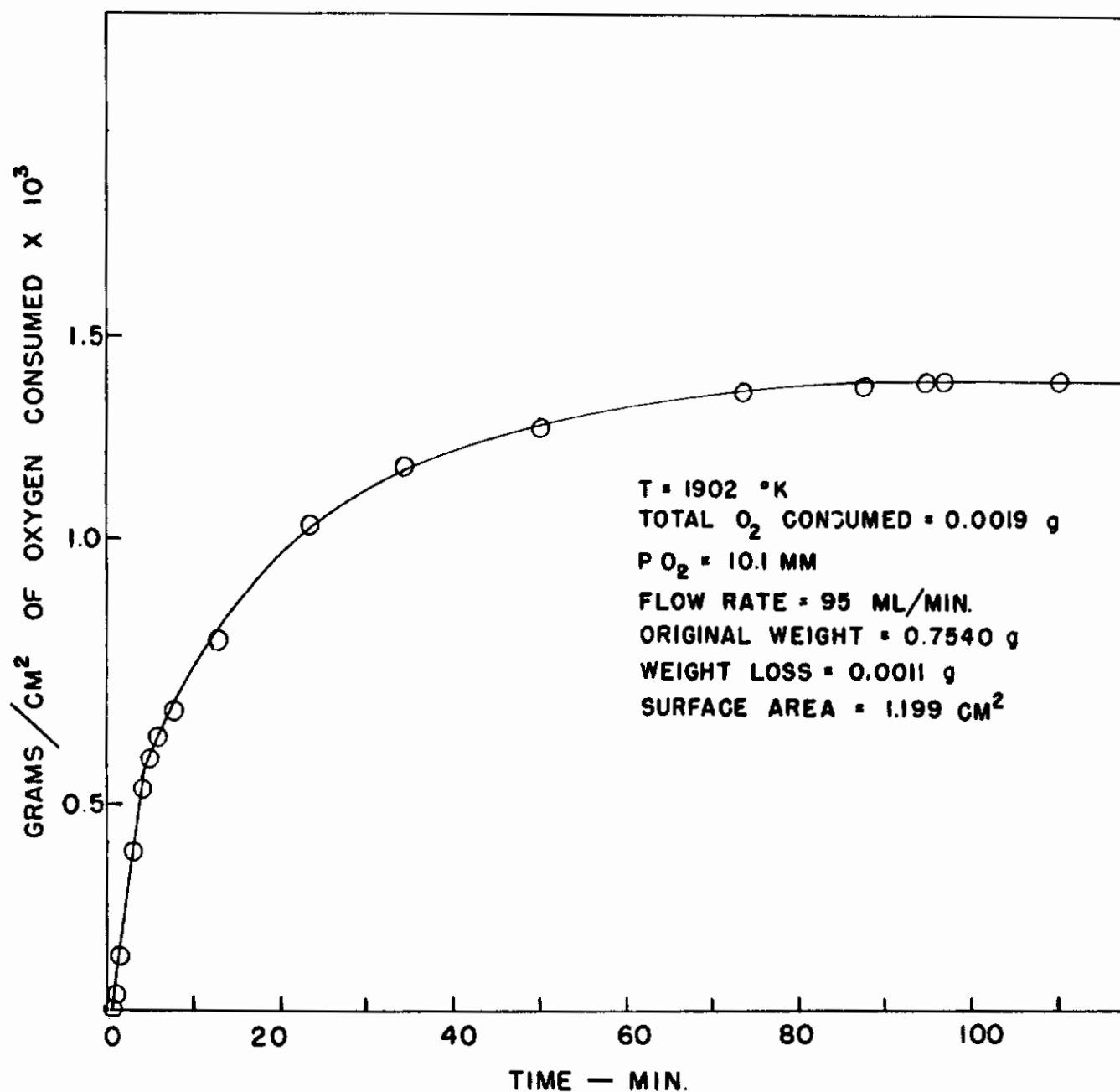FIGURE IV - 7   OXIDATION OF WSi$_2$ (XI-28) AT 1793 °K

100

FIGURE Ⅳ- 8   OXIDATION OF WSi$_2$ (XI-26) AT 1902 °K
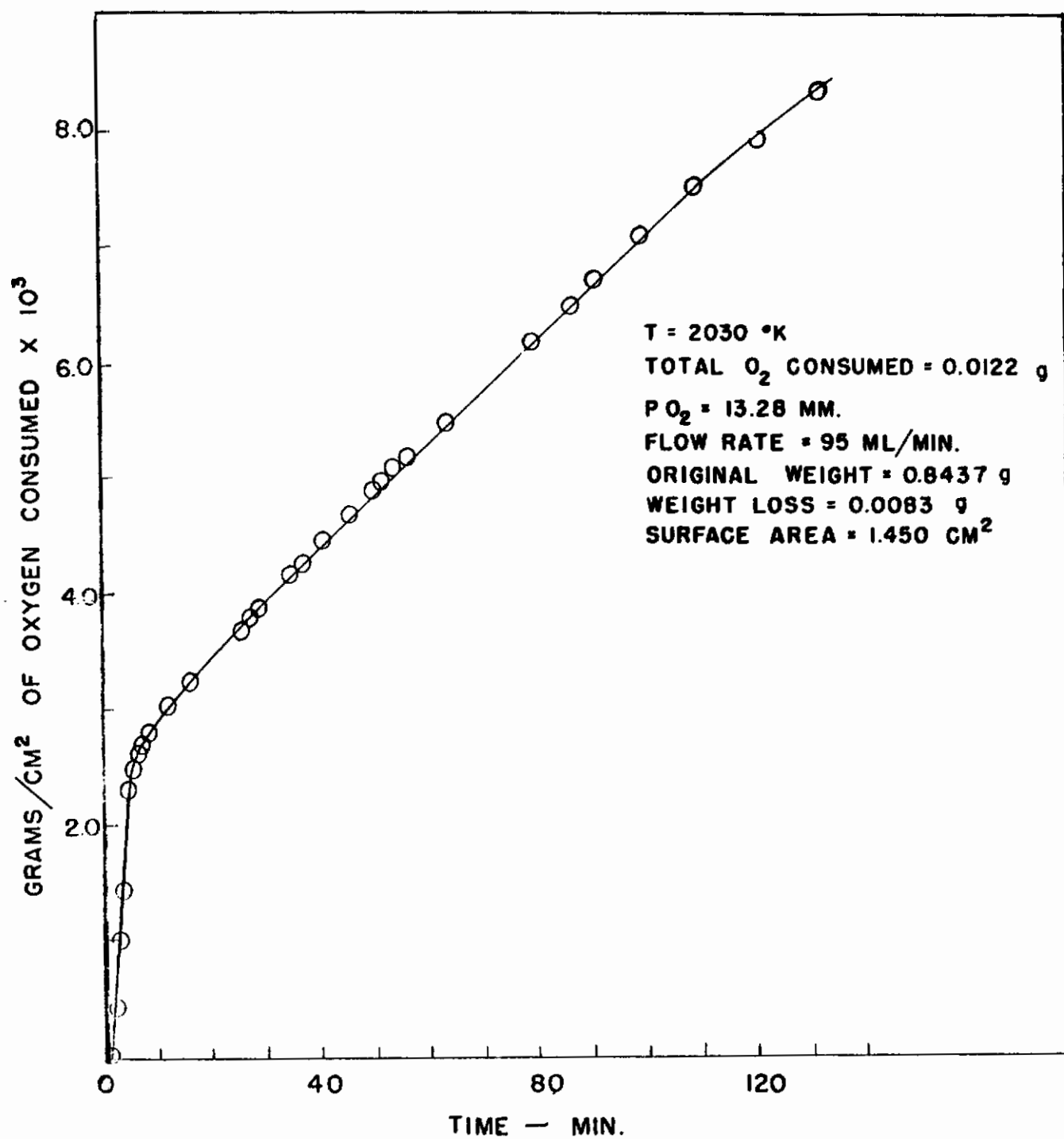
101

FIGURE Ⅳ-9   OXIDATION OF WSi$_2$ (XI-23) AT 2030°K

self-healing. Small brown mushroom-like projections on the surface of the glass after oxidation provide further evidence for this type of mechanism.

(c) Comparison between Molybdenum and Tungsten Silicides

Between 1700° and 2000°K rates of oxygen consumption after one hour's exposure are lower for both W_5Si_3 and WSi_2 than for $MoSi_2$, the most oxidation resistant molybdenum silicide. Net weight changes on oxidation, however, are higher for the tungsten compounds than for $MoSi_2$ under comparable conditions. Previous weight change measurements[1,2] suggested that WSi_2 is inferior in its oxidation resistance to $MoSi_2$. In point of fact, the tungsten compounds are as good or superior to the molybdenum compounds, and the higher weight changes for WSi_2 and W_5Si_3 reflect the higher molecular weight of W and the higher density of the tungsten silicides.

X-ray lines for $SiO_2(s)$ were detected after oxidation of all of the tungsten silicide samples, but were picked up only occasionally for molybdenum silicide samples, when a protective oxide had formed during exposure. The barrier oxide may therefore be more crystalline over W_5Si_3 and WSi_2 than over $MoSi_2$. For $MoSi_2$, total oxidation decreases markedly with increasing temperature, below the melting point of silica. For the tungsten silicides, the temperature dependence is not pronounced.

2. TANTALUM BERYLLIDE, Ta_2Be_{17}

A pellet of Ta_2Be_{17} was kindly supplied by the Brush Beryllium Co.,[3] and a single measurement of oxygen consumption vs time was made at a temperature of 1664°K (assuming an emissivity of 0.6), and an oxygen partial pressure of 8.4 Torr. Results are plotted as oxygen consumption vs time in Figure 10, and as oxygen consumption vs the square root of time in Figure 11. It is clear that the rate of oxidation does decrease with time, and that therefore a protective oxide is probably developing on the beryllide surface as reaction proceeds. However, there is insufficient data to determine definitely whether oxidation becomes diffusion controlled once a sufficiently thick layer of solid oxide has been built up, or whether a rate law slower than the parabolic
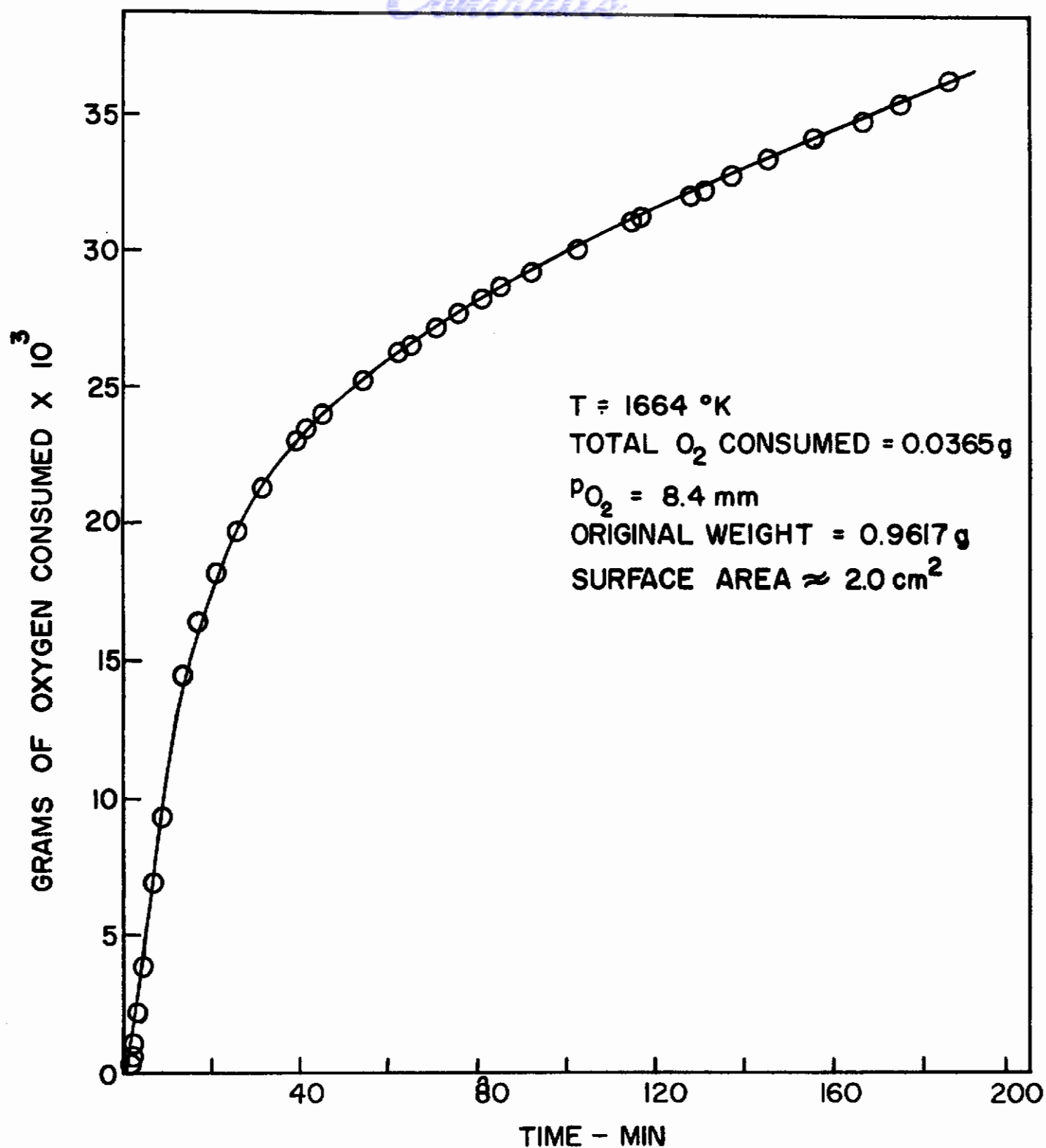
T = 1664 °K

TOTAL O_2 CONSUMED = 0.0365 g

p_{O_2} = 8.4 mm

ORIGINAL WEIGHT = 0.9617 g

SURFACE AREA $\approx$ 2.0 cm^2

GRAMS OF OXYGEN CONSUMED X 10^3

TIME — MIN

FIGURE IV — 10   OXIDATION OF Ta_2Be_{17} (XI-51) AT 1664 °K
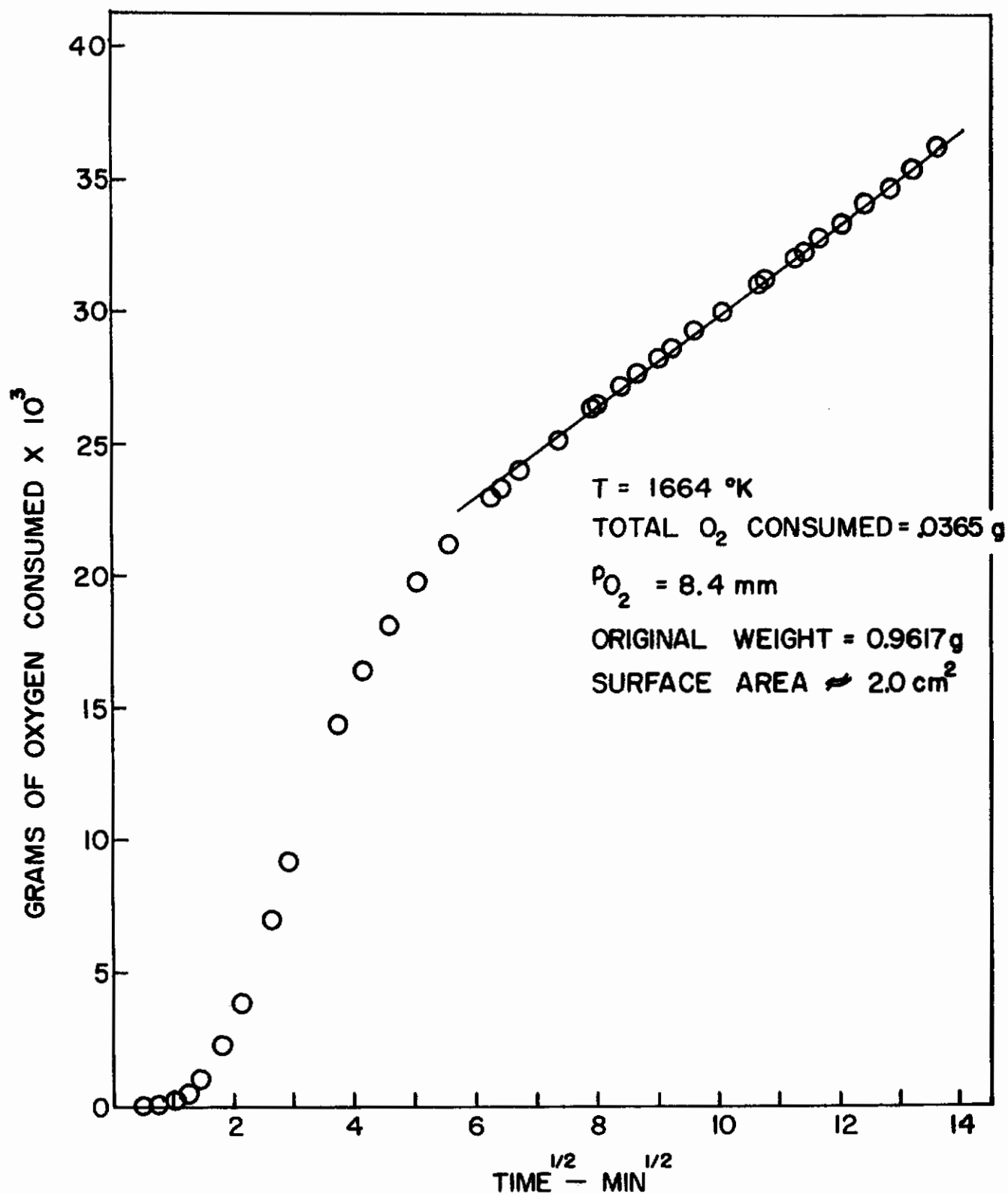
FIGURE IV-11   OXIDATION OF Ta_2Be_{17} (XI-51) AT 1664 °K

105

might fit the data over a longer period of time. Because of the limited
facilities for handling beryllium compounds in this laboratory, no attempt
was made to characterize the oxide film by X-ray or metallographic examina-
tion. Although the observed total oxygen consumption of 0.0365 g in a period
of 186 minutes, for a solid sample with original weight of 0.9617 g, is
considerably higher than that observed for $MoSi_2$ under comparable conditions,
nonetheless, the protective nature of the oxidation process makes Ta_2Be_{17}
a promising material for further study.

SECTION IV - REFERENCES

(1) R. Kieffer and E. Cerwenka, Z. f. Metallk. <u>43</u>, 101 (1952).

(2) R. Kieffer, F. Benesovsky, E. Gallistl, Z. Metallk. <u>43</u>, 284 (1952).

(3) Brush Beryllium Co., Cleveland, Ohio